2009

A Large-Scale Model of Spatio-Temporal Patterns of Excitation and Inhibition Evoked by the Horizontal Network in Layer 2/3 of the Visual Cortex

Symes, Andrew John

A Large-Scale Model of Spatio-Temporal Patterns of Excitation and Inhibition Evoked by the Horizontal Network in Layer 2/3 of the Visual Cortex

Andrew John Symes

Centre for Theoretical and Computational Neuroscience

University of Plymouth

A thesis submitted to the University of Plymouth in partial fulfillment of the requirements for the degree of

Doctor of Philosophy

Posthumous

September 2009

A Large-Scale Model of Spatio-Temporal Patterns of Excitation and Inhibition Evoked by the Horizontal Network in Layer 2/3 of the Visual Cortex

by

Andrew John Symes

Abstract: Cortical processing of even the most elementary visual stimuli can result in the propagation of information over significant spatiotemporal scales. To fully understand the impact of such phenomena it is essential to consider the influence of both the neural circuitry beyond the immediate retinotopic location of the stimulus, including pre-cortical areas, and the temporal components of stimulus driven activity that may persist over significant periods. Two computational modelling studies have been performed to explore these phenomena and are reported in this thesis.

1) The plexus of long and short range lateral connections is a prominent feature of the layer 2/3 microcircuit in primary visual cortex. Despite the scope for possible functionality, the interdependence of local and long range circuits is still unclear. Spatiotemporal patterns of activity appear to be shaped by the underlying connectivity architecture and strong inhibition. A modelling study has been conducted to capture population activity that has been observed in vitro using voltage sensitive dyes. The model demonstrates that the precise spatiotemporal spread of activity seen in the cortical slice results from long range connections that target specific orientation domains whilst distinct regions of suppressed activity are shown to arise from local isotropic axonal projections. Distal excitatory activity resulting from long range axons is shaped by local interneurons similarly targeted by such connections. It is shown that response latencies of distal excitation are strongly influenced by frequency dependent facilitation and low threshold characteristics of interneurons. Together, these results support hypotheses made following experimental observations in vitro and clearly illustrate the underlying mechanisms. However, predictions by the model suggest that in vivo conditions give rise to markedly different spatiotemporal activity. Furthermore, opposing data in the literature regarding inter-laminar connectivity give rise to profoundly different spatiotemporal patterns of activity in cortex.

2) The second computational modelling study considers simple moving stimuli. These stimuli are implicated in the 'motion streak' phenomenon whereby the movement of a visual feature can give rise to trajectory information that is not explicitly present. Published experimental data of an in vivo study in the cat has shown that a single small light square moving stimulus elicits activity in populations of neurons in primary visual cortex that are selective for orientations parallel to stimulus trajectory (Jancke 2000). In more recent, unpublished data, this work is extended to consider long term persistent cortical activity that is generated by similar stimuli. These data indicate that following initial cortical activation that appears to result directly from the stimulus, iso-orientation domains display persistent activity. Furthermore, initial activity is broadly tuned with respect to orientation whilst later activity is strongly selective for orientations that are parallel to the stimulus trajectory. Currently the generative processes involved have not been clearly defined. Hence the proposed thesis will contribute to a more complete understanding of the mechanisms responsible for such cortical representations of moving visual stimuli. More specifically this will be achieved by a large scale mean field model that will enable a thorough investigation of the anatomical and electrophysiological elements concerned with the observed spatiotemporal dynamic behaviour and will represent a significant region of cortex. In conjunction, an existing computational model of the retina will be integrated. In doing so this thesis will offer the notion that certain cortical representations are inextricably linked with earlier stages of the visual pathway. As such consideration of retinal processing is fundamental to the understanding cortical functions and failure to do so can only result in erroneous conclusions.

Contents

List of Figures

Acknowledgements

From the acknowledgement in Symes & Wennekers (2009):

> "Many thanks to Thomas Tucker for additional data and its interpretation. Thanks to Zoltán Kisvárday for supplying orientation maps of cat area 18. This project was supported by funding under the Sixth Research Framework Programme of the European Union under the grant no. FP6-2004-IST-FETPI 15879 (FACETS)."

The editor would like to thank Dr. Martin Coath (University of Plymouth) for providing his LaTeX thesis style file, which was used to typeset this thesis.

Acknowledgements by Andy's friends and collegues follow:

> "Andy Lymbo-Symes, for all those surfing times and Chai lattés I thank you. We experienced a lot of peace amongst those waves, away from the life of the PhD. Keep on surfing..."
>
> Maria Campbell

> "Brother Symes – for all the fun, laughter, endless arguments, Wikipedia moments, kindness, coffee made, wine drunk, cocktails bought and meals shared, for being the greatest sparring partner and biscuit catcher and, above all, for being the best of friends – thankyou Andy"
>
> Lucy Davies

> "Thanks for the stimulating conversations, the alarmingly anti-macho climbing partnership and the precision cooking. Thanks more generally for the experience of watching your analytical intelligence apply itself to

almost anything that entered into your environment. I expect that my future will be populated with people who are a 'bit like Andy' but few as unique as you."

Shaun Lewin

"Thanks for all your help and support during my first scary months, for your sarcastic sense of humour and, of course, for all those delicious chocolate biscuits."

Salvador Dura-Bernal

"Andy was a great guy, totally dedicated to his research, and a font of knowledge on important things like kite surfing, sailing and snowboarding. It is a remarkable tribute to him that his work and ideas on early visual processing have culminated (with the help of Thomas Wennekers) in a PhD thesis. I consider it a great privilege to have known and worked with Andy."

Sue Denham

"Andy, thanks for all the conversations on snowboarding and the lovely visual image I have of the relaxed manner you sprawled yourself out in the chair in my office to discuss what was happening with your PhD. A real gent."

Debbie Petherick

"I got to know Andy Symes in the late 1990s when we had adjacent offices in the Computing Department at the University of Kent. Andy was a hard-worker and a dedicated researcher - but he was also a person who knew how to have fun. We quickly became great friends, in part due to a shared love of winter sports but mainly because he was a lovely and very entertaining person to be with. We all missed him when he left Kent and

miss him all the more now."

Aliy Fowler
Lecturer in Computing
University of Kent

"Andy made a substantial contribution to the BT-sponsored PERMA-BASE project (Performance modelling for ATM-based applications and services, 1995-1998) at the University of Kent. He worked hard, with patience and intelligence and with good humour. I am sure that Peter Utton and Gino Martin of BT, Professor Peter Linington of the University of Kent and Andy's fellow researcher, David Akehurst, would all join me in acknowledging his work. Andy deserves warm congratulations for his achievements in the work leading to this thesis in the different field of Neural Networks."

Gill Waters, University of Kent (now retired)

"When I put the thesis together I found among the thousands of electronic publications that Andy left a directory of papers named "unhelpful". This directory contained just a single file. I thought how well this reflects how Andy was able to extract information from all he read, and also how he dealt with things more generally. Everything was critically evaluated and detail important. You will note the spirit throughout this thesis."

Thomas Wennekers

Editor's declaration

This is the thesis of my student Andy Symes who died July 2008 from a heart condition. It is compiled from material that Andy left, and submitted to the University of Plymouth in application for the title of a posthumous Ph.D.

At no time during the registration for the degree of Doctor of Philosophy has the author been registered for any other University award.

This study was financed with the aid of a studentship from the European Union as part of the project "Fast Analog Computing with Emergent Transient States in Neural Architectures (FACETS)".

Scientific seminars and journal clubs were regularly attended at which work was often presented. Meetings of the EU FACETS project were regularly attended. Part of this work was presented as a poster at the Computational Neuroscience Conference, CNS 2006. One paper has been accepted for publication in a refereed journal.

Publications :

Symes, A. & Wennekers, T. *Spatiotemporal dynamics in the cortical microcircuit: a modelling study of primary visual cortex layer 2/3.* Neural Networks 22, 1079–1092, 2009.

Posters and conference presentations :

Symes, A. & Wennekers, T. *Spread of activation along specific lateral pathways in microcircuits of the primary visual cortex.* Computational Neuroscience Conference, CNS 2006, Edinburgh. Poster presentation, 2006.

Word count for the main body of this thesis : $\approx$ 34.000

Signed: Thomas Wennekers

Date: 9. Dec. 2009

Chapter 1

Introduction

Study of the central nervous system continues to undergo dramatic changes, with significant progress made in recording techniques. The boundaries of investigation at both the micro- and macroscopic levels are constantly pushed back, with the possibility of recording the kinetics of synaptic transmitters through to the activity of multiple cortical areas. In recent years there has been considerable progress in neurophysiological recording techniques with respect to the number of cells which may be simultaneously recorded. From early techniques which recorded from a single cell, it is now possible to collect data from multiple cells through such diverse methods as multielectrode recordings of local field potentials (van der Togt, Spekreijse & Supér 2005), voltage sensitive dyes (Fitzpatrick 2000, Tucker & Katz 2003), intrinsic signals (Bear, Connors & Paradiso 2000, Payne & Peters 2001), magnetic imaging (Kandel, Schwartz & Jessell 2000, Muckli, Kohler, Kriegeskorte & Singer 2005), and calcium imaging (Cossart, Aronov & Yuste 2003, MacLean, Watson, Aaron & Yuste 2005). The advent of such methods has revealed hitherto unexpected cortical behaviour. One salient aspect of cortical processing is the role of coherent population activity. Correlation in population activity is observed in both spatial and temporal domains. The resolving power of these imaging techniques leaves little doubt to the presence of such concerted activity. However, less clear are the underlying mechanisms involved. The pervasive nature of such activity suggests it is a fundamental operating state of cortical circuitry and as such bears investigation.

More traditional views of cortical processing have been within a feedforward para-

digm operating across multiple resolutions, from discrete areas, such as the retina/lateral geniculate nucleus (LGN)/primary visual cortex (V1) route of the visual pathway, to the individual layers, 1 – 6, of V1. As such, cortical processing is often been viewed more as a functional transformation of its inputs. However, the temporal correlation observed within cortical activity calls into question the validity of purely feedforward models. A more appropriate view point might be that of a dynamical, context dependent system, where the current and ongoing cortical state is potentially as important as the stimulation transformation itself. Even the most cursory view of the visual cortex reveals multiple feedback loops, both vertically between layers and horizontally within layers. The presence of such circuits suggests that at any instant cortical processing of any stimulus is modulated by the current cortical state. Indeed, such considerations become particularly relevant when considering that stimulus induced activity may constitute a relatively small proportion of the overall observed activity in vivo (Fiser, Chiu & Weliky 2004), and of that activity which directly results from a stimulus, only a small proportion is correlated to functional tuning (Sharon, Jancke, Chavane, Na'aman & Grinvald 2007). Evidence suggests that certainly in V1, the cortex is in a spatiotemporal dynamic state even in the absence of stimulus (Tsodyks, Kenet, Grinvald & Arieli 1999) and that this ongoing activity is related to its functional architecture (Kenet, Bibitchkov, Tsodyks, Grinvald & Arieli 2003). Furthermore, such ongoing states provide a context by which stimulus driven response can be more accurately predicted (Albright & Stoner 1995) rather than simply being regarded as background noise to be averaged out. The view of processing in V1 as a predominantly feedforward mechanism is further questioned by the observed connectivity. The modelling study presented by Binzegger, Douglas & Martin (2004) of afferent and efferent connectivity observed in cat primary visual cortex highlights previous observations that intra-, rather than intercortical connections, dominate (Thomson & Bannister 2003).

This thesis proposes that the proliferation of corticocortical connections dominate the dynamic spatiotemporal population behaviour observed in primary visual cortex. It will be shown that the specific lateral connectivity accounts for activity profiles observed in vitro and in vivo. Furthermore, it is hypothesised that the same connectivity, in concert with early processing of the visual pathway, gives rise to activity in subpopulations that have a functional tuning orthogonal to stimulus characteristics. Specifically, a mean field model of primary visual cortex is developed that clearly demonstrates that specific patterns of spatiotemporal activity elicited by extracellular stimulation of in vitro slices (Tucker & Katz 2003) is a direct consequence of lateral connectivity patterns. The model is subsequently expanded to incorporate an existing retinal model that has been developed to investigate contrast gain control. In doing so it is shown that combining temporal integration characteristics of the retina with specific feedforward and lateral connectivity in V1 gives rise to motion streak effects observed in vivo (Jancke 2000) and proposed as a possible enhancement to motion processing (Geisler 1999). Finally the model is used to investigate data from ongoing in vivo studies of lateral activity spread observed in the cat primary visual cortex as a result of small moving stimuli (Jancke, unpublished). This work suggests that relatively small moving stimuli can evoke a disproportionately large response across an extensive region of cortex. Furthermore such activity is highly correlated to a specific feature of the underlying functional architecture. It will be demonstrated that such observations of population activity are a direct consequence of very specific and strong lateral connections that enable reinforcing feedback, rather than feedforward, mechanisms to generate precise spatiotemporal patterns of activation.

This thesis presents the current stage of development including background research which constitutes a foundation literature review, the model subsequently developed and preliminary results. It is structured as follows.

Chapter 2 presents a synopsis of the early stages of the mammalian visual pathway. This comprises the retina, lateral geniculate nucleus (LGN) and primary visual cortex (V1). Specific emphasis is placed on visual processing within the cat for three specific reasons. Firstly there is perhaps a more extensive and complete source of data on the cat visual pathway than any other mammalian visual system. Secondly, two of the experimental studies have been conducted using the cat, whilst for the in vitro experimental data (Tucker & Katz 2003) the ferret anatomy bears many similar characteristics to the cat, in particular the patchy long range connections observed in layer 2/3 (Bosking, Zhang, Schofield & Fitzpatrick 1997, Kisvárday, Tóth, Rausch & Eysel 1997). Finally, maintaining internal consistency within the model with respect to specific sources of anatomical and physiological data used can only lend credibility to the results.

Chapter 3 presents the model. This large scale mean field model has currently undergone two incarnations. The first of this focused on representing a single layer (2/3) within the primary visual cortex for investigation into the afore mentioned in vitro study (Tucker & Katz 2003) which formed the basis of a poster presentation at CNS 2006. A subsequent development of the model has expanded the cortical representation with an additional input layer for V1 (layer 4) and has also incorporated an existing retinal model, which will also be reviewed.

Chapter 4 reports preliminary results. These include comparison with the in vitro study of Tucker and Katz (Tucker & Katz 2003) where extracellular stimulation of ferret cortical slices was shown to produce spatiotemporal patterns of excitation that were consistent with the anatomical patterns of excitatory and inhibitory connectivity. Also presented are observations from a moving stimulus paradigm that shows motion streak effects (Jancke 2000) and lateral spreading activation. The later effect is congruent with both the underlying functional architecture and connectivity observed in

V1. In addition a relatively small stimulus is seen to elicit activation with an extensive proportion of the population that persists over a significant period. Both these results appear to have been observed experimentally in vivo (Jancke, personal communication and 2000), and thus comparisons will be made.

Chapter 5 reviews the state of the thesis. The results obtained thus far are discussed in the context of the experimental data with potential issues and discrepancies addressed. Future research directions are presented which propose to focus on a more stringent validation and verification of the model against standard functionality of the primary visual cortex and investigation of the ongoing work of Jancke (personal communication). Possible issues with these proposed directions are also considered. In particular the potential ramifications of interpreting voltage sensitive dye recordings and the inclusion of additional V1 layers from the model are examined.

This work is funded by the FACETS project – Fast Analog Computing with Emergent Transient States in Neural Architectures - (FP6-2004-IST-FETPI 15879). The FACETS project is a pan-European endeavour, with the goal of investigating new biologically inspired approaches to computation. As such it synthesises a broad spectrum of research fields including experimental biology, computer hardware and computational and theoretical neuroscience. The remit of Plymouth University's contribution is the coarse grain modelling of large populations of cells in the early stages of the visual pathway. The breadth of experience that the many participants bring to the project encourages collaboration. As a result of this, the retinal model adopted for this thesis has been developed by INRIA (Sofia-Antipolis, France), a partner in the FACETS consortium, and the cortical model incorporates further data from the experimental labs of Zóltan Kisvárday (Debrecen, Hungary) and Alex Thomson (London, UK).

Chapter 2

Early Visual Pathway

2.1 Overview

As mentioned previously, the work presented here is primarily concerned with the early processes constituting the visual pathway, and in particular the retina, lateral geniculate nucleus (LGN) and primary visual cortex (V1) components. In order to appreciate this context, a relatively brief synopsis of the early visual pathway is presented here (Bear et al. 2000, Kandel et al. 2000, Payne & Peters 2001). Again, whilst the information presented is within the realms of the mammalian visual system, particular emphasis is placed on that of the cat as this serves as the paradigm for the modelling studies conducted.

Visual stimuli from the external environment first enter the visual system via the retina with information subsequently relayed to the LGN and thence V1. This is an exceptionally gross simplification, as will be seen, and does not accommodate the multiple feedbacks pathways present; however it does serve to position the retina, LGN and V1 with respect to one another. A visual scene presented to the eye is reflected about both vertical and horizontal axis before projection onto the retina. Thus the right half of the visual field projects onto the left hemiretina whilst the left half of the visual field projects to the right hemiretina. It is common practice to employ the terms nasal and temporal hemiretina dependent on whether it is closer or further from the sagittal plane (strictly speaking this is in relation to the fovea). Hence the left half of the visual field projects to the nasal hemiretina of the left eye, and the temporal hemiretina

of the right eye. Similarly, the lower half of the visual field projects onto the upper (dorsal) half of the retina, or superior hemiretina, and conversely the upper half of the visual field projects onto the lower (ventral) or inferior hemiretina. The majority of the visual field is binocular and projects an image onto both retinas, however the periphery of the visual field is marked by regions of monocularity, and projects onto only one or other retina. The retinofugal project (optic nerve) describes the bundle of axons leaving each eye via the optic disc that combine to form the optic chiasm. From the optic chiasm two bundles of axons, the optic tracts, project to the lateral geniculate nucleus. Individual axons follow specific routes through this pathway. At the optic chiasm axons are segregated such that the right optic tract represents the left half of the visual field by combining axons from the nasal and temporal hemiretinas of the left and right eyes respectively. In doing so the axons from each nasal retina cross to the other side of the brain, whilst axons from the temporal hemiretinas do not. The majority of axons of the left and right optic tract maintain this lateral division by making thalamic projections that innervate the left and right lateral geniculate nuclei. Whilst the LGN is not the sole subcortical recipient of retinal efferents –hypothalamus, superior colliculus and pretectum are also targeted by the retina– it does play an important role in the early visual pathway through its close coupling with retina and primary visual cortex, to which it conveys a significant proportion of sensory information (Sherman & Guillery 2002, Sillito & Jones 2002). It is for this reason that it is the only direct recipient of retinal axons that is considered here and in the subsequent models. Axons from the LGN form the optic radiation that projects directly to the primary visual cortex. An overview of the early visual pathway is given in Figure 2.1.

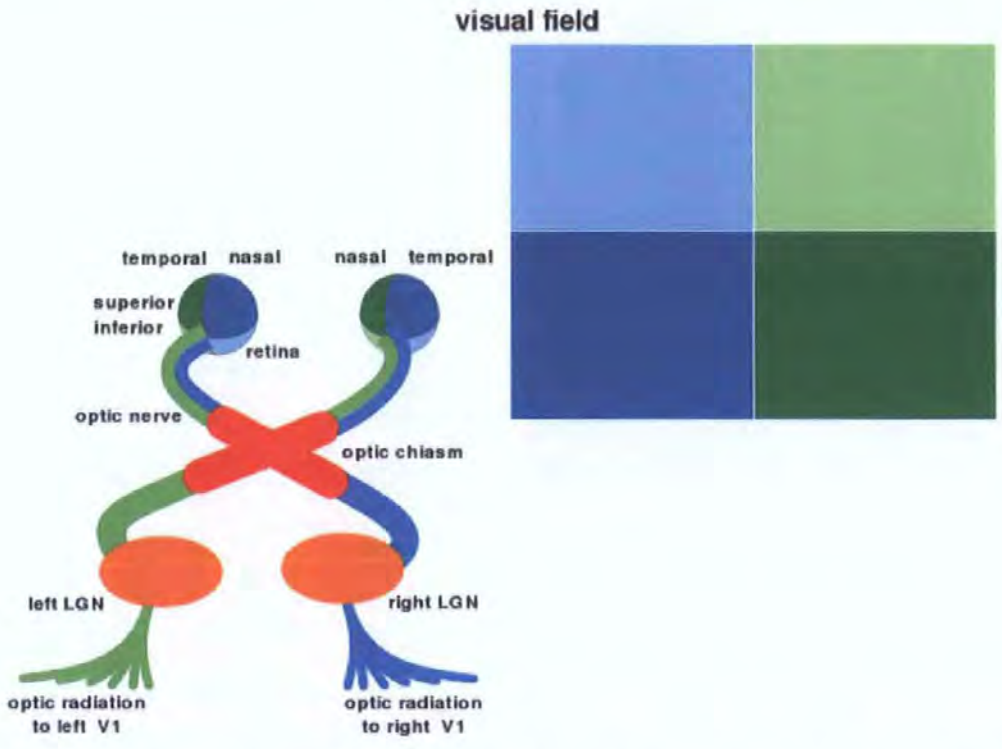

Figure 2.1: Schematic representation of the early visual pathway. The broad divisions of the visual field illustrate how it is projected onto the retina of each eye. As the visual system reorganises its representation of the nasal and temporal hemiretinal projections of the visual field only these distinctions are made in the retinofugal projection. The optic chiasm is seen to redirect information pertaining to left and right halves of the visual field to the contra lateral regions of the lateral geniculate nucleus and then, via the optic radiation, to primary visual cortex.

2.2 The Retina

A general overview of the retina is presented here before a more detailed review of certain aspects of the retinal circuitry (Bear et al. 2000, Hubel 1995, Kandel et al. 2000, Masland 2001). The retina is a light sensitive region of cells covering the posterior surface of the eye interior and subserves phototransduction. It comprises four distinct layers which are generally considered in order of the layer furthest from the centre of the eye to the innermost layer that lies closest to the centre of the eye. The

first layer in this ordering is composed of two types of light sensitive photoreceptors termed rods and cones due to their distinct morphology. Rods are primarily associated with sensitivity to very low light levels, scotopic vision, whilst cones dominate vision under high luminance, photopic vision. These two operating modes are not distinctly partitioned and thus mesopic vision combines both rod and cone signals as luminance transitions from nominally low to high levels. The cell bodies of the photoreceptors themselves form the outer nuclear layer. Adjacent to this, towards the centre of the eye, the inner nuclear layer contains three broad classes of cells, bipolar, horizontal and amacrine. Whilst there are many distinct types of each (Kolb, Nelson & Mariani 1981, Masland 2001), the inner nuclear layer is discussed only in terms of these three broad categories. The region of synapse connecting photoreceptors to bipolar and horizontal cells between the outer and inner nuclear layers is termed the outer plexiform layer. The ganglion cell layer is situated beyond the inner nuclear layer towards the centre of the eye, and as its name suggests contains the soma of retinal ganglion cells. Amacrine and bipolar cells synapse with ganglion cells in the inner plexiform layer between ganglion cell and inner nuclear layers. As a result of this structure, light must pass through the ganglion cell, outer nuclear and inner nuclear layers before reaching the photoreceptors. Unlike many other types of neurons, in the retina, all but the ganglion cells produce a graded response to stimulation, whilst only the ganglion cells have a spiking output. Two common features of the mammalian retina are a central area with increased cone density that gives rise to high acuity, commonly referred to as the fovea (or area centralis in the cat), and a blind spot called the optic disc where the optic nerve leaves the retina.

A central concept of visual processing is the notion of a receptive field (RF). Simply put, the receptive field of a cell is the region of visual space to which it is responsive. That is, a stimulus, such as a bright dot, falling within a cell's receptive field will

elicit a response, whilst any stimuli lying beyond the receptive field will have no effect on the cell. Note that as understanding of the microcircuitry of the visual system improves it has become apparent that the spatial extent over which stimuli in the visual field can influence a given cell is significantly greater than was originally thought. In turn this has given rise to such terms as the 'classical' and 'non-classical' receptive field. However, such concepts are generally the preserve of primary visual cortex (Bringuier, Chavane, Glaeser, Y. & Frégnac 1999, Seriés, Lorenceau & Frégnac 2003) rather than the retina where the receptive fields of cells are relatively compact. Retinal receptive fields are essentially circular regions of the visual field which the cell is responsive to. The response profile is generally not uniform across this region but has Gaussian like characteristics. Ganglion cells (Barlow, Fitzhugh & Kuffler 1957, Bear et al. 2000, DeAngelis, Ohzawa & Freeman 1995, Hubel 1995, Kandel et al. 2000, Peichl & Wässle 1979, Rodieck 1965, Rodieck & Stone 1965) appear to have an antagonistic centre surround structure whereby the receptive field is divided into a circular centre region and an annular surround as seen in the left diagram of Figure 2.2. Whilst ganglion cells undoubtedly have centre surround receptive field structures, the same certainty cannot be said for all cone and bipolar cells where evidence is less clear (Dacey, Packer, Diller, Brainard, Peterson & Lee 2000, Nelson 1977, Smith & Sterling 1990). The illustration is typical of retinal ganglion cells with the centre region marked by "+" symbols indicating that a light stimulus in this region has an excitatory effect on the cell. Conversely, the surround, marked by the "-" signs, inhibits the cell when stimulated. This organization gives rise to the term ON centre cell, with cells having reversed polarities in centre and surround referred to as OFF centre cells. As mentioned previously, the receptive field response has Gaussian characteristic as illustrated in the right plot of Figure 2.2. This corresponds to the response of the afore mentioned receptive field in profile along an axis through its centre. As the receptive

Figure 2.2: Centre surround receptive field structure of retina cells. The left diagram illustrates a typical ON centre cell with facilitatory centre region and inhibitory surround. The right diagram shows the response profile of the along an axis through the centre of the receptive field. The maximum response is observed at the centre of the receptive field.

field has circular symmetry the orientation of the axis is not important. It can be seen that the response is maximal at the centre of the receptive and drops of sharply towards the surround where the negative values indicate inhibition. Such profiles are often modelled using a difference of Gaussians (Rodieck 1965, Smith & Sterling 1990).

2.2.1 Outer Nuclear Layer

The outer nuclear layer is populated by two types of photoreceptor cells, specifically rod and cone cells. The names arise from the morphology of the outer segments which are cylindrical in rods, and tapering in cones, however they also differ on a number of different characteristics. Rods are far more numerous than cones yet the number of bipolar cells driven by cones is greater than that receiving input from rods. As alluded to earlier, the rod system operates predominantly at low levels of luminance. Whilst this is due in part to the higher sensitivity of rods to light, the higher convergence of rods to bipolar cells also contributes. The single photosensitive visual pigment present in all rods results in a population that responds only to a single frequency band. By contrast, cones can be divided into subpopulations each of which has a different photosen-

sitive visual pigment, and as a result sensitivity to a different frequency band, forming the basis of colour vision. Retinal circuitry can compare the response of cones tuned to different frequencies and thus determine more accurately the wavelength of the incident light. Both cones and rods display a nonlinear response to stimulus intensity, termed light adaptation. Light, or background, adaptation (Fain, Mathews, Cornwall & Koutalos 2001, Mante, Frazor, Bonin, Geisler & Carandini 2005) reflects the fact that the response of a photoreceptor is influenced by the mean background luminance in an effectively divisive relationship. Thus as the ambient luminance increases, the sensitivity, and thus response, of a photoreceptor to stimuli decreases. From Fain et al. (2001) p.118, this relationship can be described by

$$\frac{S_F}{S_F^D} = \frac{I_0}{I_0 + I_B} \tag{2.1}$$

where

S_F is the sensitivity of the photoreceptor to a stimulus flash, and is defined by $S_F = \frac{photoreceptor\ response}{stimulus\ intensity}$.

S_F^D is the sensitivity in darkness.

I_B is the background intensity.

I_0 is the intensity of the background necessary to reduce sensitivity by half.

Given that D_F^D and I_0 are constants, then for $I_B \gg I_0$

$$photoreceptor\ response \sim \frac{photoreceptor\ response}{background\ intensity}. \tag{2.2}$$

A concurrent adaptation process to luminance called bleaching adaptation (Fain et al. 2001) also takes place in photoreceptors whereby the visual pigment is bleached

at high light levels. The level of bleaching at which rods become saturated and unresponsive to an increase in luminance is much lower than observed in cones which maintain response over a significantly wider range of luminance values (Knox & Solessio 2006). Recovery of photoreceptor bleaching is termed dark adaptation and contrasts with light adaptation which describes the process employed by the retina to facilitate operation over a wide range of luminance (Lamb & Pugh 2004). The two processes differ significantly in time scale, with dark adaptation operating over several minutes compared with the relatively rapid adjustment of light adaption.

2.2.2 Inner Nuclear Layer

Connecting to the outer nuclear layer via the outer plexiform layer, the inner nuclear layer is home to bipolar cells, often differentiated as cone and rod bipolar dependent on the photoreceptors that drive them. As there is only one type of rod only a single type of rod bipolar is recognised, however, the multiple types of cones allows subpopulations of cone bipolar to be identified. Whilst a photoreceptors' response to stimulation is the release of a single neurotransmitter, glutamate, the impact on individual bipolars as either facilitatory or depressive enables the further classification of this type of cell as ON or OFF. A further distinction can be made in terms of their temporal response as either sustained or transient, giving rise to low and high frequency tuning respectively. Photoreceptor drive of cone bipolar cells demonstrates an overlap in the cone population, with a single cone contributing to the response of a number of cone bipolar cells (Cohen & Sterling 1992, Sterling 1999). Thus the pathway from cones to bipolar exhibits both convergence, with many cones driving a single bipolar, and divergence, as a single cone may synapse onto a number of bipolar cells. In contrast to the cone mediated pathway which is relatively direct from bipolar cells to ganglion cells, the rod pathway is more circuitous. Rod bipolar cells access ganglion cells through an

intermediary amacrine cells which then synapses onto cone bipolar axons. Horizontal cells provide a feedback mechanism for the photoreceptors, influencing the receptive field structure and response to overall luminance. Amacrine cells are numerically the most diverse population in the retina. This is reflected in both, morphology –dendritic arbours can extend from hundreds of micrometres to millimetres– and physiology – amacrine cells are implicated in such functionality as contrast gain control (Smirnakis, Berry, Warland, Bialek & Meister 1997) and directional tuning. As mentioned above, amacrine cells provide a gateway for rod bipolar drive to reach ganglion cells, indeed the majority of synaptic contacts on ganglion cells are made by amacrine cells.

2.2.3 Ganglion Cell Layer

Ganglion cells in the cat fall into as many as 20-23 different categories (Kolb et al. 1981, O'Brien, Isayama, Richardson & Berson 2002), however those most considered are α, β or γ, which are also synonymous with the oft cited Y, X and W cells. Proportionally, β and γ cells are the more numerous, whilst only a small fraction of retinal ganglion cells belong to the α class. These distinctions can be seen in the morphology of the cells; α retinal ganglion cells have large somata and dendritic arbours; β cells have smaller somata and arbours, whilst γ have small cell bodies and various forms of dendritic arbour. This variety in dendritic morphology offers the possibility of further subdivision, however, these subpopulations are often simply collectively termed γ cells. Ganglion cells make more synapses with those bipolar cells central to their dendritic arbour, and less with those peripheral (Sterling 1999). In parallel with morphology, the physiology of each cell type is also quite separate. As a result of the large dendritic arbour, α retinal ganglion cells have a large receptive field. This receptive field follows the classic centre surround structure and tends to exhibit low spatial frequency tuning and transient response which gives rise to a higher temporal resolution

and velocity response. In contrast β cells have smaller receptive fields, but with the same structure, and produce a sustained response to higher spatial frequencies. Hence they have low pass properties in the temporal domain and high pass in the spatial domain. The distribution between α and β retinal ganglion cell response under high contrast is dependent on the spatial frequency of the stimuli, with β cells predominant under higher spatial frequency regimes (Payne & Peters 2001). Ganglion cells exhibit maintained discharge at all levels of background luminance in the absence of a specific stimulus (Kuffler, Fitzhugh & Barlow 1957, Barlow & Levick 1969, Cleland, Levick & Sanderson 1973). This is observed even in complete darkness where ongoing spiking activity is still observed.

Both the density and receptive field size of α and β ganglion cells change retinal location (Cleland, Harding & Tulunay-Keesey 1979, Peichl & Wässle 1979, Stein, Johnson & Berson 1996, Stone & Keens 1980). In the area centralis, estimates of β cell densities as high as 7000 cell/mm^2 are reported by Stein et al. (1996) who suggest that the figure may be even higher. This figure drops significantly in more peripheral areas. Higher cell densities closer to the area centralis enables the visual field to be sampled at a much higher resolution. To accompany this, receptive field size decreases as the area centralis is approached and consequently improves the spatial resolution of cells located there (Cleland et al. 1979, Peichl & Wässle 1979).

2.3 The Lateral Geniculate Nucleus

The main target of retinofugal efferents after the optic chiasm is the lateral geniculate nucleus (LGN) which belongs to the posterior nuclei thalamic group (Kandel et al. 2000). More accurately, it is the dorsal structure of the lateral geniculate nucleus that is concerned with the transfer of visual information to the primary visual cortex (Payne & Peters 2001) and contains left and right lateral geniculate nuclei (Bear et al. 2000). As

seen in Figure 2.1, the left and right LGN receive visual information from the right and left halves of the visual field respectively. Each LGN has a laminar structure consisting of six layers which in the cat are labelled from most ventral to dorsal, A1, A2, CM, C1, C2 and C3 (Payne & Peters 2001). Within the laminae, X and Y pathways both terminate in the A layers, whilst only Y innervates layer CM (Payne & Peters 2001, Sherman & Guillery 2002). The W pathway is confined exclusively to dorsal C1 and C2 layers which do not receive any X or Y input. In addition to this segregation by lamina, there is no evidence to support the interaction of pathways within the LGN, even when they are further categorised as originating from ON or OFF centre retinal cells (Guillery & Sherman 2002, Sherman & Guillery 2002). The cat LGN shares with primates a highly specific structure to innervations by retinal afferents. In cat, from dorsal to ventral, laminae receive alternating retinal input, thus layer A1 is innervated by input from the contralateral retina, layer A2 by the ipsilateral retina through to layer C2 (Sherman & Guillery 2002, Tumosa, McCall, Guido & Spear 1989), whilst layer C3 does not receive retinal projections (Payne & Peters 2001). Clearly from section 2.2, laminar input also alternates between nasal and temporal hemiretina. In primates the laminar distribution of retinal projects differs, with layers 1, 4 and 6 targeted by the contralateral retina and layers 2, 3 and 5 by the ipsilateral retina (Bear et al. 2000, Kandel et al. 2000). Each of the laminae maintains a retinotopic map of the visual field region that projects to it such that the receptive fields of adjacent cells are centred on adjacent points within the visual field. The high visual acuity near the centre of the retina leads to a distortion in the retinotopic map with a disproportionately large number of cells of each layer given over to representation of more central regions of the retina. Additionally, not only does each layer preserve a separate retinotopic map of the visual field, but all maps are in retinotopic register with one another (Casagrande & Ichida 2002, Sherman & Guillery 2002). LGN cells can be viewed as either relay

cells which make excitatory projections to the striate cortex, or interneurons whose inhibitory synapses contact only LGN cells (Casagrande & Ichida 2002). In the A laminae approximately 25% of cells are interneurons (Peters & Payne 1993).

Receptive fields are little changed by the passage through LGN (Bear et al. 2000, Casagrande, Guillery & Sherman 2005, Casagrande & Ichida 2002, DeAngelis et al. 1995, Guillery 1995), with lateral geniculate cells inheriting many characteristics from retinal ganglion cells. However the transfer ratio (a comparison of the retinal input to an LGN cell as the synaptic or S-potential, against the output or action potential) is less than 1, in fact less than half (Casagrande & Ichida 2002). Thus the LGN is attenuating the signal. As mentioned, LGN receptive fields are generally regarded as circular, however there is evidence for elliptical and offset centre surround structures (Cai, DeAngelis & Freeman 1997). Furthermore, LGN cells exhibit distinctive spatiotemporal receptive fields; including mono- bi- and triphasic; that in some cases are nonseparable, that is the receptive field cannot be decomposed into separate functions of space and time whose product yields the original receptive field (Cai et al. 1997). In such cases the centre response develops to a peak response before that of the surround. Such spatiotemporal inseparability is quite different to that encountered in cortical simple cells (DeAngelis et al. 1995) where it is implicated in direction selectivity. The characteristics of these cells is in some respects similar to the mono- and biphasic layer 4 simple cells implicated in direction selectivity in primate (Valois & Cottaris 1998, Valois, Cottaris, Mahon, Elfar & Wilson 2000), with potentially a similar mechanism observed in the cat (Peterson, Li & Freeman 2004). LGN receptive fields can be represented by a modified difference of Gaussian (DoG) model as used for retinal ganglion cells (Rodieck 1965). There is little difference between the temporal profiles of ON and OFF centre cells in the cat. The temporal profile of lagged and non-lagged cells exhibit tri- and biphasic properties, for ON centre cells this is manifest as a significant

initial dark response and the reverse in OFF centre.

The historical perspective of the LGN as simply a relay circuit between retina and striate cortex has been challenged by Guillery and Sherman (Casagrande et al. 2005, Guillery 1995, Guillery & Sherman 2002, Sherman & Guillery 2002). By means of anatomical and functional evidence it is argued that thalamic relays fall broadly into one of two categories, either "first order" or "higher order". The term relay is employed as individual nuclei in themselves do not always enable clear delineation of first and higher order characteristics (Guillery & Sherman 2002). The distinction of first and higher order relays relies on the identification of the majority of thalamic afferents as either "drivers" or "modulators". The former is seen as the source of information that is functional acted upon by the nucleus, whilst the latter provides a mechanism by which this functionality may be adapted. Whilst divers are referred to as primary afferents they may not be numerically dominant over modulators, in the cat only approximately 10% of LGN afferents are retinal in origin, whilst roughly 30% are projections from striate cortex layer 6 (Sillito & Jones 2002). Interestingly, this figure for retinal input is at odds with the 5:1 ratio of extraretinal to retinal LGN input cited by Casagrande & Ichida (2002). Given this premise of drivers and modulators, higher order nuclei are those whose driver afferents come from cerebral cortex, in particular layer 5, whilst first order drivers are projections from non-cortical centres such as the sensory system. Within this scheme, the lateral geniculate nucleus is considered a first order nucleus as its primary afferents are the retinofugal projection. Modulators, including corticothalamic feedback from layer 6 (see Figure 2 in Guillery & Sherman (2002)), are considered to facilitate synchronisation of activity produced by different, but related, sources, and also enable cells to switch between tonic and bursting modes (Guillery 1995). It is suggested that possible roles for these two modes are improved detection under a bursting regime, and higher fidelity of stimulus representation by tonic firing

(Sherman & Guillery 2002). Thus it would appear that modulation by the lateral geniculate nucleus is more concerned with how (e.g. tonic versus bursting mode) rather than what (e.g. receptive field characteristics) visual information is transferred to cortex. The firing mode of relay cells is a function of membrane potential. Depolarisation inactivates a particular ion channel that is gated by membrane voltage resulting in tonic firing mode. Hyperpolarisation "de-inactivates" the channel resulting in burst mode firing following subsequent depolarisation. This transition between the two modes is a function not only of membrane potential but also time. Retinogeniculate transmission occurs exclusively via ionotropic receptors which permit the faithful transfer of higher frequencies. Modulators additionally activate metabotropic synapses which may play a role in the switch between tonic and burst modes.

Perhaps the main proposal of Guillery & Sherman (2002) is a more significant role of thalamic relays in all processing in opposition of the purely cortical processing that is traditionally considered. However, in the context of the work presented here this particular aspect of their hypothesis is no different from ignoring feedback from other cortical areas such as MT. In particular if the transthalamic route involves a number of centres, then the overall delay is possibly such that is impact is severely attenuated. However, given the time scale involved in the observations of Jancke (2000), it is unlikely that any transthalamic delays are that extensive. Given the lack of understanding of the impact that the specific functionality of the thalamocortical feedback has it is difficult to include in any model.

With respect to the tonic/burst firing modes of thalamic cells, if it is assumed that LGN relay cells are in a relatively depolarised state, perhaps reflecting tendency to maintained discharge (Levick & Williams 1964), then further depolarisation by stimuli will place them in tonic firing mode, in which case they might be considered more a simple relay and thus the retinal output can be assumed to feed directly into the

cortex. It perhaps needs a more temporally complex stimulus in order for the relay cells to switch between tonic and bursting modes over the course of the stimulus. Sillito and Jones suggest that hyperpolarisation resulting from centre surround interaction can switch relay cells to bursting mode (Sillito & Jones 2002). For the work presented here stimuli are such that the presence of such surround influences is questionable, or at least minimal. They also show that changing the response magnitude of layer 6 cells can switch LGN relay cells between the two firing modes. Again, for the simple stimulus used herein it is debatable whether they would generate sufficiently large response in layer 6 cells to influence the behaviour of LGN relay cells. If such switching does not occur, then this functional characteristic of the LGN is effectively ignored. Indeed, it would appear that for simple stimuli such as sinusoidal gratings in anaesthetised cat (Sherman & Guillery 2002), relay cells can maintain both bursting and tonic firing modes over periods of several seconds. In the later mode LGN response is extremely linear and thus cells behave far more as simple relays. The bursting mode of LGN relay cells is proposed to form a "wake-up call" that directs attention, with some evidence to support this (Casagrande et al. 2005, Casagrande & Ichida 2002, Sillito & Jones 2002, Wörgötter, Eyding, Macklis & Funke 2002). However, such data demonstrates that bursting behaviour is concomitant with inattentive states and presentation of novel stimuli; persistent stimuli are associated with tonic firing. For the stimuli used by Jancke (2000), the initial movement phase does not contribute to the analysis thus it is likely that LGN relay cells are firing in a tonic mode for the duration of data acquisition and may thus be treated more as simple relays. It is claimed that during bursting mode the lower spontaneous activity in relay cells contributes to a higher signal-to-noise ratio and consequently improves detectability. With respect to the synchronisation aspects of LGN functionality the stimuli used are simple and singular in nature and thus limit the possibility of containing multiple features that are in

some sense related. Such functionality will possibly enhance salient features, however, arguably at a certain resolution there is only one feature, the square or dot, whilst at a resolution where it might be considered as several features, i.e. the sides of the square, then there are no other stimulus features in the visual field from which to distinguish it as it is projected on a blank screen. Thus it might be argued that the functionality of LGN proposed by Guillery and Sherman (Guillery 1995, Guillery & Sherman 2002, Sherman & Guillery 2002) would have little impact on processing of the extremely simple stimuli considered here.

Sillito & Jones (2002) argue that whilst the corticothalamic feedback loop from layer 6 preserves the retinotopic mapping, the projection is more diffuse than from the retina and so may influence LGN cells outside their classic receptive field. Indeed, evidence suggests that the feedback projection from layer 6 to LGN is related to the orientation tuning of presynaptic cells. The retinotopic organization of the recipient LGN cells form an axis that is either parallel or perpendicular to the orientation tuning of the layer 6 cells. Furthermore they propose that the latency of this mechanism may be as short as 3-5ms. It has been proposed that layer 6 to LGN projections form an antagonistic centre surround scheme with facilitatory centre and inhibitory surround (Wörgötter et al. 2002). Cat layer 6 cells projecting to LGN are mainly simple cells which tend to have low maintained activity but strong orientation tuning with short receptive fields, and are strongly direction selective and monocular. One feature of cortical feedback is the influence that the surround has on LGN cell response. For drifting gratings, altering properties of the annular surround on the circular centre can significantly increase the observed suppression. The most striking of these effects is when both centre and surround are co-oriented and have the same spatial and temporal frequencies. Additionally, feedback is implicated in supralinear gain resulting from synchronisation of LGN cells to oriented contours. One effect observed by Sillito and

Jones that may have a bearing on the work presented here is the influence of feedback from the middle temporal area (MT, or V5), via V1, to LGN. MT is primarily associated with motion in monkeys (Albright & Stoner 1995, Bear et al. 2000, Born & Bradley 2005, Kandel et al. 2000, Newsome & Salzman 1993) with the lateral suprasylvian sulcus (area PMLS) its counterpart in the cat (Payne 1993). However, given that the motion detection studied here is resulting from orientation selective cells tuned parallel to the motion streak it is not clear what contribution direction selective cells tuned for motion parallel to the motion streak will make. This is particularly relevant when considering feedback from MT and its relatively large receptive fields (Bear et al. 2000), approximately 10 times that of V1 in monkeys (Born & Bradley 2005, Kandel et al. 2000), in conjunction with the small stimuli presented. Such small stimuli, particularly those used in Jancke (2000), may be insufficient to produce a large enough response in MT cells that is not attenuated during feedback to LGN through V1. However, it is conceivable that amplification by V1 could lead to an MT impact on LGN.

The impact of these observations on the studies presented here is questionable. Clearly for the modelling study of extracellular signals in vitro conducted by Tucker & Katz (2003) activity is independent of any influence of the corticothalamic feedback loop. With regards to modelling the data of Jancke (Jancke 2000 and unpublished data) the stimuli used are simple small dots and squares on a uniform background. As such there is no context and therefore little scope for any surround interaction effect. The only possibility is the generation of a context resulting from motion streak effects. This is particularly relevant however, as it is a central tenet. Hence it is essential to consider the spatial extent of any motion streak effects in comparison to the influence of surround. Further to this, centre-surround effects may be of more significance for the validation and tuning studies of simple orientation/direction/spatial/temporal tuning.

From Wörgötter et al. (2002), δ-wave states, as found in sleep, reduce the responsiveness of LGN. More synchronised EEG states, i.e. where δ-waves predominate, are suggested to result in more phasic responses, akin to bursting, whilst tonic firing is observed in less synchronised states. Similar response behaviour to that observed during transition from less to more synchronised EEG states is also seen during inactivation of cortical feedback by cooling. As a result there is potential ambiguity with regard the source of change in LGN activity. Wörgötter et al. (2002) suggest that corticothalamic facilitation is the result of direct excitatory projections as opposed to disinhibition via a bi-synaptic circuit of two inhibitory LGN interneurons. Removal of corticothalamic feedback by abolition of LGN-projecting layer 6 cells shows an increase in stimulus driven activity of the remaining layer 6 cells and their receptive field width. Whilst the experimental data does not unequivocally point to a corticothalamic mechanism, observation of similar results in LGN cells does support this hypothesis.

Alitto & Usrey (2003) propose that corticothalamic feedback may sharpen the receptive field properties of cortical cells. For the small spot stimuli modelled here the lack of a wide field stimulus is unlikely to activate such functionality.

2.4 The Primary Visual Cortex

Via the optic radiation, the LGN makes projections to the primary visual cortex (Bear et al. 2000, Callaway 1998, Hubel 1995, Kandel et al. 2000). The notion of a cortical area corresponding to primary visual cortex, often termed V1 or striate cortex, is relatively straight forward in primates, however, in the cat the issue is less clear cut. Whilst areas 17 and 18 in the cat have traditionally been equated with areas V1 and V2 in the monkey (Payne & Peters 2001), and consequently equating area 17 with primary visual cortex, there is a rationale for considering both area 17 and 18 within the scope of primary visual cortex (Payne & Peters 2001). As mentioned previously, the work

presented here uses the cat as a model for visual processing to comply with the in vivo data considered (Jancke 2000) and due to the significant amount of data available in the literature. However, within the scope of this exposition on the early visual pathway references are also made to the mammalian, and in particular primate, visual system. Thus the many terms for the primary visual cortex, e.g. striate cortex, V1, are often used herein, but with respect to the cat area 17 should be inferred.

Area 17 is notionally divided into 6 layers, as with primate V1, on the basis of the excitatory neuron population (Payne & Peters 2001) which in the main are either spiney stellate or pyramidal cells. Together they constitute approximately 80% of all cells, with the remaining 20% GABA-ergic inhibitory interneurons (Payne & Peters 2001, Peters & Yilmaz 1993). Layer 1 is sparsely populated solely by inhibitory neurons and is more characterised by neurite projections from deeper layers (Bear et al. 2000). The lack of a well defined boundary between layers 2 and 3 invariably leads to them being referred to together as layer 2/3. Excitatory cells in this layer are pyramidals whose soma size increases with depth. In contrast layer 4 excitatory neurons are predominantly spiney stellate cells with some pyramidal cells (Payne & Peters 2001, Peters & Payne 1993, Peters & Yilmaz 1993). Layer 4 is the primary recipient of thalamofugal efferents and can be further subdivided on the basis of innervations by LGN X and Y cells in the cat. Upper layer 4, layer 4a, receives input predominantly from LGN Y cells, and lower layer 4, layer 4b, from LGN X cells (Payne & Peters 2001, Peters & Payne 1993, Peters & Yilmaz 1993), although both X and Y streams are seen to make projections throughout layer 4 and lower layer 3 (Humphrey, Sur, Uhlrich & Sherman 1985, Lund, Henry, MacQueen & Harvey 1979, Payne & Peters 2001). In the primate layer 4 has different subdivisions giving rise to layers 4A, 4B, 4Cα and 4Cβ (Callaway 1998, Kandel et al. 2000). Layers 5 and 6 are both subdivided into a and b layers with all but layer 6b containing pyramidal cells (Payne & Peters 2001, Peters

& Payne 1993, Peters & Yilmaz 1993). In addition to the main innervations of layer 4 by X and Y LGN relay cells, both cell types also make projections to layer 6, with W cells of LGN laminae C1 and C2 project to layers 1, 3 and 5b (Lund et al. 1979, Payne & Peters 2001).

Perhaps one of the most salient features to emerge in the primary visual cortex is the elaboration on the basic centre surround receptive field structure observed in both retinal ganglion and lateral geniculate nucleus cells. In contrast to the receptive fields found earlier in the visual pathway, cells in the primary visual cortex tend to respond optimally to linear features such as bars and edges that are oriented according to their individual preference or orientation tuning (Bear et al. 2000, DeAngelis et al. 1995, Dayan & Abbott 2005, Hubel 1995). Such cells are further classified as either simple or complex. Simple cells have specific inhibitory and excitatory spatial regions within the receptive field whilst complex cells have no such subregions. The subregions of simple cells are elongated in order to facilitate orientation tuning (Ferster & Miller 2000, Jones & Palmer 1987, Mullikin, Jones & Palmer 1984). Thus a simple cell will respond more vigorously when a bar stimulus is correctly oriented over an excitatory region and is attenuated by similar stimulation of inhibitory subregions. Conversely, complex cells respond optimally to a correctly oriented stimulus swept across any part of the receptive field, and indeed often produce little or no response to a static stimulus. Unfortunately such descriptions do not uniquely differentiate the two classes of cells, rather exclusions seem to be a more useful method of identifying complex cells (Martinez & Alonso 2003). In addition, cortical receptive fields have a temporal component that reflects how cell activity develops over time in response to a stimulus. Receptive fields that can be represented as a product of their spatial and temporal functions are termed spatiotemporal separable receptive fields. Perhaps more interesting are the inseparable spatiotemporal receptive fields which indicate direction selectivity

(DeAngelis et al. 1995, Valois & Cottaris 1998, Valois et al. 2000, Livingstone 1998, Peterson et al. 2004). The precise mechanism underlying orientation tuning is still unresolved; the two main proposals favour either thalamocortical feedforward (all simple cells receive direct LGN input (Martinez & Alonso 2003)) or lateral recurrent models (Ferster & Miller 2000, Martinez & Alonso 2003).

In addition to orientation tuning, cells can have a number of other functional properties including spatial frequency (Issa, Trepel & Stryker 2000), reflecting the optimal stimulus width, directional selectivity or sensitivity to directed motion (Valois & Cottaris 1998, Valois et al. 2000, Livingstone 1998, Peterson et al. 2004) and ocular dominance which indicates from which eye visual information originated (Anderson, Olavarria & Sluyters 1988, Bear et al. 2000, Hubel 1995, Kandel et al. 2000, LeVay, Connolly, Houde & Essen 1985). As with the lateral geniculate nucleus, cells in the primary visual cortex also maintain a retinotopic map of visual space (Albus & Beckmann 1980, LeVay et al. 1985, Rosa, Schmid & Calford 1995, Tusa, Palmer & Rosenquist 1978) with the maps of all layers in register with one another. A further similarity is the biased retinotopic mapping of visual space towards the area centralis as can clearly be seen in Figure 6 of Tusa et al. (1978).

Simple cells seem to dominate layers receiving thalamic input, i.e. layers 4 and 6. Layers 2/3 and 5 appear to be populated by complex cells which are also present in layer 6 alongside simple cells (Martinez & Alonso 2003, Martinez, Wang, Reid, Pillai, Alonso & Sommer 2005). In layer 2/3 cells appear to be complex responding irregularly to flashing spot stimuli but more robustly to moving stimuli (Hirsch, Martinez, Alonso, Desai, Pillai & Pierre 2002, Martinez et al. 2005). In contrast layer 4 simple cells are equally well driven by flashed spots and moving bars (Hirsch et al. 2002). Such properties are also observed in layers 5 and 6 (Martinez et al. 2005) with cells of all three layers often tuned to a single stimulus polarity. Complex inhibitory cells

in layer 4 have are apparently not orientation selective. Hirsch et al. (2002) suggest that layer 4 to 2/3 differences arise from excitatory synaptic transmission and dendritic characteristics and not inhibition.

Unlike the LGN, the primary visual cortex also has a number of other maps that are related to the functional properties of cortical cells such as orientation tuning (Bear et al. 2000, Hubel 1995, Kandel et al. 2000), directional selectivity (Roerig & Kao 1999) and ocular dominance (Anderson et al. 1988, Bear et al. 2000, Hubel 1995, Kandel et al. 2000, LeVay et al. 1985). With regard the orientation tuning of cell in striate cortex, vertically aligned cells throughout the cortical layers display the same orientation preference leading to the notion of an orientation column (Bear et al. 2000, Hubel 1995, Kandel et al. 2000). Furthermore, the observed map is in general continuous with adjacent cells invariably having similar orientation preferences analogous to neighbouring cells representing adjacent points in the visual field. This leads to the oft mentioned "pinwheel" structures where the orientation tuning of cells varies smoothly in a circle around a central discontinuity. Similarly the notion of a hypercolumn is used to describe a region in the cortex where all orientations are represented and is often associated with pinwheels. Also observed in orientation maps are large areas of similarly oriented cells or iso-oriented domains.

In the cat, cytochrome oxidase (CO) blobs –neurons rich in cytochrome oxidase which is involved in cell metabolism– are found from upper layer 4, 4A, through the layer 3/4 boarder into lower layer 3 and are independent of ocular dominance columns unlike in the macaque (Payne & Peters 2001). In the monkey they are associated with monocular cells that are tuned for colour but not orientation, and have low spatial frequency preference (Kandel et al. 2000, Payne & Peters 2001), although these findings are not unequivocal (Sincich & Horton 2005). X cell innervations of layer 4B are independent of blobs, equally targeting the inter-blob space. Y cells from LGN lamina

C target the blobs as do W cells, but in layers 3. Intrinsic cortical connections strongly target blobs in the monkey yet this has not been observed in the cat.

Layer 1 connectivity in cat (Payne & Peters 2001) appears to be in common with other mammals in general (Thomson & Bannister 2003) as the cell population target invading dendrite of deeper layer cells. In addition to local connections, layer 2/3 pyramidal cells make extremely long range horizontal projections within the layer (Bosking et al. 1997, Buzás, Kovács, Ferecskó, Budd, Eysel & Kisvárday 2006, Gilbert, Das, Ito, Kapadia & Westheimer 1996, Hirsch & Gilbert 1991, Kisvárday et al. 1997, Sincich & Blasdel 2001, Tanigawa, Wang & Fujita 2005) and to layer 5 (Kandel et al. 2000, Lund et al. 1979, Payne & Peters 2001, Thomson & Bannister 2003). The major projections of layer 4A spiney stellate cells ascend to target layer 2/3 and descend to innervate layers 5 and 6 (Payne & Peters 2001). By comparison the axons of layer 4B cells predominantly descend to 6 with collaterals branching in layer 5 (Lund et al. 1979, Payne & Peters 2001). Collectively, the pyramidal cells of layers 5A and 5B make strong projections to layer 2/3 and 6 with layer 6A pyramidal axons ascending to layer 4 (Lund et al. 1979, Payne & Peters 2001). These data are largely corroborated by an extensive modelling study of cat primary visual cortex (Binzegger et al. 2004). Of particular note from the later is the preponderance of lateral connections observed in layer 2/3, whilst layers 4 and 6 also have a significant number of horizontal axon collaterals. On a cautionary note it would be unwise to draw too many conclusion based solely on the number of connections. In the case of the lateral geniculate nucleus, despite the numerical dominance of cortical projections from layer 6 over retinal input (Casagrande et al. 2005, Guillery & Sherman 2002, Sillito & Jones 2002), the two streams are proposed to assume modulation and driver roles respectively (Casagrande et al. 2005, Casagrande & Ichida 2002, Guillery 1995, Guillery & Sherman 2002, Sherman & Guillery 2002). Indeed, if numerical dominance were the sole criteria for

assigning functional roles then it might be hypothesised that the LGN and cortex have very different roles (Casagrande et al. 2005, Guillery & Sherman 2002). Furthermore, retinal EPSPs are relatively large (Sherman & Guillery 2002) perhaps in the same way that vertical projections in primary visual cortex generate larger EPSPs than horizontal connections (Martinez & Alonso 2003, Yoshimura, Sato, Imamura & Watanabe 2000) and LGN thalamocortical synapses are many times stronger than intercortical connections of layer 4 (Martinez & Alonso 2003), up to 5 times in rat (Ferster & Miller 2000). Indeed Sherman & Guillery (2002) draw comparisons between LGN relay cells and layer 4 cortical cells that are postsynaptic to the LGN where it is suggested that they contribute 35-46% of excitatory responses (see also Ferster & Miller (2000)).

Of particular interest to the work presented here is the extensive plexus of horizontal axon collaterals observed in layer 2/3. Long range lateral connections appear to be preferential for ocular dominance as projections in monocular regions favour monocular areas representing the same eye, whilst projections from binocular regions target binocular areas (Malach, Amir, Harel & Grinvald 1993) although it is not entirely clear if these data are exclusively from layer 2/3. Such projections are also tuned for orientation, and display a tendency to contact cells that have similar orientation selectivity (Bosking et al. 1997, Buzás et al. 2006, Kisvárday et al. 1997, Malach et al. 1993, Schmidt, Goebel, Löwel & Singer 1997, Sincich & Blasdel 2001). In conjunction, a number of observations have also indicated that such long range connections display anisotropies, with a bias towards projections made coaxially to the orientation preference of the presynaptic pyramidal cell (Bosking et al. 1997, Schmidt et al. 1997, Sincich & Blasdel 2001). The distribution of long range connections in macaque has been observed to display anisotropies (Malach et al. 1993, Tanigawa et al. 2005), however this has not been studied in conjunction with orientation preference, but was linked to ocular dominance (Malach et al. 1993) and suggested that when considered

with respect to the retinotopic map the distribution way appear more circular in the visual field. Interestingly the model of Buzás et al. (2006) does not appear to reflect any anisotropy in the long range lateral connections of the cat although long range connections do appear to deviate to some extent from coaxial alignment with orientation preference (Kisvárday et al. 1997, Schmidt et al. 1997). The long range connections made by layer 2/3 pyramidal cells within the layer appear to be mirrored by projections to layer 5 where axon collaterals are just as extensive and are also aligned below those in layer 2/3 (Gilbert & Wiesel 1983). In contrast to the long range connections in layer 2/3, local dendritic and axonal connections do not respect either orientation or ocular preferences and appear to form a uniform halo about the presynaptic cell (Bosking et al. 1997, Buzás et al. 2006, Kisvárday et al. 1997, Malach et al. 1993, Schmidt et al. 1997, Sincich & Blasdel 2001). Both the extent and anisotropic projection of pyramidal horizontal connections made to inhibitory cells is less clear. Observations of area 17 indicate that numerically, synapses with inhibitory cells are dwarfed by those with excitatory cells, and possible anisotropic projections are uncertain (Kisvárday et al. 1997). Modelling evidence based on anatomical data appears to contradict this, suggesting that excitatory connections with inhibitory cells are almost as numerous as those made between excitatory neurons (Binzegger et al. 2004). Such axonal projections do not appear to be exclusively the preserve of layer 2/3 as extensive clustered projections have been observed in all layers (Gilbert & Wiesel 1983) with a limited sample of layer 5 cells exhibiting axons co-aligned with orientation tuning.

As with retinal ganglion cells (Barlow & Levick 1969, Cleland et al. 1973, Kuffler et al. 1957) and neurons in the lateral geniculate nucleus (Levick & Williams 1964, Levine & Troy 1986), those in the primary visual cortex also display maintained discharge in the absence of an apparent stimulus (Arieli, Shoham, Hildesheim & Grinvald 1995, Arieli, Sterkin, Grinvald & Aertsen 1996, Sanseverino, Galletti & Maioli 1977,

Tsodyks et al. 1999). Firing rate of such activity is observed to vary both with cortical layer (Snodderly & Gur 1995) and putative excitatory/inhibitory cell type (Gibber, Chen & Roerig 2001).

Chapter 3

Computational Model

The model presented here represents a significant portion of the early visual pathway. Specifically, the retina and layers 4 and 2/3 from primary visual cortex are modelled however the lateral geniculate nucleus and layers 5 and 6 of primary visual cortex are not or only in a very simplistic manner. The recurrent nature of neural computation has already been emphasised with reference to the unique roles that may be played by LGN and layer 6, whilst the relationship of layer 5 to other striate layers has also been highlighted. In light of this and the premise of this thesis that feedback, rather than exclusively feedforward systems, are essential in the understanding of visual processing it may seem contradictory to adopt such selective modelling. However, this decision was motivated by two overriding factors; first incorporating complete models of the retina, lateral geniculate nucleus and six layers of V1 is in itself a significant task requiring considerable resources and as such is not within the remit of this thesis; secondly, as discussed in Section 2.3, for many of the experimental protocols modelled it is entirely feasibly that much of the specific functionality attributed to the LGN (Casagrande et al. 2005, Casagrande & Ichida 2002, Guillery 1995, Guillery & Sherman 2002, Sherman & Guillery 2002, Sillito & Jones 2002, Wörgötter et al. 2002) is not observed or is severely attenuated and consequently will not contribute to observations reported herein. Indeed, as a general observation, one of the most salient features of the brain is the interconnection between disparate areas; as such any modelling study must make, to some extent, the relatively arbitrary decision of those regions that are represented and those that are not.

A coarse grain modelling approach has been adopted with the primary visual cortex represented using a mean field model. The retina model is an implementation of work conducted by partners in the FACETS consortium (Wohrer, Kornprobst & Viéville 2006) that fits well within the mean field paradigm. In terms of implementation, the gross structure of retina and striate cortex does form a simple feedforward circuit with no feedback between the two. This has enabled a certain degree of independent modelling of the two systems, with the retina acting as a pre-processor of visual information before input into the primary visual cortex. Both describe the time dependent activity of retinal and cortical cells expressed as a series of ordinary differential equation that are numerically solved by Euler's method (Cheney & Kincaid 2003). Both retina and cortical models adhere to object oriented design methodologies (Booch 1993, Josuttis 2002) and are implemented in C++ (Josuttis 2002), with visualisation via a runtime interface with Matlab (Palm 2005).

3.1 Retina Model

The original INRIA retinal model (Wohrer et al. 2006) consists of four distinct processing stages that correspond to the functions of the combined photoreceptor and horizontal cells of the inner and outer nuclear layers, the bipolar cells of the inner nuclear layer, the amacrine cells populating the inner nuclear layer, and the retinal ganglion cells of the retinal cell layer. This gives a vertical view of how activity in the retinal laminae is emulated and may be thought of as a feedforward chain of three processes and a single feedback mechanism between bipolar and amacrine cells. As a result the convergence seen in the retina, such as photoreceptors to bipolar cells is not replicated. In this way, the model is similar in nature to a mean field model and certainly has a columnar structure. Thus from a lateral perspective, each layer is composed of a grid of cells each corresponding to spatial position, with all layers in spatial register. A gross

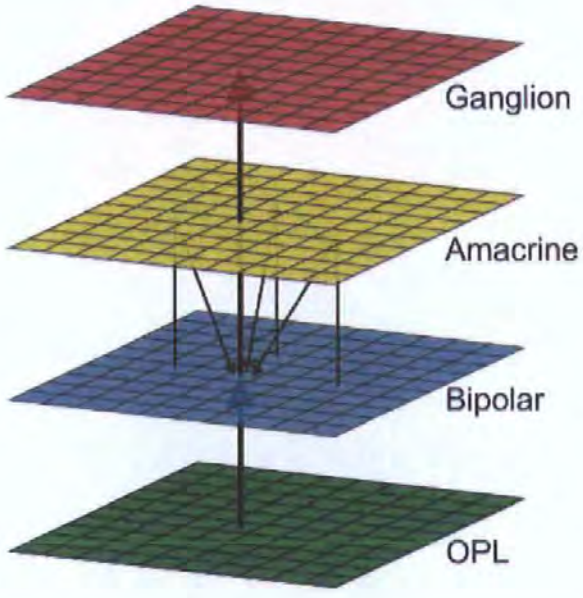

Figure 3.1: INRIA Retina Model Schematic. The model is comprised of four layers representing various anatomic laminae observed in the retina (Wohrer et al. 2006). The OPL layer combines inner and outer nuclear layers, whilst the remaining layers are self explanatory. Layers provide successive processing of a visual stimulus in a feedforward chain, with activity in the bipolar layer modulated by the amacrine layer which itself is driven by the bipolar layer. Each layer is a square point lattice representing cells of that type.

overview of the retinal model structure can be seen in Figure 3.1. As retinal ganglion cells effectively form the final tier in this hierarchical convergence they are used as a basis on which to parametrise spatial coordinates. In the cat retina the mosaic of beta ganglion cells exhibits characteristics of both square and hexagonal tiling (Wässle, Boycott & Illing 1981). Due in part to the coarse grain nature of the model and for the sake of simplicity, a square point lattice is used to specify the spatial location of cells in a given layer. It is then a simple matter to determine the minimum distance between retinal ganglion cells for a given distance from the area centralis using their density (Cleland et al. 1979, Peichl & Wässle 1979, Stein et al. 1996, Stone & Keens 1980, Wässle et al. 1981). Since visual space is normally specified in terms the angle

subtended on the retina (Hubel 1995), it is useful to convert the anatomical separation of cells, e.g. in μm, into degrees for comparison with the visual field. This is done simply by means of distance a given angle subtends on the retina (Barlow et al. 1957, Bishop, Kozak & Vakkur 1962, Crocker, Ringo, Wolbarsht & Wagner 1980, Kuffler et al. 1957, Peichl & Wässle 1979, Rodieck & Stone 1965, Stein et al. 1996, Vakkur & Bishop 1963).

In the original INRIA model initial processing of visual stimuli in the OPL captures the functionality of both photoreceptors and horizontal cells and thus effectively spans both inner and out nuclear layers of the retina (section 3.1.1 later considers separate cell types and especially more detailed receptor models). A simple antagonistic centre surround receptive field structure is modelled by two spatial Gaussian filters that have exponentially decaying temporal profiles. Thus temporal activity is defined by

$$OPL(x,y,t) = g(C(x,y,t) - S(x,y,t)) \tag{3.1}$$

and

$$\tau_{RF}\frac{dRF(x,y,t)}{dt} = -RF(x,y,t) + GF_{RF}(I(x,y,t)) \tag{3.2}$$

where

$OPL(x,y,t)$ is the activity of the OPL cell at position (x,y) and time t.

$C(x,y,t)$ is the activity of the centre cell at position (x,y) and time t.

$S(x,y,t)$ is the activity of the surround cell at position (x,y) and time t.

RF can take the value C or S representing centre or surround.

τ_{RF} is the time constant of cell type RF.

GF_{RF} is the Gaussian receptive field cell type RF.

$I(x,y,t)$ is the luminance of the visual stimulus at position (x,y) and time t.

g is a gain term for the output of the OPL layer.

Within this definition, the two spatial filters GF_C and GF_S are defined by the corresponding standard deviations, σ_c and σ_s, of each Gaussian function. Setting $\sigma_s > \sigma_c$ gives rise to the stereotypical centre surround receptive field.

From Figure 3.1 the output of each OPL layer cells feeds directly into the corresponding bipolar cell which also receives feedback from the amacrine layer. As with the centre and surround cells of the OPL layer, bipolar cells are characterised by a simple exponential function with definition

$$\frac{dB(x,y,t)}{dt} = -lB(x,y,t) + OPL(x,y,t) + kA(x,y,t)(E - B(x,y,t)) \tag{3.3}$$

and

$$\tau_A \frac{dA(x,y,t)}{dt} = -A(x,y,t) + GC_A(T(B(x,y,t),r)) \tag{3.4}$$

where

$B(x,y,t)$ is the activity of the bipolar cell at position (x,y) and time t.

$OPL(x,y,t)$ is the activity of the OPL cell at position (x,y) and time t.

$A(x,y,t)$ is the activity of the amacrine cell at position (x,y) and time t.

E is the reversal potential associated with amacrine cell inhibitory feedback.

l is a leak conductance of the bipolar cells.

k is a gain term for the output of the amacrine layer.

τ_A is the time constant of amacrine cells.

GC_A is the Gaussian connectivity pattern from bipolar to amacrine cells.

$T(x,r)$ is a transfer function representing the synaptic input from bipolar to amacrine cells.

r is a threshold for the transfer function.

The connectivity pattern GC_A is parametrised by the standard deviation σ_A which determines the spatial extent over which the amacrine cells sample the bipolar layer. The transfer function $T(x,r)$ is given by

$$T(x,r) = R(x,r) + R(-x,r) \tag{3.5}$$

and

$$R(x,r) = \begin{cases} 0 & : \quad x < r \\ x - r & : \quad x \geq r \end{cases} \tag{3.6}$$

where

$R(x,r)$ represents synaptic transmission to a presynaptic cell.

r is a threshold for the transmission function R.

The definition of the transfer function is selected such that amacrine cell feedback is driven by both contrast polarities, that is bipolar input from both ON and OFF cells is captured by the terms x and $-x$, respectively.

The final ganglion cell layer models the output of retinal ganglion cells as a firing rate rather than individual spikes. The activity of each bipolar cell is rectified and high pass filtered to determine the firing rate of the corresponding retinal ganglion cell and is defined by

$$F(x,y,t) = h(R(B(x,y,t),p) - wG(x,y,t)) \tag{3.7}$$

and

$$\tau_G \frac{dG(x,y,t)}{dt} = -G(x,y,t) + R(B(x,y,t),p) \tag{3.8}$$

where

$F(x,y,t)$ is the firing rate of the ganglion cell at position (x, y) and time t.

$B(x,y,t)$ is the activity of the bipolar cell at position (x, y) and time t given by equation (3.3).

$G(x,y,t)$ is the low-pass filtered bipolar cell activity at position (x, y) and time t.

$R(x,r)$ is the rectification function representing bipolar cell output and is defined as in equation (3.6).

p is a threshold at which bipolar cells produce an output.

w is the relative weighting of high and low pass terms.

τ_G is the time constant of ganglion cells.

h is a gain term for the output of the ganglion layer.

Of interest is the use of a threshold in equations (3.7) and (3.8) for the output of the bipolar layer as these cells, along with photoreceptors and horizontal cells, produce a continuous graded change of membrane potential in response to stimuli as opposed to the spiking output of ganglion cells (Dayan & Abbott 2005).

As discussed in Section 2.2, the retina is populated by morphologically identified cell types α, β and γ which in turn correspond to the physiological distinct Y, X and W cell types, each of which may be designated either ON or OFF dependent on receptive field structure. Beta cells have the characteristics of high special resolution and sustained response to visual stimuli, and are the more numerous cell type (Cohen &

Sterling 1992, Peichl & Wässle 1979, Stein et al. 1996, Wässle et al. 1981). For these reasons they are taken as a prototype for parameterising the retina model. However, a later incarnation of the model contains, both, X and Y cells, cf., section 3.1.4. The results in section 4.2.1 and section 5 Figure 5.1 use both cell types, whereas results in section 4.1 only use X cells.

Since ON and OFF β cells form two independent populations within the retina (Wässle et al. 1981), the retinal model as illustrated in Figure 3.1 represents the processing pathway of a single β cell type, either ON or OFF, and is duplicated for the complementary population of β cells but with equation (3.1) rewritten as $OPL(x,y,t) = g(S(x,y,t) - C(x,y,t))$. With this qualification for retinal ganglion cell type it is possible to stipulate a generic receptive field width from experimental data (Cleland et al. 1979, Peichl & Wässle 1979, Rodieck 1965, Rodieck & Stone 1965). As with the majority of model parameters it is acknowledged that they can be expected to vary over a specific range, however a single value is often used for simplicity and also in keeping with the mean field approach adopted herein.

3.1.1 Photoreceptor Preprocessing

The original INRIA model lumps photoreceptors and horizontal into a single outer plexiform layer (Wohrer et al. 2006). This section considers more detailed implementations of photoreceptors.

Even at the most fundamental level the retina of vertebrae exhibits light adaptation. Whilst initial evidence suggested that light adaptation did not take place in the mammalian photoreceptor system (Shapley & C. Enroth-Cugell 1984, Steinberg 1971), this is contradicted by studies of cones in the primate (Valeton & Norren 1983) and rods in the cat (Tamura, Nakatani & Yau 1989) and other mammals (Nakatani, Tamura & Yau 1991). Light adaptation in the rod system can manifest itself in a number of ways,

including variation in the time to peak response, relaxation of initial peak response, or reduction in stimulus sensitivity in the presence of adapting background luminance (Nakatani et al. 1991). The first two of these characteristics are also observed in the response behaviour of ganglion cells (Levick & Zacks 1970). Variation in response latency and peak output adaptation do not readily lend themselves to inclusion in the retinal model adopted here (Wohrer et al. 2006). However, reduction in stimulus sensitivity in the presence of an adapting background luminance is more amenable to implementation as part of the retinal model. The rod photocurrent model presented here is based on observations made in the cat and other mammals (Tamura et al. 1989, Nakatani et al. 1991). The rod system is considered as the stimuli used in Jancke (2000) fall within the range of scotopic vision (Grand 1968).

The normalised response data from Tamura et al. (1989) is presented in Figure 3.2 and fitted using the adapted Michaelis-Menten equation of Valeton & Norren (1983) (called Naka-Rushton function in Shapley & C. Enroth-Cugell (1984)) which allows control of the response slope and has the form

$$r = \frac{1}{1 + \left(\frac{\sigma}{I}\right)^n} \tag{3.9}$$

where

r is the normalised response.

I is the stimulus luminance in photons $\mu m^{-2}\ s^{-1}$ at 500nm.

n controls the steepness of the response curve.

σ is the half saturation of the response curve.

The response data is first transformed by $y = \log(1/r - 1)$ and $x = \log(I)$ in order to allow a linear fit of the form $y = mx + c$, to give $n = -m$ and $c = nlog(\sigma)$. As such

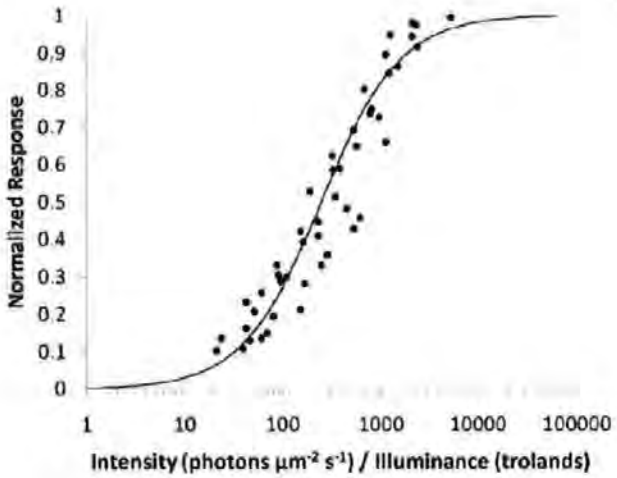

Figure 3.2: Normalised luminance response for isolated cat rod. The normalised response of seven isolated rods is plotted against light intensity at 500nm. The fitted curve is of the form $r = (1 + (\frac{\sigma}{I})^n)^{-1}$.

data taken from Figure 3.2 where $r = 1$ is not included in the fit which gives values of $\sigma \approx 247$ and $n \approx 1.0778$. The curve appears to provide a reasonable fit to the data over the majority of data points. Whilst it does not appear to saturate as quickly as the experimental data suggests, the actual saturation figure reported by (Tamura et al. 1989) is approximately 11400 photons $\mu m^{-2}\ s^{-1}$.

Tamura et al. (1989) determined the flash intensity, S_F^D necessary to elicit a just detectable response in a dark adapted rod. For rods adapted to different background intensities they determined the intensity of a superimposed flash necessary to also elicit a just detectable response, S_F. These two quantities are related by

$$\frac{S_F}{S_F^D} = \frac{1}{1 + \frac{I_S}{I_D}} \tag{3.10}$$

where

S_F^D is the sensitivity to a flashed stimulus with no background luminance. It is given

by r^D/I^D where I^D is a flashed stimulus of 6.51 photons μm^{-2} and r_D is the resultant peak response of 1.35 pA.

S_F is the sensitivity to a flashed stimulus with background luminance.

I_0 is a constant with value of 100 photons μm^{-2} s^{-1} at 500nm.

I_S is the background luminance in photons μm^{-2} s^{-1} at 500nm.

For the model proposed here taking the sensitivity as $S_F = dr/dI$ the resultant relationship is given by differentiating equation (3.9)

$$\frac{dr}{dI} = \frac{cn}{I^{n+1}(1+\frac{\sigma^n}{I^n})^2} \tag{3.11}$$

Normalising with respect to the model definition to give the normalised sensitivity gives

$$\frac{S_F}{S_F^D} = \frac{cn}{I^{n+1}(1+\frac{\sigma^n}{I^n})^2}\frac{I_D^n+\sigma^n}{I_D^n} \tag{3.12}$$

where I_D is the luminance used to determine sensitivity with no adapting background luminance. From (Tamura et al. 1989) this is set to 6.51 photons μm^{-2}. From their figure 1A, the rod response plateaus well before 1 second. Thus for a luminance of 6.51 photons μm^{-2} s^{-1} and assuming a duration of 1 second will result in a stimulus of 6.51 photons μm^{-2}, the normalised response which is given by equation (3.9). Clearly different combinations of luminance and duration may result in a stimulus of 6.51 photons μm^{-2} but potentially a different normalised response. Levick & Zacks (1970) observe that for equal energy stimuli, i.e. where the product of luminance and duration are equal, response amplitude is constant for durations up to 32ms beyond which it begins to decline. For such short durations Tamura et al. (1989) observe that the rod response has not reached its peak and consequently neither has the normalised response predicted by the model of equation (3.9). For durations up to at least 150ms

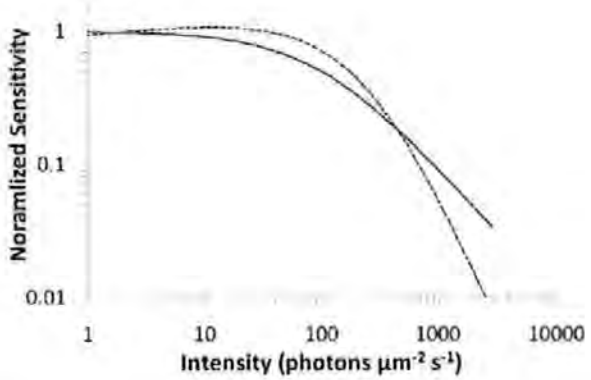

Figure 3.3: Sensitivity of response to background luminance. Sensitivity of responses to flashed stimuli at different levels of background luminance is normalised by the sensitivity in the absence of background luminance. The solid line shows the sensitivity observed experimentally by Tamura et al. (1989) whilst the dashed line shows the sensitivity derived from the proposed model.

equation (3.9) overestimates the rod response. Consequently equation (3.12) represents an underestimate, as the term $\frac{I_D^n+\sigma^n}{I_D^n}$ will be smaller than the experimentally observed value for D_F^D. The resultant relationship is given in Figure 3.3 where the solid line gives the relationship of equation (3.10), and the dotted line equation (3.12).

In attempting to use this model to fit the complete retinal model to the experimental data of Sakmann & Creutzfeldt (1969) problems arose over the range of background luminances used. Furthermore, the model does not incorporate any adaptation with background luminance. In an attempt to address this issue the basic equation (3.9) was modified. This adaptation was guided by the change in response sensitivity observed experimentally and illustrated in Figure 3.3. Several possibilities are immediately apparent:

1. Use a single intensity/response function curve and simply rescale stimulus intensities, dependent on background intensity, to a range commensurate with a background intensity of 0. This is similar to the curve shifting of (Valeton &

Norren 1983) where a prototype response curve is shifted according to the adapting background luminance. Whilst this would aid replication of the curves of figure 8 in (Sakmann & Creutzfeldt 1969) it would not utilise any of the feedback mechanisms in the INRIA model which would become largely redundant. Furthermore at different background levels, contrast gain results would result from the same contrast value and would not exhibit the nonlinearity observed by Enroth-Cugell & Robson (1966), amongst others.

2. Make n a function of background intensity I_B with the half saturation point remaining the same. In general this would require n decreasing as a function of I_B. This would mean that for $I > \sigma$, the response function would decrease relative to that for $I_B = 0$ as require, but would *increase* for $I < \sigma$.

3. Make n a function of background intensity I_B with $\sigma^n = \sigma^{n_0}$ where n_0 is the value of n for $I_B = 0$, i.e. when there is no background luminance. Hence the term σ^n becomes a constant with the result that for values of I greater than 1 the response decreases with increasing background luminance. Whilst for $I < 1$ the response will *increase*, proportionally this is negligible. Thus equation (3.9) becomes

$$r = \frac{1}{1 + \frac{c}{I^n}} \tag{3.13}$$

The later solution is adopted which requires determining a function of I, $f(I) = n$, to minimise

$$g(t) = \left(\frac{1}{1 + \frac{I_S}{I_D}} - \frac{cn}{I^{n+1}(1 + \frac{\sigma^n}{I^n})^2} \frac{I_D^n + \sigma^n}{I_D^n} \right)^2 \tag{3.14}$$

For lower values of background luminance n can be found such that $g(t) = 0$. For background a luminance of 1000 photons μm^{-2} s^{-1} the minimum must be found,

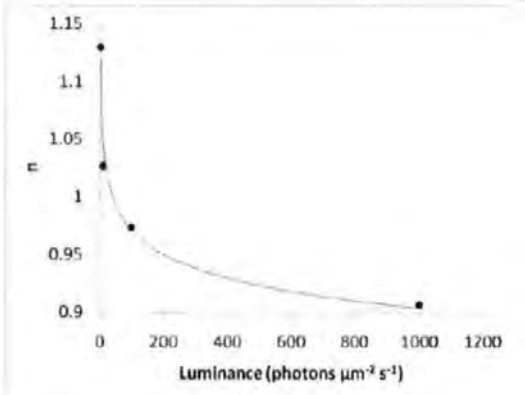

Figure 3.4: Exponent values to produce experimental sensitivity. The filled circles show the values of n that minimise equation (3.14) and thus produce sensitivities in equation (3.13) that match experimentally observed values.

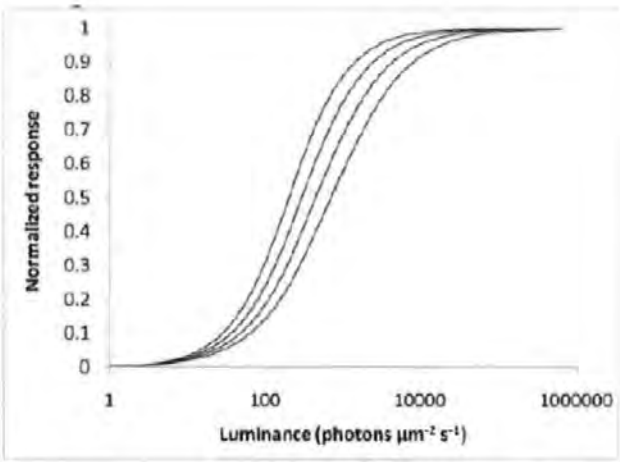

Figure 3.5: Response sensitivity for different background luminance values. The curves from left to right show the normalised response at background luminance values of 1, 10, 100 and 1000 photons $\mu\text{m}^{-2}\ \text{s}^{-1}$

whilst further increasing the background luminance results in an increase in this minimum as the two curves diverge. Setting $c = \sigma^{n_0} = 247^{1.0778} \approx 379$ and solving graphically gives the results of Figure 3.4 which shows a fit to the data by $n = 1.12I^{-0.031}$.

Response curves at different luminance values can be seen in Figure 3.5. From left to right the curves shown the response at the four background luminance values of 1, 10, 100 and 1000 photons $\mu m^{-2}\, s^{-1}$.

3.1.2 Parameters of the Retina Model

The retinal model was parameterized where possible with data taken from the literature (Rodieck 1965, Rodieck & Stone 1965, Cleland et al. 1979, Peichl & Wässle 1979, Lankheet, Rowe, Wezel & van de Grind 1996, O'Brien et al. 2002, Kenyon, Moore, Jeffs, Denning, Stephens, Travis, George, Theiler & Marshak 2003, Wohrer et al. 2006).

Centre and surround filter sizes of OPL cells were based on ganglion cell data (Rodieck & Stone 1965, Peichl & Wässle 1979) since only amacrine cells provide any lateral integration of information, and this is purely for inhibitory feedback. The parameters σ_C and σ_S, controlling the centre and surround filters, were adjusted such that the receptive field centre of X and Y cells had diameters of 0.5° and 1.15° given that $\sigma_S = 3\sigma_C$ (Rodieck 1965). Both centre and surround filters are two dimensional Gaussian functions of the form

$$R = Ae^{-\frac{x^2+y^2}{2\sigma^2}}. \tag{3.15}$$

The function is normalized by, A, such that the response, R, is in the range $[0,1]$. The spatial extent of the filter over retinal positions (x,y) is determined by σ. In an ideal case where a filter extends infinitely in x and y directions, the normalization term

is given by

$$A = \frac{1}{2\pi\sigma^2} . \tag{3.16}$$

To ensure that the centre and surround filters combine to give a receptive field centre diameter of d, by virtue of their radial symmetry, let $y = 0$, and $x = d/2$, to give

$$\frac{1}{2\pi\sigma_c^2} e^{-\frac{x^2}{2\sigma_c^2}} = \frac{w}{2\pi\sigma_s^2} e^{-\frac{x^2}{2\sigma_s^2}} , \tag{3.17}$$

where σ_c and σ_s control the spatial extent of centre and surround filters respectively, and w determines their relative contribution. For a given ratio of centre and surround filters given by $\sigma_s = r\sigma_c$:

$$\frac{1}{2\pi\sigma^2} e^{-\frac{x^2}{2\sigma^2}} = \frac{w}{2\pi(r\sigma)^2} e^{-\frac{x^2}{2(r\sigma)^2}} \tag{3.18}$$

and therefore

$$\sigma = x \sqrt{\frac{1 - \frac{1}{r^2}}{2\ln\left(\frac{r^2}{w}\right)}} , \tag{3.19}$$

where σ controls the spatial extent of the centre filter. Within the model the convention is adopted that the maximum extent of a dendritic field is three times the spatial extent parameter σ. This convention was adopted to limit computational costs and reflect spatial limits of dendritic fields. Selecting a maximum extent of 3σ, input at the extremities of the dendritic field was approximately 0.01 of the maximum.

Time constants for OPL, centre cells, OPL surround cells, bipolar cells and amacrine cells were set to 10ms, 20ms, 10ms and 10ms respectively. Ganglion X and Y cells had passive membrane time constants of 25ms and 4.5ms, although as noted by O'Brien et al. (2002) the passive membrane time constant for Y cells may be even smaller which would further emphasise the temporal resolving power of Y cells as modelled here. Amacrine cells receive filtered input of the bipolar layer. Amacrine cells are identified

as narrow, small, medium and wide field dependent on the spatial extent of their dendritic arbour (Kolb et al. 1981, Masland 2001). The receptive field of model amacrine cells is assumed to be wide as this provides a feedback that integrates both narrow and wide field cells. However, if narrow, small, medium and wide field amacrines all contribute to the feedback mechanism it is possible that a bias will be seen for more proximal parts of the combined receptive field. In the cat retina wide-field amacrines have dendritic fields that extend between 500 and $1000\mu m$ from the soma (Kolb et al. 1981). Values of σ for Gaussian representations of amacrine dendritic fields from modelling studies range from 0.5° (Hennig, Funke & Wörgötter 2002) to 3° (Wohrer et al. 2006). If the spatial limits of the dendritic field are assumed to by 3σ as discussed earlier, this would suggest a value of $\sigma = 250\mu m$ or 1.1° (assuming 226μm in the retina represent 1° of visual space), given an average field diameter of 1500μm. Figure 3.6 shows the spatial extent of amacrine dendritic fields for these different values of σ. The solid line results from $\sigma = 1.1°$ as adopted here and is in good agreement with the observations of Kolb et al. (1981) for wide field amacrine cells. The remaining parameters were taken from the initial presentation of the retina model by Wohrer et al. (2006).

Within the area centralis Cleland et al. (1973) observe of 88 recorded cells 50% ON X-cells, 30% OFF X-cells, 3.4% ON Y-cells, and 5.7% OFF Y-cells. Conversely for X and Y cells, ON and OFF proportions of 48% and 52% were observed by Wässle et al. (1981). Across the retina Wässle et al. (1981) observe X, Y and W cell proportions as 55%, 4% and 41% respectively. They also estimate ON and OFF X cells to be separated by approximately 21 and 19 μm, whilst ON and OFF Y cells would be 107μm apart. Using their figure of 226μm to 1°, ON and OFF X cell separation is $\approx$0.09° and $\approx$0.47° for ON and OFF Y cells. The authors also observe that the mosaic of cells exhibits both square and hexagonal tiling characteristics (Wässle et al. 1981). For simplicity a square lattice is adopted. Peichl & Wässle (1979) observe a

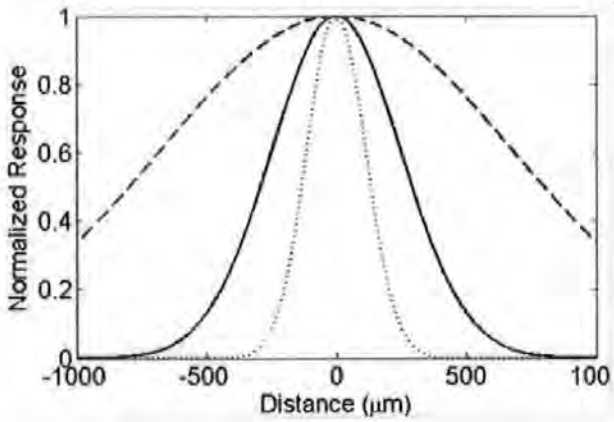

Figure 3.6: Comparison of amacrine dendritic fields. The spatial extent of amacrine dendritic fields represented by a Gaussian function is shown for different values of σ. The dotted and dashed lines indicate dendritic fileds assuming $\sigma = 0.5°$ and 3° respectively. The solid line shows the spatial extent for $\sigma = 1.1°$ as used here and is in good accordance with observations in the cat for wide field amacrine cells (Kolb et al. 1981).

combined ON and OFF X cell density of 6500/mm^2 in the area centralis and 200/mm^2 for ON and OFF Y cells. This later figure is in general agreement with others (Stone 1978). Stein et al. (1996) propose X cell densities as high as 7000/mm^2. Using a ratio of 10:1 for X to Y cells in the area centralis (derived from (Cleland et al. 1973)) the suggested figure of Stein et al. (1996) would give a Y cell density of 700/mm^2. Assuming a square lattice and no difference in cell densities between ON and OFF cells, the distance between X ON or OFF cells would be in the range 16.9 - 17.5μm and for Y cells the range would be 53 - 100μm. In terms of degrees of visual field X and Y cells would be separated by 0.075 - 0.078° and 0.24 - 0.44°, using a figure of 1° to 225μm (Barlow et al. 1957, Kuffler et al. 1957, Bishop et al. 1962, Vakkur & Bishop 1963, Rodieck & Stone 1965, Peichl & Wässle 1979, Crocker et al. 1980, Stein et al. 1996). These figures are consistently lower than those of Wässle et al. (1981). This is due predominantly to the high density suggested by Stein et al. (1996). Even using the Y proportion of Wässle et al. (1981), the figure of Stein leads to a distance of

0.28° between cells. For X cells Stein et al. (1996) suggests 7000 cells per mm^2 at the area centralis dropping to ≈3000 cells per mm^2 at 1mm eccentricity. Using an average figure of 5000 cells per mm^2 for a give type, ON or OFF, this translates to $\sqrt{2500} = 50$ cells per mm, or $50/1000 = 0.05$ cells per μm or $0.05 \times 225 = 11.25$ cells per degree of visual space. For the resolution of 0.1 degree used in the model, X ganglion cells sample the space every ≈1 model cells. Similarly, assuming an X to Y cell ratio of 55:4, gives the distance between Y cells as ≈0.33°.

From the above, the 0.1° spatial resolution of the model is greater than the spatial separation of ON and OFF X cells and so each model cell corresponds to one or more X cells as per a mean field approach. However, ON and OFF Y cell density is less, with cells separated by 0.4° in the model. This is greater than the spatial resolution of 0.1° invariably used in the model which is not changed when simulating X or Y cells. However, the preceding argument refers to ganglion cell densities only. Cell densities in the other retinal layers, OPL, bipolar and amacrine, has not been investigated in the current literature survey. Indeed the distinction of cells in these layers appears to focus on their role in cone or rod circuits. As such cell densities of OPL, bipolar and amacrine cells are assumed to be the same when simulating X and Y cells. A simulation of Y cells using a spatial resolution of 0.1° will then over-represent the number of ganglion cells. To solve this problem the population of ganglion cells is subsampled by cortical cells at a resolution suggested by the above argument, currently 0.4 degrees.

Both ON and OFF centre cells are modelled.

3.1.3 Further Calibration of the Retina Model

Many parameters of the retina model were fixed by values from the experimental literature, section 3.1.2. However, the retinal model still contains six free parameters whose values require determining as detailed in Table 3.1. Calibration of these parameters

Parameter	Location	Description
g	OPL layer	Gain term for the output of the OPL layer.
r	Bipolar layer	Threshold for the transfer function from bipolar cells to amacrine cells.
k	Amacrine layer	Gain term for output of the amacrine layer.
p	Ganglion layer	Threshold for transfer function from bipolar cells to ganglion cells.
w	Ganglion layer	The relative weighting of the high and low pass terms.
h	Ganglion layer	Gain term for the output of the ganglion layer.

Table 3.1: Retinal model free parameters. Where possible parameters for the retinal model have been taken from the literature. However certain parameters, in particular gain values are not readily available from experimental data. These free parameters are listed here.

was conducted against experimental data by extensive fitting. Given the wealth of experimental data available in the literature, it was decided to select that most applicable to the data being modelled (Jancke 2000). A study by Sakmann & Creutzfeldt (1969) recorded the response of retinal ganglion cells to flashed spots at various luminance values against uniform backgrounds and also of different luminance values. Note that a potential shortcoming is that the selected calibration stimuli are static and do not reflect the moving stimuli of Jancke (2000). Furthermore, similar stimuli used by Levick & Zacks (1970) produced significantly higher firing rates.

The data presented by Sakmann & Creutzfeldt (1969) is given in terms of candela per square metre (cd/m^2) (Wyszecki & Stiles 1967), whilst the photoreceptor model presented above is in terms of photons μm^{-2} s^{-1}. To provide comparison between the two, and other experimental data, values are often converted to trolands (Wyszecki & Stiles 1967). At 507nm 4.46 $\times$ 10^5 quanta degree^{-2} s^{-1} is equivalent to 1 troland (Lennie, Hertz & Enroth-Cugell 1976, Shapley & C. Enroth-Cugell 1984) whilst in the cat 1 degree^2 is equal to 4.8 $\times$ $10^{-4}cm^2$ (Shapley & C. Enroth-Cugell 1984).

Hence in the cat 1 troland is equal to ≈ 9.3 photons μm^{-2} s^{-1}, it should be noted that there is a slight discrepancy in that the data generated by Tamura et al. (1989) results from stimuli with wavelength 500nm as compared to 507nm. From Tamura et al. (1989) saturation of rods occurs at approximately 4000 Rh^* s^{-1} (rhodospin photoisomerizations per second) which is equivalent to $\approx$ 11400 photons μm^{-2} s^{-1} given a collect area of $0.35\mu m^2$ (given that Rh^* s^{-1} = collecting area $\times$ photons μm^{-2} s^{-1}), or $11400/9.3 \approx 3.1$ log trolands. These figures compare favourably with those of Steinberg (1971) where saturation in two separate cases occurs at approximately 3.25 and 3.35 log trolands. Whilst they are relatively high in comparison to saturation values suggested by Lennie et al. (1976), the criteria adopted by the later is possibly more lenient.

The data presented in figure 8 of Sakmann & Creutzfeldt (1969) for background luminance values of 0.00001, 0.0001, 0.001, 0.01 cd/m^2 were used to calibrate the model. Whilst it is acknowledged that these potentially represent very high firing rates (the slope of the response curves were the highest observed) they are the most complete set of data presented. Furthermore, the specific ratio of stimulus size to receptive field size is not specified; consequently, parameters were determined for a range of ratios. Parameters were fit using a microbial genetic algorithm (Harvey 2001) with a crossover probability of 0.5 and mutation probability of 0.25. Mutation values were taken from a normal distribution N(0, 0.01). For most runs of the genetic algorithm populations of between 60 and 100 genotypes were evolved over 1000 generations. The difference in population size appeared to make no discernable difference in the resultant fitness values. The fitness function, f, was given by

$$f = \frac{1}{n}\sum_{i=1}^{n} a_i b_i (e_i - m_i)^2 \tag{3.20}$$

where

n is the number of spot and background combinations used to calibrate the model.

e_i is the firing rate observed by Sakmann & Creutzfeldt (1969) for the ith spot/background combination.

m_i is the firing rate produced by the model for the ith data point, i.e., spot/background combination.

a_i penalises excessive firing rates by setting $a_i = 4$ when $m_i > e_i$ and $a_i = 1$ when $m_i \leq e_i$.

b_i weights the importance of the ith spot/background combination.

The factors, a_i, were used in an attempt to encourage parameters that produced firing rates below the experimental data as these were potentially excessively high as mentioned above.

From the observation of Sakmann & Creutzfeldt (1969) that the response curves appear to have the same slope but shifted half saturation point, the data from their figure 8 was shifted so that all curves coincided with that of the response for a background luminance of -5 log cd/m^2. This data was then fit by a function of the form $r = (1 + c/I^n)^{-1}$ where r is the normalised response assuming a peak spike rate of 350Hz. To produce an estimate of the average response, the fitted curve was then shifted back and the slope adjusted to coincide with the average value of 180 as observed by Sakmann & Creutzfeldt (1969). Note that from the fit to the combined data the slope was 279 which is higher than the average value of 234 from Table 1 in Sakmann & Creutzfeldt (1969). Also the constant c was not changed to keep the half saturation point the same. These estimated fits are potentially erroneous in that they simply adjust the slope to coincide with that of the observed average and do not take into account how the half

saturation is a function of background luminance. Thus they may not be reliable as reference points.

In an attempt to produce a more accurate fit to the experimental data, the two parameters used to fit the curve of Figure 3.4 were added to the parameters set with mutation probability increased to 0.5. This did produce more accurate fits to the data however the resultant rod response curves were not realistic. For background luminance values of -2 log cd/m^2, saturation occurred for stimuli towards 8 log cd/m^2. Consequently this approach was not pursued and the original fit of Figure 3.4 was used. Evolving parameters that closely fit the calibration data was not possible. It is entirely possible that a solution exists but the genetic algorithm was unable to find it. Despite several attempts and increasing the number of generations a close fit was not obtained. One feature of note was that all the genotypes in a given final population were quantitatively very similar as is illustrated by Figure 3.7 which shows the parameters evolved when the maintained rate was not included. Graphs A – D represent the results for stimulus diameters of 0.2 – 0.5 degrees and each plots 70 parameter sets. Clearly there is very little variation in the range of values of each parameter in the final population. Similar results were observed when the maintained firing was included in the evolutionary process. This suggests that at this point mutation becomes the driving force of the algorithm. Why such a "cloned" population emerges is unclear; it may be because there are few or no local maxima or the global maximum is very dominant or easily accessible; alternatively it may be that the small genotype allows the fittest individual to dominate the gene pool through crossover. Given the earlier observation that over many different runs of the genetic algorithm the resultant populations appear similar for different conditions suggests that one particular maximum, global or local, dominates the fitness landscape.

Also of note was that for different evolutionary runs, different ratios of stimulus

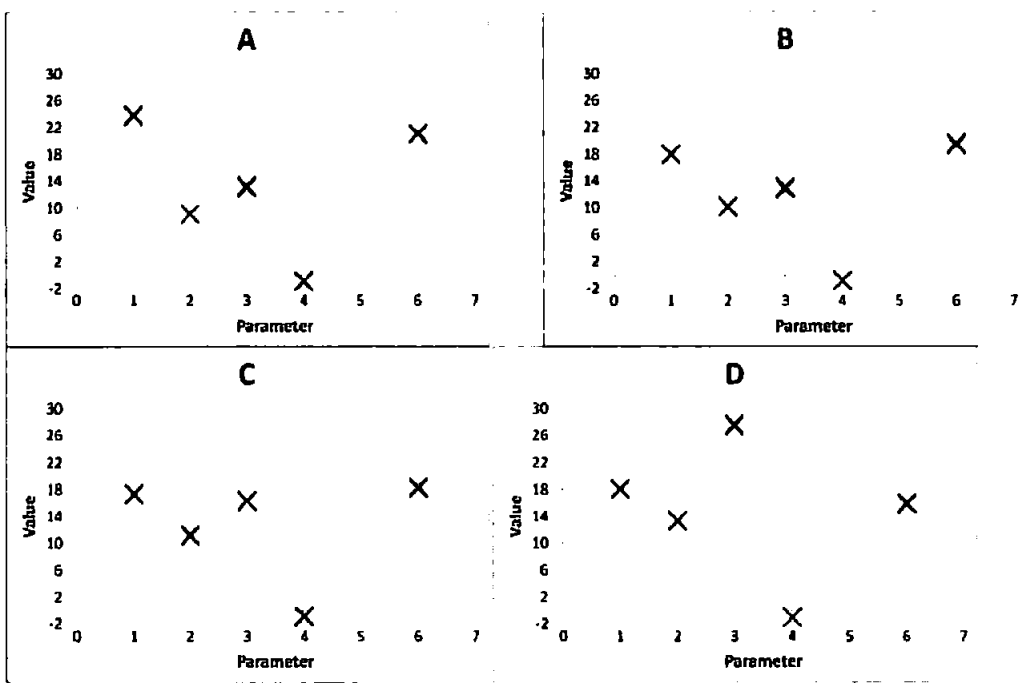

Figure 3.7: Variation in evolved parameter set. Each of the four graphs plot the final population of 70 parameter sets evolved over 1000 generations. Graphs A – D were evolved for stimulus diameters of 0.2 – 0.5 degrees. The small variation in each final parameter over the entire population gives the appearance of each graph plotting only 5 distinct points rather than 350.

Stimulus diameters	Maintained firing	No Maintained Firing
0.2 / 0.3	0.975	0.973
0.2 / 0.4	0.933	0.927
0.2 / 0.5	0.722	0.670
0.3 / 0.4	0.983	0.975
0.3 / 0.5	0.800	0.737
0.4 / 0.5	0.893	0.867

Table 3.2: Comparison of correlation coefficients for fittest parameter sets. Rows show the correlation coefficient between the fittest parameter set for the two stimulus diameters of column 1. Columns 2 and 3 show the correlation coefficients when maintained firing rate was included and excluded from the evolutionary process.

spot diameter to receptive field diameter produced qualitatively similar results. The range of each parameter value was similar for different ratios and different evolutionary runs. For the fittest member of each final population correlation coefficients were calculated and presented in Table 3.2. All the parameter sets show a close correlation, particularly so for those generated for closer stimulus diameters.

Applying the parameters evolved without maintained firing rates on large 1.5degree per side square stimuli as used by Jancke in the unpublished data but with other experimental parameters as in Jancke (2000) produced similar firing rates of the order 220Hz, for parameters based on Sakmann & Creutzfeldt (1969) stimuli of diameter 0.3 – 0.5 degrees. For the 0.2 degree diameter stimuli the simulation becomes very sensitive to the integration step with the ganglion response decaying towards zero.

It was decided to use a parameter set that best fit the data for a background luminance of -4 log cd/m^2 as this is closest to that used in Jancke (2000). The data presented by Sakmann & Creutzfeldt (1969) does not include the maintained firing rate. Parameterising the retina model then presents two options, fit the data as presented or include the maintained firing rates and thus represent maintained firing in the retinal model.

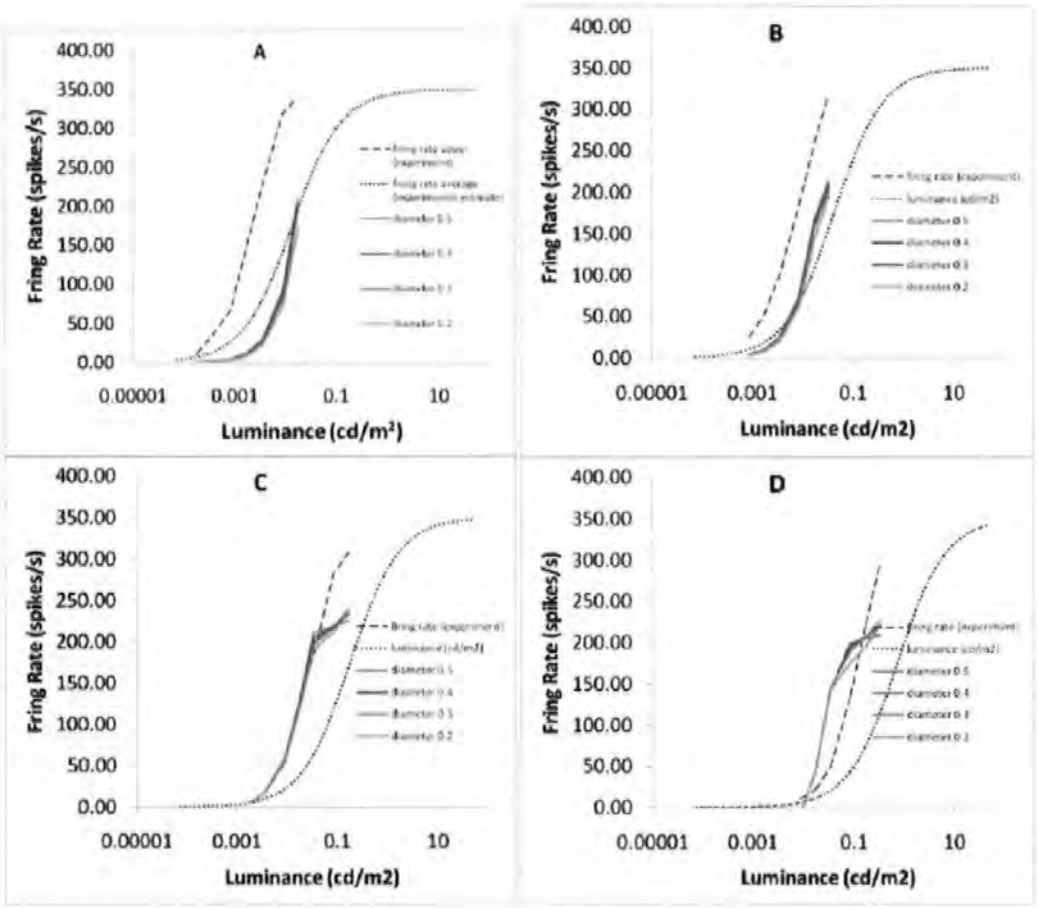

Figure 3.8: Retina model luminance response curves. Graphs A – D show the output of the retinal model for background luminance levels of -5, -4, -3 and -2 log cd/m^2. For each graph the response of stimulus diameters 0.5, 0.4, 0.3 and 0.2 degrees are shown (the receptive field centre diameter is 0.5 degrees). The dashed curves show the data as taken from Figure 8 of (Sakmann & Creutzfeldt 1969) whilst the dotted lines show the estimated average response.

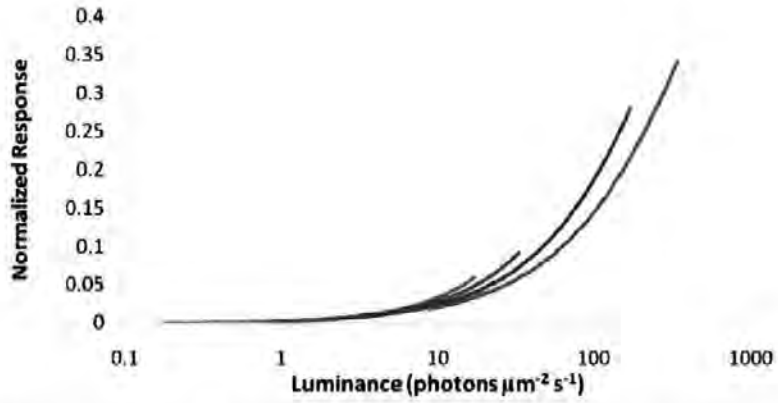

Figure 3.9: Response range for calibrating data. The luminance range and corresponding normalised response for each of the four background luminance values are shown. The red, green, purple and cyan curves show the luminance and response range for stimuli represented against backgrounds of -5, -4, -3 and -2 log cd/m^2.

Both approaches were tried but showed no particular difference.

With the maintained firing rate included in the parameter fitting process, the model firing rate was consistently higher than that observed experimentally, including those of Barlow & Levick (1969) which are very similar, irrespective of the ratio of stimulus diameter to receptive field diameter. Furthermore whilst the experimental maintained rates increase more steeply over background luminance values of -5 to -3 log cd/m^2 than -3 to -2 log cd/m^2, the reverse is observed from the model output. For parameters fit to decreasing ratios of stimulus to receptive field diameter the maintained rate increased slight (maximum increase 15Hz at background -2 log cd/m^2). The fitted response curves themselves, with maintained rate removed, were remarkably consistent irrespective of stimulus to receptive field diameter as can be seen in Figure 3.8. In spite of a fitness function biased towards a background luminance of -4 log cd/m^2 (Figure 3.8B), the closest fit is observed for background luminance of -3 log cd/m^2 (Figure 3.8C). This is due in part to the relationship of 1 troland to $\approx$9.3 photons μm^{-2} s^{-1}

as selection of suitable values enables closer fits to any of the experimental data. This issue is further highlighted when the response range for each of the background luminance values is considered as in Figure 3.9. For the lower background luminance values the range of responses are apparently too low to be amplified such that they correspond to the experimental data. In spite of this, considering Figure 3.8B which has a background luminance comparable to that of Jancke (2000), the response curve does fall between the experimental observed data and the average response estimate. Interestingly, over the more linear sections of the model response curves, the slope of the response against log luminance is relatively constant for background luminance values of -4 to -2 log cd/m^2 (averaging different ratios gives 240, 257 and 263 Hz (log(cd/m^2))$^{-1}$). These linear sections occur at progressively lower stimulus luminance values as the background luminance increases. The slope of the corresponding ranges from Figure 3.9 for increasing background luminance are approximately 0.104, 0.038, 0.090 and 0.070 Hz (log(photons μm^{-2} s^{-1}))$^{-1}$. Whilst the units are different and do not permit a direct comparison, the slope for the lowest background luminance of -5 log cd/m^2 has the highest slope at both the photoreceptor and ganglion cell level (389 for the later in Hz (log(cd/m^2))$^{-1}$). However, the slopes at the other background luminance levels do not appear as similar in the photoreceptors as they do in the ganglion cells.

With reference to clear discrepancies illustrated by Figure 3.8, the retinal model is mechanistic in nature and thus it seems reasonable to attempt to have each component comparable to and calibrated against biological data. However, the model undoubtedly does not reflect all the mechanisms present in the real retina and thus the sum of the model parts must be expected to fall short of the real retina and cannot hope to accurately model observed biological data. Thus it might be argued that the system as a whole should be treated as a "black box" model and simple parameter tuned by a

genetic algorithm here to match the observed data. Indeed this has been investigated as mentioned above and in doing so produces a better fit to the experimental data. However, in taking this stance it might be further argued that an artificial neural network, or similar mechanism, could be used and simply fit to the experimental data and thus dispense with the retinal model currently used. Whilst such an approach might prove more accurate in representing the calibration data it is difficult to justify and investigate how the system reacts to novel data. With the more mechanistic INRIA based model the reaction of the component parts to novel stimuli can be investigated and compared with experimental data and lead to potentially more plausible results. Furthermore, adopting the mechanistic approach leaves far more scope for elaboration of the model at a future date in order to capture more of the components of the retina. It might be expected that the results produced by the model over background luminance values of -5 to -3 log cd/m^2 are within the range of experimental observations. Clearly these results highlight the need for further extensions to the INRIA retinal model to produce a system capable of representing the behaviour of the cat/vertebrate retina over its range of operating values in the scotopic domain. Almost undoubtedly this is also applicable to the photopic domain simply by considering the response characteristics of the early cone photoreceptor system (Valeton & Norren 1983).

The photoreceptor model is undoubtedly not particularly accurate but is only a small part and there are many other shortcomings/inaccuracies in other parts of the model, such as the V1 model having only layers 4 and 2/3 and no LGN, and so is probably only a small contribution to the overall errors. Furthermore it is not the main focus of the work being conducted. Whilst it is acknowledged that it is fundamental to such work as it provides the foundation on which it is built in terms of initial input, provided that it does provide consistent, calibrated and verified output in the range of stimuli to be considered then this should be sufficient. Indeed it cannot be expected to

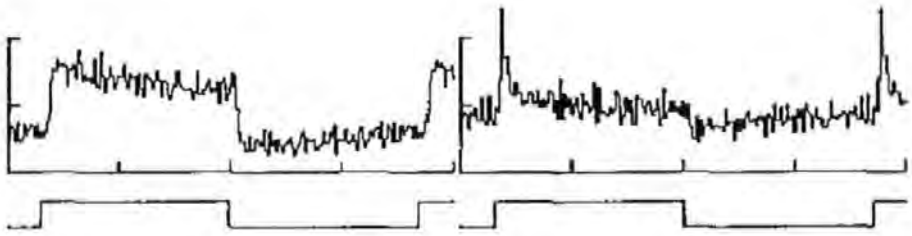

Figure 3.10: Experimental X and Y cell responses. Figure taken from (Jakiela et al. 1976).

operate over the entire range of stimuli as observed for the real retina as this was not within the scope of the initial design.

3.1.4 X and Y Ganglion cells

In later versions of the model two classes of ganglion cells, X and Y, were introduced, replacing the existing single ganglion class definition. To reflect the transient and sustained responses observed in these two classes (Jakiela et al. 1976) a new definition for the temporal response of X and Y cells was introduced incorporating a firing rate adaptation term (Dayan & Abbott 2005) to give

$$FR = FG \tag{3.21}$$

$$\tau_G \frac{dG}{dt} = -G + R(B,p) - a(G-E) \tag{3.22}$$

$$\tau_a \frac{da}{dt} = -a + gF \tag{3.23}$$

The firing rate, FR, is simple the product of G, the membrane activity of the ganglion cell, with F, a gain term. The membrane activity of the ganglion cell is a simple passive membrane model with time constant τ_G = 25 and 4.5ms for X and Y cells respectively (O'Brien et al. 2002). The bipolar input to ganglion cells, $R(B,p)$, is a half rectification, R, of bipolar cell activity, B, according to threshold p (Wohrer et al.

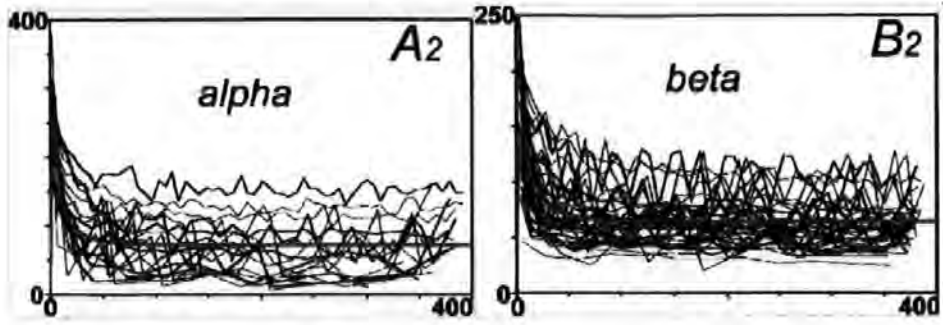

Figure 3.11: Comparison of spike frequency adaptation in model with cat X and Y cells. In both panels, the dark lines show the spike rate over time observed for maximum current injection and is taken directly from the published article by O'Brien et al. (2002) whilst the red line shows the firing rate of a model ganglion cells. The left panel shows the results for Y, or alpha, cells, and the right panel results for X, or beta, cells.

2006). The adaptation gain term g was set to 0.1 for Y cells and 0.04 for X cells, whilst the time constant τ_a had a value of 50ms. These values for g and τ_a were selected as they gave reasonable fits to observed physiological data (O'Brien et al. 2002) as can be seen in Figure 3.11. As the resting value for G is 0, E is also 0.

For comparison, model Y cells have a spike frequency adaptation (FA) 0.72 compared with 0.77 ± 0.04 observed in alpha cells of the cat, where $FA = (F_i - F_{ss})/F_i$, with F_i the initial spike rate and F_{ss} the steady state spike rate (O'Brien et al. 2002). For the purposes of the model, F_i is taken to be the maximum spike rate observed which occurs 3.7ms after initial stimulation. In X cells $FA = 0.58$ whilst O'Brien et al. (2002) record a value of 0.57 ± 0.03. To capture the non-transient nature of X cells under conditions of low background luminance (Jakiela et al. 1976), the adaptation gain term, g, was set to 0. The firing rate gain parameter F, and as a consequence adaptation gain g, is dependent on the range of the bipolar input $R(B, p)$. For a range of stimuli, the maximum bipolar input to both X and Y ganglion cells was recorded. Stimuli consisted of a uniform background of -4log cd/m^2 with a single circular spot centred on the re-

ceptive. The results for X and Y ganglion cells are presented in Figure 3.12 assuming a pupil area of 108mm^2. The pattern of bipolar input for different stimuli is similar for both cell types. However, the input to X cells is generally greater than that to Y cells. In addition, for extremely high luminance values further increases in brightness result in a reduction of peak bipolar input. Both observations are likely to result from the feedback of amacrine cells. From the data of Sakmann & Creutzfeldt (1969) it is assumed here that no appreciable gain in ganglion firing rates would be observed for stimuli with luminance greater than 0.1cd/mm^2. Conversely Figure 3.12 indicates a continued gain in bipolar activity for luminance values in excess of 0.1cd/mm^2 and a consequently continued gain in ganglion firing rate. In order for the model to operate over all possible stimuli luminance values additional gain control mechanisms need to be considered or re-evaluation of existing parameters. The work presented here is concerned with the relative activity of X and Y cells under a given stimulus protocol. Furthermore, the illuminance of these stimuli is less than the equivalent luminance of 0.1cd/mm^2 in Figure 3.12. Thus it was decided to limit the bipolar output to the maximum observed for a luminance of 0.1cd/mm^2. The maximum bipolar output was 3.84 and 2.16 for X and Y cells.

Figure 3.13 displays fitted responses of X and Y model cells to small spot stimuli at different luminance levels. Both, X and Y cells were used in the simulations of motion streak in section 4.2.1 and section 5 Figure 5.1. The simulations of lateral spread in section only made use of X cells, section 4.1.

3.2 Lateral Geniculate Nucleus

The historical perspective of the LGN as simply a relay circuit between retina and striate cortex has been challenged (Guillery 1995, Casagrande & Ichida 2002, Guillery &

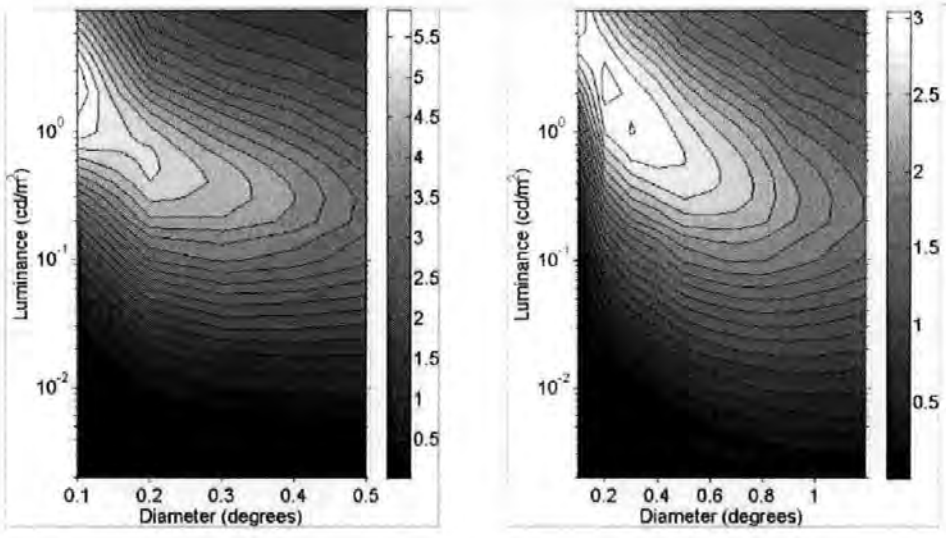

Figure 3.12: Maximum bipolar input to X and Y ganglion cells. The left and right panels show the maximum bipolar input to X and Y ganglion cells respectively. A circular spot was presented on a uniform background and centred on the receptive field of the cell. Pupil area was 108mm^2 and background luminance -4log cd/mm^2. Gray scale indicates the maximum bipolar input observed.

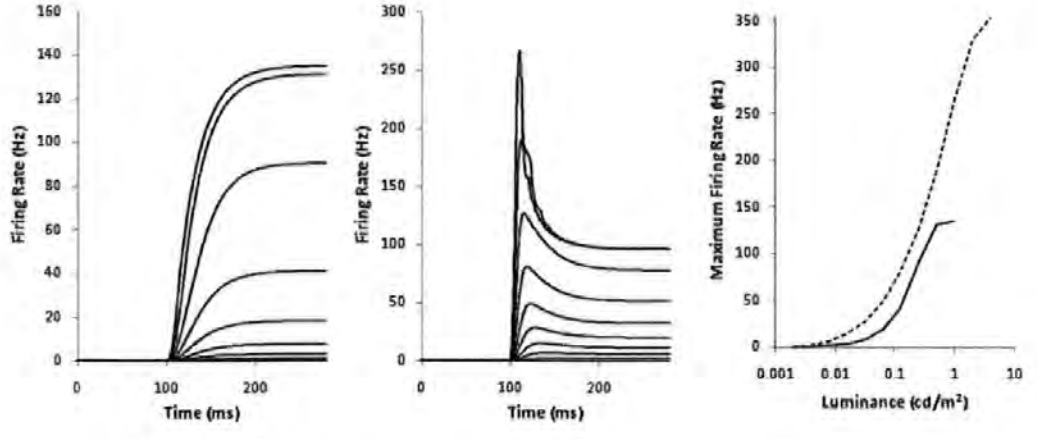

Figure 3.13: X and Y cell model responses. Responses to small spot stimuli at different luminance levels are shown for X cells (left) and Y cells (middle). The right plot shows the resulting maximal responses as a function of luminance.

Sherman 2002, Sherman & Guillery 2002, Sillito & Jones 2002, Wörgötter et al. 2002, Alitto & Usrey 2003, Sherman 2005). However, much of the evidence is concerned with non-classical receptive field effects. Given the small stimuli considered here it was decided to characterize the LGN as a simple relay from retina to cortex. This is supported by a recent modelling study of LGN cells (Casti, Hayot, Xiao & Kaplan 2008) where a simplified model was sufficient to capture the spiking behaviour of LGN cells in response to spot stimuli. Furthermore they demonstrate that under this stimulus paradigm, feedforward excitation from the retina is the dominant drive of LGN activity with limited or no inhibition and cortical feedback. As the authors observe, small spot stimuli are unlikely to elicit significant response from the large receptive fields of layer VI cells which are responsible for the bulk of V1 feedback to LGN. Results from flashed spot experiments suggest that inhibition from cortical feedback to LGN is not significant for the size of spot used here (Sillito & Jones 2002). This is definitely the case for Y stream activity as this stream provides good temporal location of the stimulus. The streak effect resulting from the X stream might be considered to activate cortical feedback due to the bar like representation of the stimulus in cortex. However, as the stimulus is moving, the retinopic position of feedback is not temporally aligned with the feedforward activation of the X stream and thus any inhibitory effect is reduced – although it might truncate the motion streak in LGN and thus attenuate the motion streak effect. Thus the LGN model presented here represents a single layer of excitatory X cells and a single layer of excitatory Y cells. All cells have temporal characteristics governed by

$$\tau\frac{dV}{dt} = V_r - V_g F_G(E-V) - a(V-E) \tag{3.24}$$

This attempts to represent the membrane potential, V, of LGN cells with passive membrane time constant,$\tau = 22.4ms$ for X cells and 14.6ms for Y cells, and resting poten-

tial, V_r = -61mV (Crunelli et al. 1987). The last term $a(V-E)$ is a spike adaption term that is applicable only to Y LGN cells and is specified as in equations (3.22) and (3.23) for Y ganglion cells. Only excitatory projections are made from retina to LGN which is captured by $gF_G(E-V)$ where F_G is the firing rate of the presynaptic ganglion cell, E the AMPA reversal potential and g a tuneable gain term. Whilst the response of X and Y LGN cells are observed to be similar to X and Y ganglion cells (Cleland & Lee 1985) the firing rate of LGN cells is a simple activation function based on that found in area 17 of the cat (Carandini & Ferster 2000) and for some threshold t is given by

$$\theta(V) = \begin{cases} 0 & : \quad V \leq t \\ g(V-t) & : \quad V > t \end{cases} \tag{3.25}$$

LGN cells share similar circular centre surround receptive field structure with retinal ganglion cells (DeAngelis et al. 1995) from which they receive selective and limited input (Usrey, Reppas & Reid 1999, Kara & Reid 2003). Here a single model ganglion projects to a single LGN cell.

Note that retinal synapses on LGN cells are only of AMPA-type but do not have the kinetics of those modelled in cortex. Neither do retinal connections have the kinetics of cortical synapses.

The transmission ratio of LGN cells is shown to be a function of stimulus parameters (contrast, temporal frequency, and spatial frequency), however, no difference is observed between X/Y or ON/OFF cells (Kaplan, Purpura & Shapley 1987). Thus the particular transmission value used might be seen as arbitrary as the model makes comparison between X and Y streams where no difference in transmission ratio is observed. The reduced transmission ratio as a result of stimulus parameters are generally similar to that observed for spot stimuli (Casti et al. 2008). For drifting gratings extending beyond the classical receptive field, at 50% contrast, the mean firing rate of

retinal and LGN cells indicates a transmission ratio of 0.5 (Kara, Reinagel & Reid 2000). The gain from retina to LGN, g, was individually tuned for X and Y cells to give a transmission ratio of 0.35.

3.3 Primary Visual Cortex Model

The cortical model represents thalamic recipient layer 4 and supragranular layer 2/3. Each cortical layer is comprised of two cell populations representing excitatory and inhibitory neurons. These populations are organised in a grid such that a given model cell captures the combined activity of individual neurons within a given spatial location. Thus dependent on scaling, an excitatory model cell might represent 40 excitatory stellate cells in layer 4 and the complementary inhibitory model cell would represent 10 inhibitory interneurons, given typical excitatory to inhibitory proportions of 80% and 20%. As there is no segregation of excitatory and inhibitory cells within a cortical layer, excitatory and inhibitory cells at the same spatial location correspond to an identical physical space. A hierarchical model of orientation tuning (Bear et al. 2000, Ferster & Miller 2000, Hubel 1995, Kandel et al. 2000, Martinez & Alonso 2003) is created by spatially specific retinal projects to layer 4 cells. All layer 4 cells, inhibitory and excitatory, are classed as simple and have odd symmetry (Jones & Palmer 1987) with two subregions. The orientation preference of individual model cells is specified by a predetermined orientation map. The initial simulation study investigating the dynamic spatiotemporal activity reported by Tucker & Katz (2003) used a synthetically generated orientation map (Section 4.1). This has subsequently been replaced by an orientation map derived from experimental data of cat area 18 supplied by a partner in the FACETS consortium, Zoltán Kisvárday. The orientation tuning of layer 2/3 cells is inherited from layer 4 cells which make direct projections to the former. As detailed later, each layer 4 cell makes a number of divergent projections to layer 2/3

thus each layer 2/3 cell receives convergent synaptic input from several layer 4 cells. These presynaptic layer 4 cells are spatially distinct and as a result can have different orientation selectivity which in turn may lead to broader tuning of orientation preference in layer 2/3. This convergence may also lead to more complex like characteristics in layer 2/3 cells as observed in vivo (Hirsch et al. 2002, Martinez & Alonso 2003, Martinez et al. 2005) due to spatial overlap of receptive fields. However, currently this is purely speculative and further investigation is required to determine the precise functional ramifications of divergent projections from layer 4 to layer 2/3.

The temporal dynamics of model cells and synaptic connections are defined by a series of ordinary differential equation. Excitatory and inhibitory cells, influenced by Song, Miller & Abbott (2000) and Gerstner & Kistler (2002), are described by

$$\tau_{ct}^{rise}\frac{dV_{ct}^{j}}{dt} = V_{ct}^{rest} - V_{ct}^{j} + f_{ct}^{j} \tag{3.26}$$

with

$$\tau_{ct}^{decay}\frac{df_{ct}^{j}}{dt} = -f_{ct}^{j} + \sum_{i} g_{i}^{ct,j}\left(E_i - V_{ct}^{j}\right) \tag{3.27}$$

where

ct is the cell type *excitatory* or *inhibitory*.

j indexes a particular cell in an excitatory or inhibitory layer.

V_{ct}^{j} is the "membrane potential" of cell j in population type ct.

τ_{ct}^{rise} is the rise time constant of cell type ct.

V_{ct}^{rest} is the resting "membrane potential" of cell type ct.

f_{ct}^{j} is an auxiliary function for cell j in population type ct.

τ_{ct}^{j} is the decay time constant of cell type ct.

i is the connection type, belonging to the set {AMPA, NMDA, $GABA_A$, $GABA_B$}.

$g_i^{ct,j}$ is the synaptic input of connection type i to cell j of type ct.

E_i is the reversal potential of connection type i.

In keeping with the notion that each model cell represents a number of individual neurons, connections between model cells similarly represent a collection of neurites. The concept of combine connections is extended to include all projections to a given model cell. Thus all connections of a given type, i, to a model cell are represented by the single ordinary differential equation

$$\tau_i^{rise}\frac{dg_i^{ct,j}}{dt} = -g_i^{ct,j} + h_i^{ct,j} \tag{3.28}$$

with

$$\tau_i^{decay}\frac{dh_i^{ct,j}}{dt} = -h_i^{ct,j} + \sum_{ct'}\sum_{l} w_{i;jl}^{ct,ct'} f^{ct'}(V_{ct'}^{l}(t-d_{jl})) \tag{3.29}$$

where

i is the connection type, belonging to the set {AMPA, NMDA, $GABA_A$, $GABA_B$} as defined in equation (3.27).

$g_i^{ct,j}$ is the synaptic input of type i to cell j of type ct as defined in equation (3.27).

τ_i^{rise} is the rise time constant of connection type i.

$h_i^{ct,j}$ is an auxiliary variable for synaptic input of type i to cell j in population type ct.

τ_i^{decay} is the decay time constant of connection type i.

l runs over all model cells presynaptic to cell j, with connection type i.

$w_{i;jl}^{ct,ct'}$ are synaptic weights of connection type i from presynaptic cell type ct' to postsynaptic cell type ct and specifically from neuron l to j.

t is the current time.

d_{jl} is the propagation delay from cell l to cell j.

$f^{ct}(x)$ is a firing rate function for cell type ct as a function of x, and is defined by $\omega^{ct}[x-\phi^{ct}]^+$ where ω^{ct} and ϕ^{ct} are the gain (in spikes per second per millivolt) and threshold for cell type ct. This is essentially the rectification model of Carandini & Ferster (2000).

The foundation of this definition of synaptic activity has been adapted from Gerstner & Kistler (2002).

The membrane potential is open to interpretation in this context. In one sense it does represent the membrane potential of a single cell which in turn characterises the activity of a number of cortical neurons. An alternative perspective is that a model cell is a model to describe firing rates averaged over a number of neurons by application of a rectification function to the "membrane potential" which is simple a mechanism to give the appropriate firing rate. In this case the notional membrane potential still has parallels with the previous view point. In either case, as highlighted by Carandini & Ferster (2000), the use of a rectification function to determine firing rate renders the concept of membrane potential above spiking threshold relatively artificial. If model cell activity is considered to represent the averaging over a number of cortical cells, in contrast to a point sample of a collection of neurons, then consideration should be given to the relative temporal activity of the individual neurons. It is unlikely that the synaptic driven activity of such a collection of neurons will be in lock step; rather

there will be some variation in the onset of individual cell responses. This dynamic is captured in some regard by the use of the difference of exponentials function used to capture model cell activity as described in equation (3.26) and, as a function of time t, is of the form

$$g(t) = \frac{1}{\tau_{decay} - \tau_{rise}} \left[e^{-\frac{t}{\tau_{decay}}} - e^{-\frac{t}{\tau_{rise}}} \right] \tag{3.30}$$

Specific values for τ_{decay} and τ_{rise} are selected such that the behaviour of $g(t)$ conforms to the membrane dynamics observed experimentally in cat visual cortex (Nowak, Azouz, Sanchez-Vives, Gray & McCormick 2003).

As mentioned above, layer 4 model cells make divergent projections to layer 2/3 and target a number of postsynaptic model cells. Modelling studies of the cat (Stepanyants & Chklovskii 2005, Stepanyants, Hirsch, Martinez, Kisvárday, Ferecskó & Chklovskii 2008) and anatomical data in the rat (Bender, Rangel & Feldman 2003) both support this notion. To model this spread in connectivity, the probability, p, of connection between layer 4 and layer 2/3 cells is given by the simple Gaussian function

$$p = e^{-\frac{(x_4 - x_{2/3})^2 + (y_4 - y_{2/3})^2}{2\sigma^2}} \tag{3.31}$$

where

(x_4, y_4) determines the position of the presynaptic model cell within the layer 4 grid.

$(x_{2/3}, y_{2/3})$ determines the position of the postsynaptic model cell within the layer 2/3 grid.

σ determines the spatial extent of divergent connections from layer 4.

Note that the grids themselves can be considered to be stack above each other along the z-axis, and that all grids for all layers are in register such that for two cells with $x_4 = x_{2/3}$ and $y_4 = y_{2/3}$, one cells lies directly beneath the other in the z direction.

However, from the modelling studies, the specificity of these connections with regard to orientation tuning is not defined. At present connections are made independent of the orientation tuning of both pre- and postsynaptic cells which may lead to undesired effects such as detuning with respect to orientation selectivity of layer 2/3 cells. In future incarnations of the model this will be investigated more thoroughly in terms of both the consequences of cell tuning within the model and literature surveyed. Currently there is no reciprocal connectivity from layer 2/3 to layer 4. Modelling studies (Binzegger et al. 2004, Stepanyants et al. 2008) and biological data (Thomson & Bannister 2003) seem to suggest that excitatory synapses by layer 4 stellate cells with layer 2/3 pyramidal cells are more numerous than those from layer 2/3 to 4. However, Binzegger et al. (2004) calculate that inhibitory synapses from layer 2/3 to layer 4 are more numerous than the reverse. Despite this, the inclusion of feedback from layer 2/3 to layer 4 will be considered for future extensions of the model.

Within layer 4, lateral connectivity is isotropic, with excitatory and inhibitory model cells making projections in a radially symmetric halo. The probability of a connection between cells is specified by a Gaussian function of their spatial separation defined similarly to the projection from layer 4 to layer 2/3. Thus

$$p = e^{-\frac{(x_{pre}-x_{post})^2+(y_{pre}-y_{post})^2}{2\sigma^2}} \tag{3.32}$$

where

(x_{pre}, y_{pre}) determines the position of the presynaptic model cell within the layer 4 grid.

(x_{post}, y_{post}) determines the position of the postsynaptic model cell within the layer 4 grid.

σ determines the spatial extent of connections from layer 4.

The less extensive connectivity of layer 4 does appear to conform to the results of modelling studies (Stepanyants et al. 2008) however experimental data (Gilbert & Wiesel 1983) does suggest that extensive long range lateral connections are observed in all layers of the cat visual cortex and also form patchy connections similar to those of layer 2/3. Furthermore, whilst the modelling study of Stepanyants et al. (2008) does suggest longer range connectivity in layer 2/3 it does not have the resolution necessary to reflect the patchy connectivity recorded experimentally (Bosking et al. 1997, Buzás et al. 2006, Gilbert & Wiesel 1983, Kisvárday et al. 1997, Malach et al. 1993, Sincich & Blasdel 2001, Tanigawa et al. 2005) or in layer 4 (Gilbert & Wiesel 1983).

Projections made by excitatory cells to excitatory and inhibitory targets in layer 2/3 uses a model based on the work of Buzás et al. (2006). A two dimensional Gaussian function is used to control the anisotropic extent of layer 2/3 connections and a one dimensional Gaussian dictates how similar the orientation tuning of pre- and postsynaptic cells must be. The product of these two functions gives a connection probability of

$$p = e^{-\frac{(\theta_{pre}-\theta_{post})^2}{2\sigma_\theta^2}} e^{-(ax^2+bxy+cy^2)} \tag{3.33}$$

and

$$a = \left(\frac{\cos\theta_{pre}}{\sigma_=}\right)^2 + \left(\frac{\sin\theta_{pre}}{\sigma_\perp}\right)^2 \tag{3.34}$$

$$b = -\frac{\sin 2\theta_{pre}}{\sigma_=^2} + \frac{\sin 2\theta_{pre}}{\sigma_\perp^2} \tag{3.35}$$

$$c = \left(\frac{\sin\theta_{pre}}{\sigma_=}\right)^2 + \left(\frac{\cos\theta_{pre}}{\sigma_\perp}\right)^2 \tag{3.36}$$

where

θ_{pre} is the orientation tuning of the presynaptic cell.

θ_{post} is the orientation tuning of the postsynaptic cell.

σ_θ determines the angular range over which different orientation tunings are connected.

(x,y) determines the relative displacement of the pre- and postsynaptic model cells within the layer 2/3 grid.

$\sigma_=$ determines the spatial extent of lateral connections in the direction parallel to the orientation tuning of the presynaptic cell.

σ_+ determines the spatial extent of lateral connections in the direction perpendicular to the orientation tuning of the presynaptic cell.

In addition, the more isotropic local connections are modelled using equation (3.32). Local to the presynaptic cell this combination can result in very dense connectivity and a bias towards cells of a similar orientation. It is unclear from the literature if this local bias occurs, however Buzás et al. (2006) support this general approach. Interestingly though, they do not appear to reflect the anisotropy in lateral long range layer 2/3 connections observed by others (Bosking et al. 1997, Gilbert & Wiesel 1983, Schmidt et al. 1997, Sincich & Blasdel 2001, Tanigawa et al. 2005). Connections from inhibitory cells are modelled using equation (3.32) only and do not include the long range anisotropic connections of excitatory cells. An example of the resultant connectivity for a single model cell can be seen in Figure 3.14. Previously it was indicated that connections between model cells reflect a number of projections between two small populations of cortical neurons. These synaptic representation can therefore not simply be parametrised using experimental data. Rather experimental data concerning the efficacy of synaptic types, e.g. AMPA, NMDA, etc., and the relative density of connections (Binzegger et al. 2004), is used to guide the tuning of these parameters.

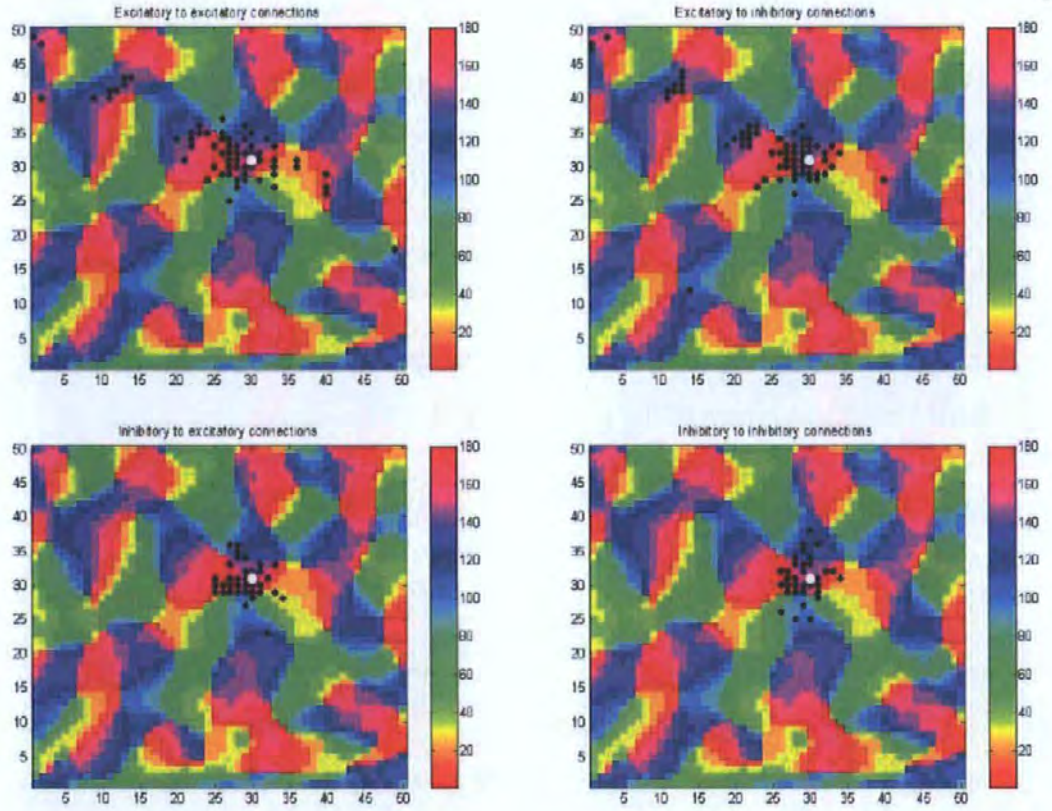

Figure 3.14: Example of layer 2/3 connectivity. The connectivity of a single layer 2/3 cell, indicated by the white dot, for each connection type is shown in the four panels. The left and right upper panels show the long range connections made by excitatory cells to excitatory and inhibitory cells, respectively. The lower left and right panels show the short range inhibitory connections made to excitatory and inhibitory cells respectively. Note that this orientation map is for Macaque visual cortex. The scale bars to the right of each plot indicate the orientation tuning of the different coloured regions.

Chapter 4

Results

Two sets of results are presented; the first attempts to replicate the observations of Tucker & Katz (2003) whilst the second investigates two sets of observations made by Jancke (Jancke 2000 and unpublished data). The experiment of Tucker and Katz was an in vitro study of the lateral spread of activity in layer 2/3 slices of Ferret visual cortex. The data from Jancke was obtained by in vivo visual stimulation of cat primary visual cortex. The first set of observations is from multi-electrode recordings used to derive a model describing the temporal dynamics of orientation tuning activity in cell populations (Jancke 2000). The second, unpublished, data set shows population activity in layer 2/3 evoked by a single moving square of light and is imaged using voltage sensitive dyes. The results that follow illustrate the current state of the computational model. As such they serve to validate the modelling decisions taken and support the assertion that the approach adopted is suitable for the proposed research.

4.1 Lateral Propagation of Layer 2/3 Activity in vitro.

Results from the model are presented in conjunction with experimental observations of Tucker & Katz (2003) for comparison.[1] Their data was obtained from optical imaging of in vitro layer 2/3 slices stained with voltage sensitive dyes. They aimed at exploring lateral activation spread and nonlinear interactions in population signals. Images represent the activity in 1.76mm $\times$ 1.76mm cortical patches. Correspondingly, the model used for this study did not incorporate either the retinal system or layer 4. Activity of

[1] The comparison figures are taken directly from the publication by Tucker & Katz (2003).

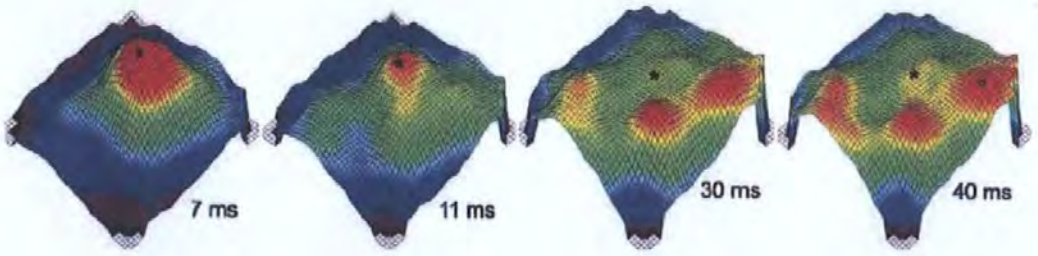

Figure 4.1: Experimental Spatiotemporal Activity. Four weak focal pulses of an extracellular stimulus were applied to the site mark ("⋆"). The plots from left to right show the induced activity 7, 11, 30 and 40ms after the initial pulse. They illustrate that an initial diffuse zone of activity centred on the stimulation site is followed by more distal patches of activity or "optical clusters".

collocated excitatory and inhibitory layer 2/3 model cells is proportionally combined to give a measure corresponding to an optical signal.

In vitro 4 weak focal extracellular pulses at 10Hz elicit a diffuse spreading zone of activity centred on the stimulus site. A number of discrete distal zones of activity, termed "optical clusters", are also produced. An example of such activity observed by Tucker and Katz is seen in Figure 4.1. The stimulus site (indicated by ("⋆") is centred on a large diffuse zone of activity, with 3 distal zones clearly seen between 20 and 30ms after the initial pulse.

In the model, focal stimulation positioned at the red area of Figure 4.2 produces similar spatiotemporal activity, as seen below.[2] A large, spreading zone of activity is centred on the stimulus site, with two distal zones of activity clearly visible after 17ms. Activation spread follows specific excitatory pathways, but propagation delays induce typical temporal response dispersal.

Activity surrounding the stimulus site is actively suppressed following each stimulus pulse. This effect is readily apparent following four pulses at 20Hz; 15ms after the

[2]These images have been smoothed using the median value of a 3×3 pixel grid centred on each pixel.

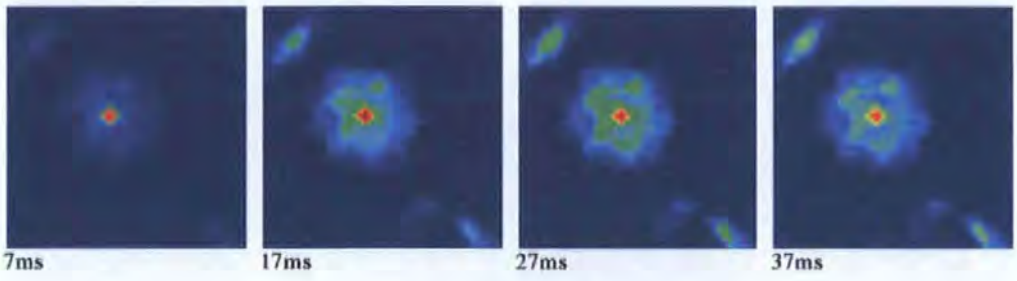

Figure 4.2: Model Spatiotemporal Activity. Four weak focal pulses of an extracellular stimulus were modelled at the site of the red cross. The plots from left to right show the induced activity 7, 17, 27 and 37ms after the initial pulse. As with the results of Tucker and Katz, an initial diffuse zone of activity centred on the stimulation site is followed by more distal patches of activity.

final pulse a distinct ring of inhibition is observed centred on the stimulus sit as shown in Figure 4.3. Figure 4.4 shows a similar inhibition is reproduced by the model with a comparable time course and a clear impact of total inhibitory efficacy and nonlinearities. The right panel of Figure 4.4 demonstrates that a slight increase in inhibitory connection efficacy results in a more distinct inhibitory ring 13ms after the final pulse and elevated activity at the stimulus site.

In vitro Tucker and Katz report that the maximum rate of decay occurs 7ms after each pulse in a series of four at 10Hz. The spatiotemporal characteristics of the maximum rate of decay can be seen below in Figure 4.5. The spatial extent of this rapid decay increases to a maximum following the third pulse.

In the model, the rate of decay had not reached a maximum before the onset of the subsequent stimulus pulse. Consequently, the maximum rate of decay was measured between 9 and 10 ms after each pulse. Under this proviso, the spatiotemporal characteristics of the maximum rate of decay in Figure 4.6 are seen to concur with

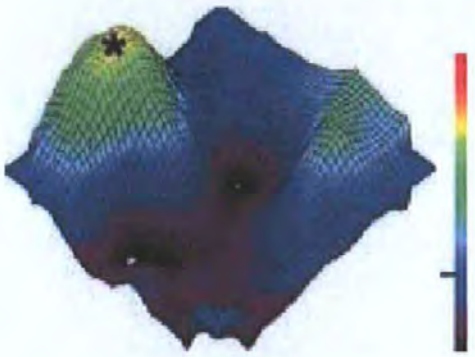

Figure 4.3: Experimental Inhibition. Four pulses applied at 20Hz to the site mark (induce a pronounced ring of inhibition around the diffuse zone of activity centred on the stimulus site 15ms after the final pulse.

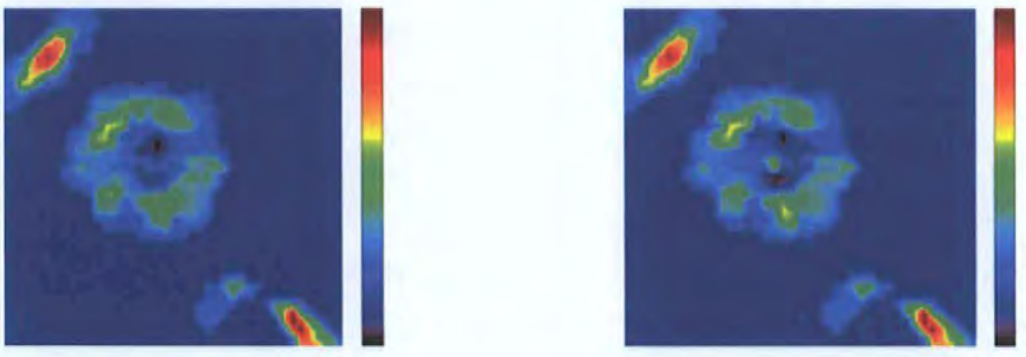

Figure 4.4: Model Inhibition. Model stimulation is sited as in Figure 6 which is just below the dark central spot of the left panel and the green central spot of the right panel. The left panel shows the result of stimulating the model as parameterised in Figure 6, whilst the right panel indicates the results of increasing inhibitory efficacy.

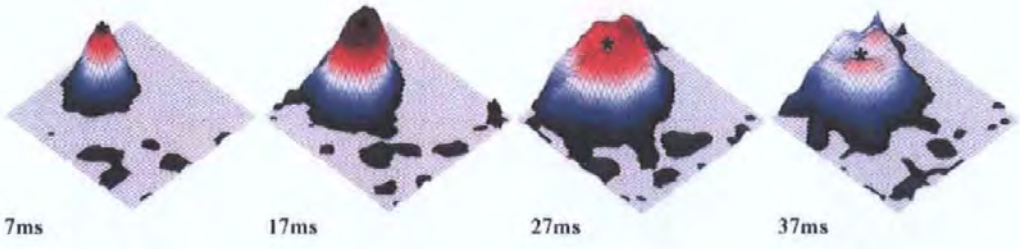

Figure 4.5: Experimental Rate of Decay. The panels from left to right show the rate of decay of activity 7, 17, 27 and 37ms after the initial pulse in a series of 4 at 10Hz. These images are calculated by taking the spatiotemporal activity data of Figure 4.1 and for each pixel at a given time, determining the rate at which the fluorescence response was changing.

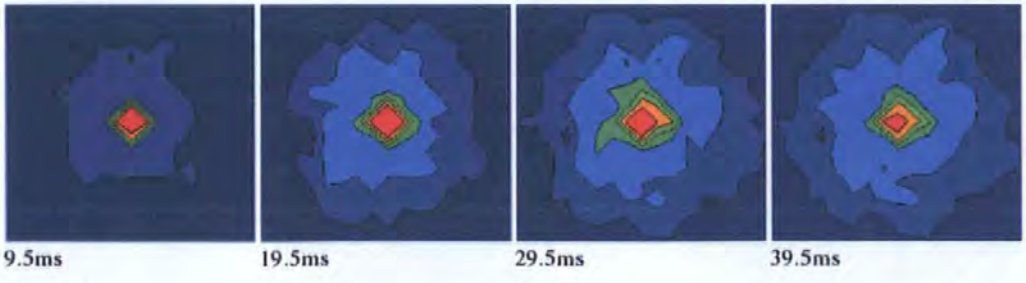

Figure 4.6: Model Rate of Decay. From left to right the rate of decay 9.5, 19.5, 29.5 and 39.5ms after the initial pulse in a series of four at 10Hz centred on the red circle. The rate of decay is seen to expand with time as observed experimentally. It should be noted that these images do not represent the entire cortical area modelled but rather show a sub region centred on the stimulation site in order to highlight the observations made.

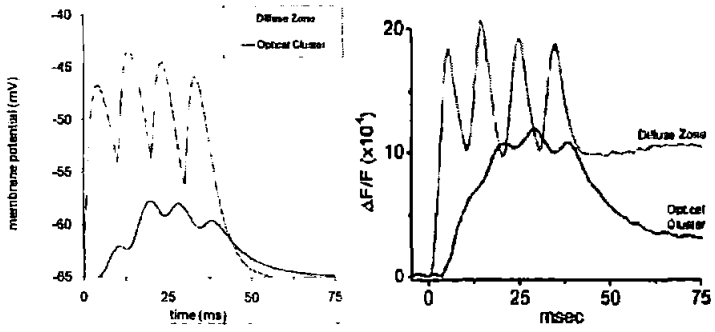

Figure 4.7: Temporal Response Profile. The activity recorded at the site of stimulation and an optical cluster is shown for model and experimental data by the grey and black traces respectively. The left graph presents data from the model and the right panel gives in vitro experimental results. Both show qualitatively similar results however there are some striking differences in terms of response amplitude and prolonged activity.

experimental observations.

The temporal response centred on the stimulus site and an optical cluster observed in vitro and in the model is presented in Figure 4.7. The upper, grey, traces in both plots show the response at the site of stimulation, with the lower, black, trace demonstrating the response elicited at a distal optical cluster. Qualitatively the two graphs are very similar. Both show large distinct peaks focused at the stimulus site that indicate a rapid response to extracellular stimulation. Conversely, at a more distal location stimulus response is attenuated; peaks become less distinct suggesting that synaptic integration produces a smeared, or blurred, response. Two points are worth considering from Figure 4.7; firstly the ratio of amplitude between proximal and distal responses, grey and black traces, is significantly different in the two graphs; secondly the in vitro recordings at both the diffuse zone and optical cluster show elevated activity over a significantly extended period in comparison to the model. In particular at the diffuse zone the optical response shows a curious, almost discontinuous, change in response after approximately 40ms. Such elevated activity in optical recordings has been observed

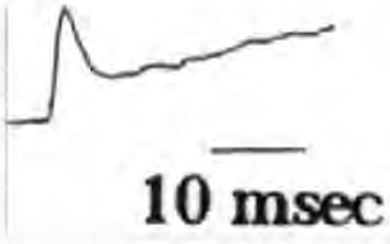

Figure 4.8: Slow component of optical signal (from Lev-Ram & Grinvald (1986)). Stimulation of myelinated rat optic nerve shows an initial transient action potential signal followed by a distinct slow component of the signal attributed to oligodendrocytes.

by others (Ebner & Chen 1995, Lev-Ram & Grinvald 1986) however in this case it is unclear the precise nature of the signal. Glial cells have been implicated in other experiments (Lev-Ram & Grinvald 1986); compare the optical signal of Figure 4.7 (right) with Figure 4.8 taken from Lev-Ram & Grinvald (1986), which shows an initial fast action potential followed by a distinct slow signal following stimulation of the rat optic nerve. Such a slow signal may be possible here as axons from inhibitory cells with myelinated sheaths have been observed in layers 2/3 and 4 (Somogyi, Kisvárday, Martin & Whitteridge 1983). However, it should be noted that different dyes preferentially bind to different neural components (Lev-Ram & Grinvald 1986). As Fitzpatrick (2000) notes, signals from optical imaging of voltage sensitive dyes indicate activity present in the upper 600μm of the cortex, thus from measurements by Peters & Yilmaz (1993) in cat primary visual cortex voltage sensitive dyes primarily image layer 2/3 and superficial layer 4.

Analysis of the time that each peak occurs at distal and proximal locations suggests nonlinear effects at the optical clusters. Figure 4.9 plots the time of each peak for optical cluster and diffuse zone as observed in vitro and in the model. At the stimulation site the model and experimental data are in good agreement and show a slight reduc-

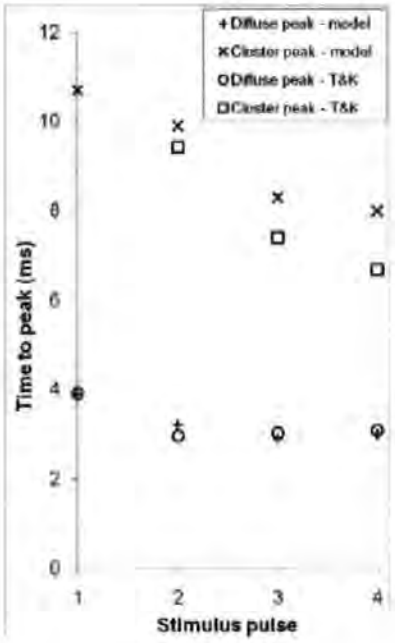

Figure 4.9: Response Nonlinearities. The time of each peak recorded at stimulation site and optical cluster for experimental and model results shown. The response at the local diffuse zones shows a small initial reduction in latency. This is more pronounced at the optical clusters, especially in the experimental data which demonstrates a clear nonlinear effect.

tion in the latency between stimulus and response after the first pulse. At the optical cluster site there is some divergence between the two data sets, however both show a decrease in the latency between stimulus and response. Tucker and Katz suggest that this decrease, or response acceleration, follows a nonlinear trend. The model results are more ambiguous in this respect with an exponential fit no better than a linear fit (R2 = 0.944 and R2 = 0.943 respectively). If only the last three points are considered then the data displays a similar nonlinearity to Tucker and Katz. The Tucker and Katz data is limited to 3 points here as a distinct response to the initial stimulus pulse is not apparent in Figure 4.7 (see (Tucker & Katz 2003) for a derived figure for response latency to the first pulse). As Figure 4.4 demonstrates, a slight change in connection efficacy

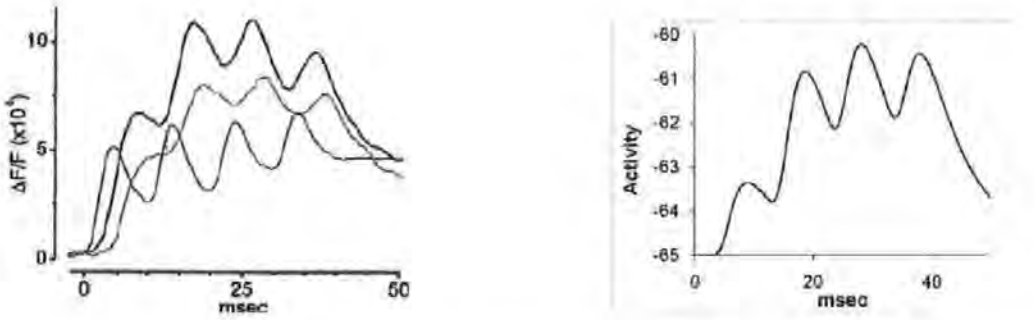

Figure 4.10: Optical Cluster Profile. The activity at optical cluster sites recorded in vitro and generated by the model. The left panel shows a number of traces recorded in vitro at optical clusters sites which all show characteristic blurring of response peaks. The right panel shows the activity of a model optical cluster site which displays a similar response.

can have a pronounced effect on the qualitative response of the model. Similarly it has been observed that a slight change in the parameter space of the model can result in optical cluster response latencies closer to the experimental data of Figure 4.9. Indeed it has already been mentioned that some values of model parameters, such as those for individual connection strengths, might be better represented by random values drawn from specific distributions rather than fixed values.

The optical response time course of three different distal zones as recorded by Tucker and Katz can be seen in Figure 4.10 on the left (note that certain annotation has been removed from the original plot for clarity). The activity time course for a distal zone in the model is given on the right (this corresponds to the upper left zone in the series of Figure 4.2) and is qualitatively similar. For further comparison consider the distal response presented in Figure 4.7. Again the temporal response profile in Figure 4.7 is characteristic of the observations reported by Tucker and Katz.

4.2 Motion Streak Representation

The following results focus on modelling investigations of experimental data from Jancke (Jancke 2000 and unpublished results). These data are presented in two sections, the first concerned with published results that highlight motion streak effects resulting from small moving stimuli (Jancke 2000). The second section presents attempts to model the extensive spread of lateral activity observed with voltage sensitive dye records when larger and faster moving stimuli are presented (Jancke, unpublished data). Both modelling studies are preliminary investigations that have simply applied the protocols defined in the experiments to the complete computation model including retina and layer 4. As might be expected, there are certain discrepancies between the modelling and experimental results, with a qualitative rather than quantitative comparison appropriate.

4.2.1 Population Representation of Motion Trajectory

Jancke (2000) uses a large sample of extracellularly recorded cells to study population activity in a two dimensional parameter space specifying orientation and visual space. The stimuli consist of single bright squares, 0.4° per side, moving at different velocities. Thus for each stimulus presentation a single square is seen to move across the visual field at a given velocity. The evolution of population activity over time can be seen in Figure 4.11. Consider the lower series of panels: in visual space population activity is seen to follow the stimulus, indicated by the white square. Along the orientation dimension broadly tuned initial activity gives way to population activity tuned to orientations perpendicular to the direction of motion, and then parallel to motion direction. This change in population activity as a function of orientation tuning can be clearly seen in the upper panels of Figure 4.11 which simply show the single

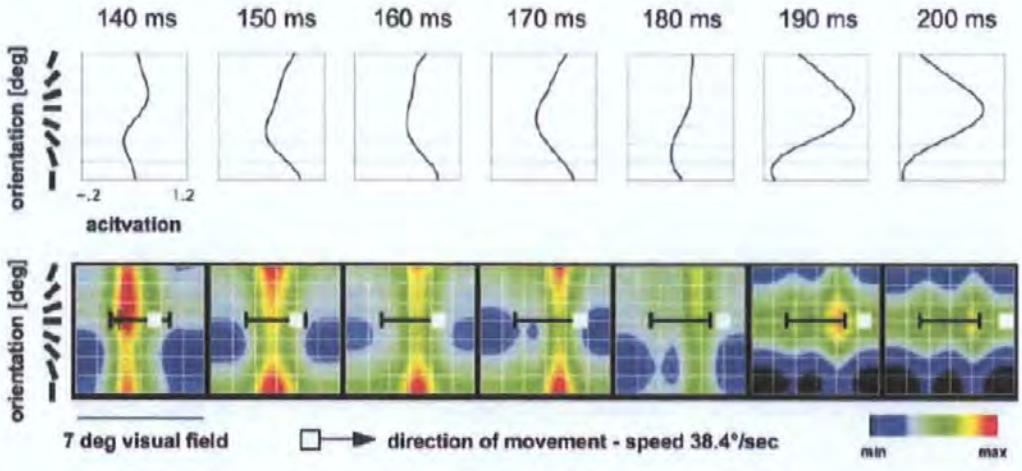

Figure 4.11: Experimental population activity for a moving square. A single moving square is seen to elicit population activity that follows the stimulus in visual space. In orientation space population activity is initially broadly tuned across orientations. As time progresses cells with orientation preference perpendicular then parallel to the stimulus direction of motion are active.

dimension of population orientation. Modelling results are given in Figure 4.12 and attempt to use the same representation of population activity. It should be noted that due to the coarse grain sampling of orientation space by the model and the bias in cat orientation maps available, the orientation domain was biased. In order to address this issue a synthetic map was used that evenly sampled the orientation space. The upper series of panels in Figure 4.12 show the evolution of population activity with respect to orientation preference in terms of membrane potential rather than spiking activity as in Figure 4.11. Despite this, the same general trend in population activity is seen with the caveats that neither the absolute times of activity nor relative amplitudes correspond to the experimental data. These differences may result from the parameters used in the model or the direct coupling of retina and visual cortex model components. Further, it was observed that biasing in the orientation domains of the map used for modelling purposes led to corresponding bias in population activity. It is possible that the use of a synthetic orientation map in the model may explain some of the differences in relative

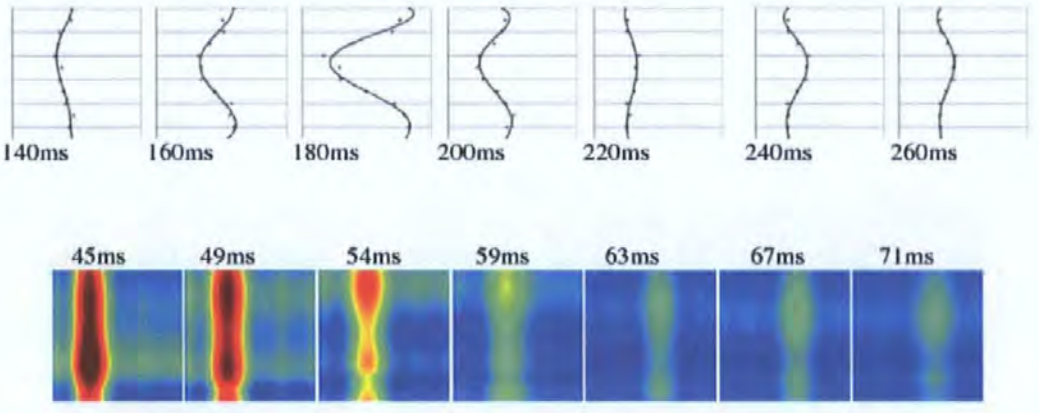

Figure 4.12: Model population activity for moving square. As with the experimental data, population activity follows the stimulus in visual space but shows that over time initial broad tuning along the orientation dimension gives way to activity in cells with orientation preferences perpendicular then parallel to the direction of motion. Not that unlike the experimental data, the upper panel here shows the membrane potential rather than spiking activity of model cells, whilst the lower series of panels have been derived from firing rates.

population activity across orientations present in Figure 4.12. The lower panel of Figure 4.12 was constructed in accordance with Figure 4.11. Again similarities in general behaviour can be seen. However there are discrepancies in the temporal evolution of activity, with the model results demonstrating a significant temporal compression in activity.

4.2.2 Persistent Activity in Population Encodings of a Trajectory

Unpublished data from Jancke shows cortical activity generated by a single moving light square stimulus, 1.5° per side, with velocity between 8-64°/*sec*. This activity is imaged using voltage sensitive dye techniques and thus represents neural responses in layer 2/3 and upper layer 4. Initial cortical responses appear spatiotemporally correlated with the stimulus showing elevated activity in retinotopic and temporal register. Activity can clearly be seen across orientation domains. Following this early phase per-

sistent attenuated activity is observed in the same patch of cortex but predominantly in iso-orientation domains that are tuned to orientations parallel to the stimulus trajectory. It is currently not possible to place exact values to the data, however it would appear that there is persistent activity for approximately 200ms after the stimulus is beyond the imaged region. The persistent activity appears to be about 20% of the signal induced during the early phase of the recording.

Simulation studies have produced data that displays some of these characteristics. Figure 4.13 shows how the activity in layer 2/3 evolves as the visual stimulus proceeds from left to right across the visual field region represented in cortex. The activity directly resulting from the stimulus does appear to coincide with orientation patches that are tuned parallel and orthogonal to the stimulus trajectory. The activity seen in Figure 4.13 is directly driven by layer 4 which shows very similar spatiotemporal dynamic behaviour. It should be noted that this simulation utilised a large stimulus that was in fact twice the size and thus 3° per side, and moving at $64^{\circ/sec}$. Subsequent simulations using a smaller stimulus of 1.5° per side in line with the experimental protocol have yielded similar results.

Persistent activity observed in the model is presented in Figure 4.14. Again a similar pattern of spatiotemporal activity is also seen in layer 4 suggesting that this layer is generating the activity in layer 2/3 where it is sharpened and slightly amplified. The patchy activity of iso-orientation regions is similar to that observed by Jancke. Unlike such data, the activity shown here is far more transient and does not appear to be as strongly correlated with a single orientation, however, there is a potential bias towards orientations parallel to the stimulus trajectory.

Increasing connectivity contralateral to the orientation of layer 2/3 cells as appears to be the case in the model of Buzás et al. (2006) produces the markedly different

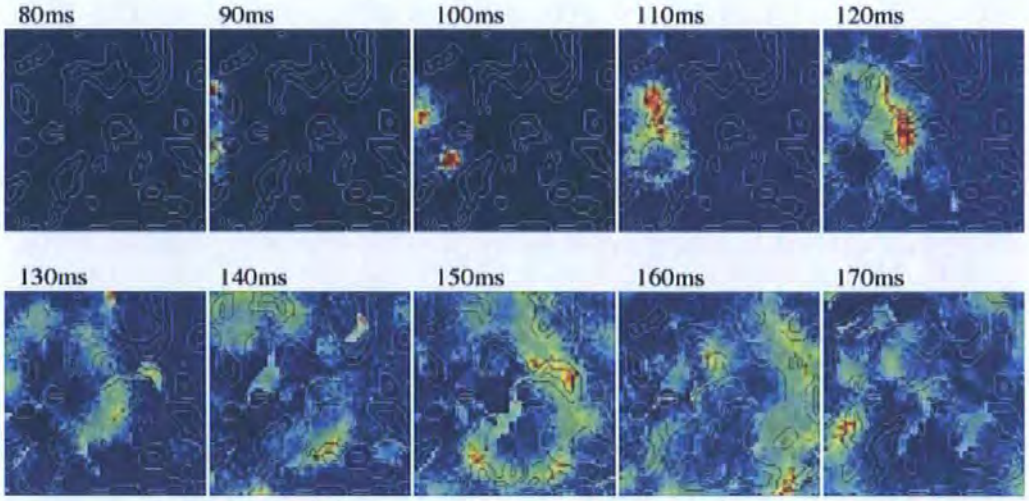

Figure 4.13: Spatiotemporal evolution of layer 2/3 activity induced by a moving square stimulus. Each panel shows the simulated activity in layer 2/3 at a given time which is indicated above the top left corner. The stimulus (not shown) moves from left to right and has half crossed the left boarder of the panel at 80ms. By 160ms it is beyond the right hand boarder of the panel. The concentric black rings denote iso-orientation domains roughly 15° either side of horizontal. The white concentric rings show iso-orientation domains roughly 15° either side of vertical. Activity appears to be biased toward vertical and horizontally tuned iso-orientation domains. There is perhaps more focal activity in cells that are tuned for horizontal orientations that are parallel to the stimulus trajectory.

behaviour illustrated in Figure 4.15. Here the spatiotemporal dynamic activity in layers 4 and 2/3 begins to diverge. In layer 2/3 the pattern of activity becomes much more stable than in either Figure 4.13 or Figure 4.14 yet seems to reflect orientation tunings that are between parallel and orthogonal to the stimulus trajectory. Furthermore, the level of activity in this stable state is significantly higher than that under the previous regime. This in conjunction with the very precise demarcation of activated isoorientation domains does not suggest particularly realistic results, however is does demonstrate that persistent activity is possible through the specific lateral connectivity observed in layer 2/3. With regards the orientation tuning of the activated patches

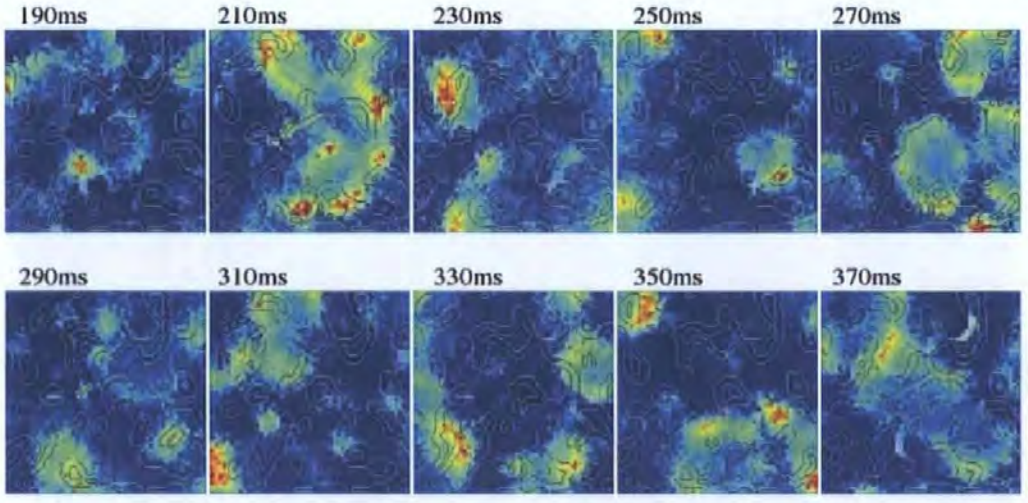

Figure 4.14: Evolution of persistent layer 2/3 spatiotemporal activity. The eight panels show the continuation of spatiotemporal activity presented in Figure 4.13. Note that the interval between successive panels is now 20ms rather than 10ms as in Figure 4.13.

Figure 4.15 suggests that oblique rather parallel and orthogonal selective regions are stimulated. Preliminary investigations have shown that this results from the connection density within the model which in turn is driven by biases in the orientation map and the specific connectivity model adopted. Changes in the orientation map such that isoorientation domains tuned parallel and orthogonal to stimulus trajectory have the highest connection densities result in activated regions that show orientation selectivity parallel and orthogonal to the stimulus trajectory. Further to this, more anisotropic connectivity can also be adopted that has similar connection densities to those used for Figure 4.15, and consequently can also produce persistent activity. Reduction of these connection densities mitigates the elevated activity presented in Figure 4.15 but also introduces more transient behaviour as in Figure 4.14.

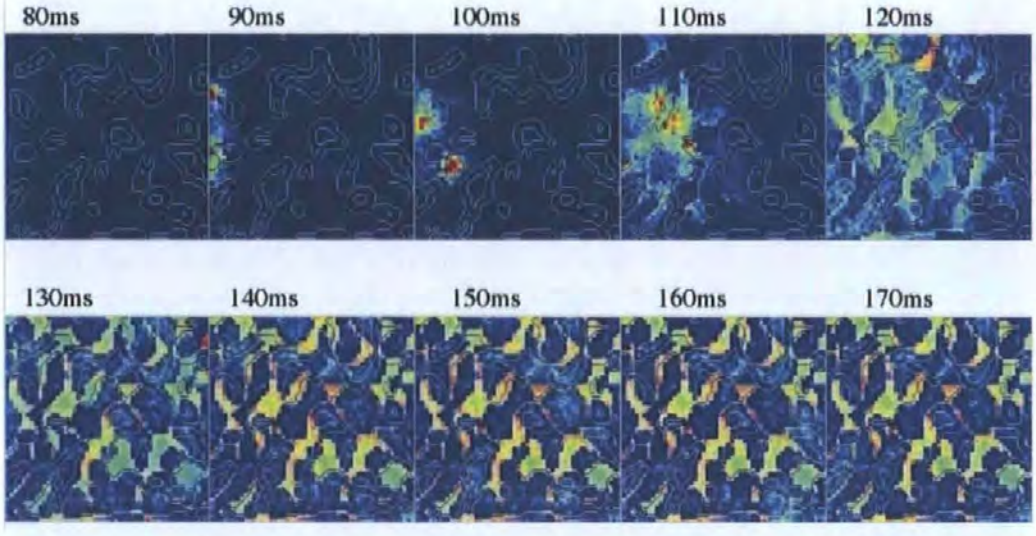

Figure 4.15: Evolution of layer 2/3 activity with stronger connectivity. The eight panels show spatiotemporal, activity as for Figure 4.13, for isotropic long range connectivity. As a result the connectivity is denser resulting in more synaptic input to each cell. The activity is seen to evolve similarly to that in Figure 4.13 up to approximately 110ms. After this, the network enters a stable state in which cells selective for orientations approximately 30° either side of 135° and 45° are extremely active at levels significantly above that induced by the stimulus in Figure 4.13. The network then remains in such a state for 100s of milliseconds before it is abolished by $GABA_B$ mediated inhibition.

Chapter 5

Discussion of Future Work

Work conducted in this thesis has focused on

- the background survey as presented in Chapter 2, necessary for computational modelling of the early visual pathway from retina to primary visual cortex,
- the development of a computational model of the early visual pathway that incorporates a multilayer retinal model and layers 4 and 2/3 of primary visual cortex (Chapter 3),
- a model study of the spatiotemporal behaviour of layer 2/3 in-vitro slices under extracellular stimulation (Section 4.1),
- a preliminary study of moving stimuli representations in the two dimensional parameter space of spatial location and orientation tuning (Section 4.2.1),
- and an initial investigation of the encoding of stimulus trajectory information and subsequent persistent representation mediated by long range lateral connections within layer 2/3 (Section 4.2.2).

The results reported in Chapter 4 are encouraging, however they may lack formal rigour. Consequently the initial goal of subsequent work is to calibrate the model against more experimental data. In particular, more established stimulus protocols need to be considered, such as full field grating and moving bars, in order to specify selectivity characteristics such as orientation, spatial frequency and possibly directional preference and contrast gain control. Additional validation can be addressed through

use of data regarding maintained activity in the absence of specific stimuli (Barlow & Levick 1969, Cleland et al. 1973, Gibber et al. 2001, Kuffler et al. 1957, Levick & Williams 1964, Levine & Troy 1986, Sincich & Blasdel 2001) to further calibrate the retinal and cortical model components; the relative contribution of feedforward and lateral components to synaptic input (Ferster & Miller 2000, Sillito & Jones 2002); and possibly motion direction signals from moving spot stimuli (Geisler, Albrecht, Crane & Stern 2001, Wörgötter & Eysel 1989). However, it is expected that there will be nontrivial discrepancies between the resultant model and validation data primarily as a result of nonlinearities observed in the later. For example: the maintained activity observed in the discharge of retinal ganglion cells follows a nonmonotonic function (Barlow & Levick 1969) whilst the feedback relationship between layer 6 of striate cortex and lateral geniculate nucleus indicates that the later can no longer be regarded as a simple relay. It has been argued previously in Chapter 2 that for the moving dot stimuli of Jancke (2000 and unpublished data) the hypothesised mechanisms in the LGN (Casagrande et al. 2005, Casagrande & Ichida 2002, Guillery 1995, Guillery & Sherman 2002, Sherman & Guillery 2002, Sillito & Jones 2002, Wörgötter et al. 2002) will have minimal impact on the transfer of information from retina to visual cortex. In contrast, the validation stimuli such as full field gratings would be expected to modulate the behaviour of LGN cells and consequently cortical neurons. This dichotomy between calibration stimuli and the paradigms that are the focus of the subsequently suggested modelling studies will undoubtedly result in discrepancies between model and experimental data which will require measured consideration. The results of this initial phase will not only serve to validate and verify the model but may also provide further insight into the mechanisms that underlie both simple and complex cells (Ferster & Miller 2000, Martinez & Alonso 2003).

Subsequent work should also be directed to motion streak phenomena (Burr 2000, Geisler 1999, Geisler et al. 2001) and in particular extend the preliminary investigation of observations made by Jancke (2000 and unpublished data). As detailed in Section 4.2.2 a single square stimulus moving across the visual field gives rise to activity in layer 2/3 and upper layer 4 that is imaged by voltage sensitive dyes. The initial response has a strong spatiotemporal correlation with the stimulus, and appears to be a relatively simple transformation of stimulus features. However, a more persistent, but attenuated, signal is also observed predominantly in cells that are not in spatiotemporal register with the stimulus and have specific orientation selectivity (parallel its trajectory). Similar behaviour is also generated by the computational model. Initial activity is observed shortly after stimulus onset in cells that have a corresponding retinotopic representation. Activated cells are principally selective for orientations orthogonal and parallel to stimulus trajectory, with the later more so. Cells tuned orthogonal to stimulus trajectory respond to its corresponding edges. The activity of those cells tuned to orientations parallel to the trajectory is comprised of similar edge detection but also temporal integration, i.e. a motion streak. Maximal response is observed in retinal cells aligned with the leading corners of the stimulus which in turn are temporally integrated to enhance the response of cortical cells that are oriented parallel to its trajectory, resulting in a greater response than orthogonally tuned cells. This temporal integration effect by the retina can be seen in Figure 5.1 where the ON centre retinal ganglion cell response is greatest near the leading corners of the stimulus (interestingly, the author is unaware of any similar findings reported as a result of experimental observations). Thus, one aspect of the data reported by Jancke can possibly be explained as a consequence of spatiotemporal characteristics of the retina coupled with specific feedforward connectivity to the visual cortex. Further, it is unclear whether, in the absence of the specific retinal model used here, such results would be observed in models

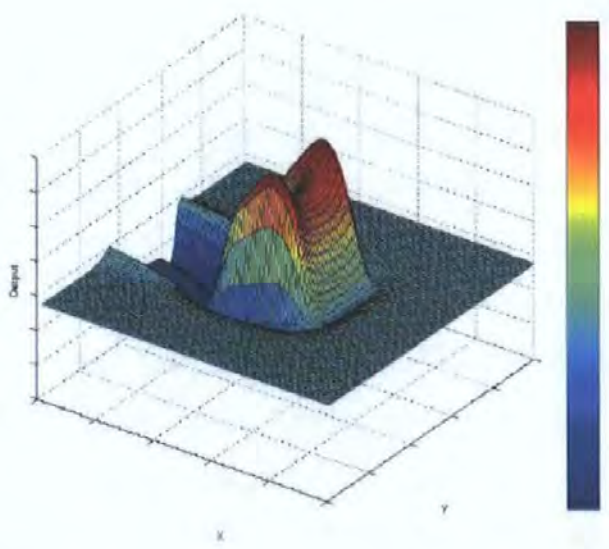

Figure 5.1: ON Retinal Ganglion Cells. The output of the on retinal ganglion cells can be seen for a square stimulus moving from left to right across the visual field in the X direction. The large output in the centre corresponds closely to the retinotopic representation of the actual spatial location of the stimulus in the visual field. The maximal output of cells coincides with the two leading corners of the stimulus. Temporal integration in turn leads to elevated regions of activity parallel to the trajectory of the stimulus.

where the stimulus is simply convolved with simple cell receptive fields (DeAngelis et al. 1995, Dayan & Abbott 2005).

Subsequent persistent activity can also be generated in the model and bears some similarities to the optical signal recorded in vivo, in particular the preference for orientation tunings parallel to stimulus trajectory. Thus far separate mechanisms have been considered, NMDA and AMPA/$GABA_B$ and connection densities, respectively. However, uncertainty with respect to the experimental protocols and disparities between the optical and computational data dictate that resolving the precise mechanisms involved will constitute the majority of future work. As such the following considerations need to be addressed.

Orientation Map Statistics. Preliminary investigation of the two dimensional spatio-orientation parameter space of cell populations reported in Section 4.2.1 does produce similar results to the experimental data. Whilst encouraging a more thorough study is warranted to resolve inconsistencies and to produce a more rigorous hypothesis of the underlying mechanisms. The relative distribution of iso-orientation domains plays a significant role in the observed population activity. Biases clearly exist in the orientation map used herein and biases are observed in the orientation statistics of natural scenes (Coppola, Purves, McCoy & Purves 1998). It is less clear whether such a bias is a general feature of cortical orientation maps in area 17 of the cat. Clarification of the precise statistics of such maps will give a more solid basis on which to determine the cortical microcircuitry that generates the observed population activity. In addition, the source of the latency between orientation activity and spatial activation needs to be established. A comprehensive understanding of these experimental data is seen as a fundamental prerequisite to computational modelling of the more recent unpublished optical imaging data by Jancke.

Persistent Activity through Propagation Delays. In perhaps the simplest case, persistent activity observed at a given spatial location may result from increasingly distant presynaptic input. This would require a relatively precise relationship between the velocity of the retinotopic projection of the stimulus and the synaptic propagation velocity. Under such a regime the postsynaptic potentials of spatially sequential activated cells would temporally overlap at a given cortical location. This may be resolved simply by clarification of the specific experimental protocol, or may require further computation studies.

Interpretation of Voltage Sensitive Dye Signal. Neurite activity would appear to be the dominant component of optical signals from voltage sensitive dyes (Ebner & Chen 1995, Grinvald, Lieke, Frostig & Hildesheim 1994). This is in stark contrast to the

modelling work conducted thus far where the notional membrane potential of model cells (Section 3.3 equation (3.26)) is seen as an indicator of the optical signal. Such an inconsistency may necessitate the re-evaluation of current model results and serve as to direct future work. In particular the persistent signal has hitherto appeared severely attenuated in comparison to the initial response. However, the early signal generated directly by the stimulus will contain components generated by projections from layer 4 (both vertical and horizontal) and probably later 5, which in turn have larger EPSPs than those of the horizontal projections within layer 2/3 (Yoshimura et al. 2000). In addition, both X and Y pathways from the lateral geniculate nucleus projecting to area 17 are seen to innervate layer 2/3 as well as layer 4 (Humphrey et al. 1985, Lund et al. 1979, Payne & Peters 2001). Further, layer 1 receives projections from all cortical layers in area 17 and is comprised primarily of neurites. As this type of neuropil element potentially dominates any optical signal it would appear that the observed data are undoubtedly confounded by layer 1 activity. In addition, extrastriate projections to area 17 originate from a number of areas including area 18, area 19, PMLS, PLLS and area 21a (Symonds & Rosenquist 1984) and may also contribute to any optical signal, in particular PMLS and area 18. Nonetheless, delays between stimulus onset and corresponding neural responses can be, certainly in Macaque, significantly differ across cortical areas (Schmolesky, Wang, Hanes, Thompson, Leutgeb, Schall & Leventhal 1998) which may discount the contribution of certain areas to a feedback signal in layer 2/3. Accordingly, the contribution of layer 2/3 to the early part of the optical signal may be significantly less than that observed. Now consider that the persistent signal results primarily from, and is localised to, layer 2/3 then this part of the optical signal might be more comparable with the hypothesised layer 2/3 contribution to the early signal as many of the additional components such as extrastriate input, may be absent. Consequently the activity in layer 2/3 may be more consistent over time than

is initially suggested by the experimental data, and as a result closer to initial computational observations. Elucidation of this issue will be paramount to evaluating current computational data and directing future work. Further consideration of the specific connectivity between layers 2/3 and 5 (Gilbert & Wiesel 1983, Payne & Peters 2001, Stepanyants et al. 2008, Symonds & Rosenquist 1984) offers the possibility of a combined topological view of the two layers that is similar to layer 2/3 alone. As such layer 5 might be equally important in the generation of the persistent signal but is not visualised by the optical recording techniques. Translation to the computational model would suggest that current findings are biased and overestimate layer 2/3 activity as has been observed. This is clearly speculative and the assumption that the persistent activity is confined entirely to layer 2/3 is unrealistic. In spite of these caveats, this is a reasonable avenue of investigation. In a similar vein, the contribution of inhibitory GABAergic synapses to the optical signal may have been underestimated as their hyperpolarising influence on membrane potential rather than their synaptic potential has only been consider thus far. This is of particular relevance here given the extremely slow kinetics associated with $GABA_B$. Taken together, these issues highlight the significant contribution that this modelling study can make to elucidating how signals from voltage sensitive dyes should be interpreted. In order to bridge the gap between optical data and interpretation it may be necessary to consider additional single unit recordings.

Comparison of Stable States via NMDA and AMPA. One computational paradigm can achieve a stable attractor state by fast, AMPA like, glutamate receptors that is manifest as elevated activity in iso-orientation domains that are tuned to orientations oblique to the stimulus trajectory (see Figure 4.15). This stable state is abolished by the action of slow $GABA_B$ receptors. This is consistent with the distribution of fast, non-NMDA, glutamate receptors and slow $GABA_B$ receptors observed in cat visual cortex

(Allison, Kabara, Snider & Casagrande 1996, Douglas & Martin 1991, Fox, Sato & Daw 1989, Hirsch & Gilbert 1991, Rosier, Arckens, Orban & Vandesande 1993, Sato, Hata & Tsumoto 1999) and with the time scale of $GABA_B$ activity (Douglas & Martin 1991, Hirsch & Gilbert 1991). The maintenance of stable elevated activity in iso-orientation domains is demonstrated by Cai, Rangan, & McLaughlin (2005) for the purpose of explaining coherent spontaneous activity (Kenet et al. 2003, Tsodyks et al. 1999). Interestingly the dominant mechanism they employ is the slow glutamate transmitter NMDA. Thus, the model presented here offers the possibility of a significantly different means of generating comparable behaviour.

The Role of Different Receptor Types. The distribution of the glutamatergic and GABAergic receptors does not appear to be uniform across the different layers in area 17 of the cat. NMDA contribution to visually evoked response is observed in layer 2/3 and is questionably present in layer 4, 5 and 6 of adult cat, although it does appear to play a role in spontaneous activity (Fox et al. 1989, Sato et al. 1999). This appears in agreement with imaging studies of NMDA receptor sites which are mainly in layer 2/3 (Rosier et al. 1993). As mentioned previously, in this and other modelling studies, different receptors have been implicated in the generation of persistent cortical activity. Indeed $GABA_B$ does not currently play a significant role in modelling layer 4 processing yet its activity in layer 2/3 drives one computation paradigm (Figure 4.15) and is observed to play a role in all cortical layers (Douglas & Martin 1991, Hirsch & Gilbert 1991). This must be addressed in conjunction with the potential influence of layer 5 and the various feedback paths between all the layers, only some of which are currently represented. Whilst two possible microcircuits have been identified here, alternative schemes informed by a more complete anatomical picture must be considered.

Extrastriate Contribution to Persistent Activity. The observed persistent activity may result from feedback from extrastriate areas. It might be expected that the moving

stimulus would evoke activity in PMLS (equated with the motion specific area MT (Payne 1993)), however, this issue is unclear as the stimulus is relatively small. If the stimulus does induce activation of PMLS cells then it has been shown that this area makes feedback projections to layer 2/3 in area 17 (Rosier et al. 1993). In addition there are strong projections from area 18, an area that can be argued to be inseparable from area 17 (Payne & Peters 2001) and thus would be co-activated by the same stimulus. Other areas also project to area 17 although the relative latencies and selectivity of constituent cells mean that it is purely speculative as to whether they might provide feedback to layer 2/3 in area 17. Notwithstanding, it is reasonable to hypothesise that the persistent activity observed in the optical signal results from extrastriate feedback.

Implementation Resources. The avenues of investigation proposed above will undoubtedly require exploration of an extensive parameter space. It is envisaged that this will be achieved by exploiting available parallel computing resources in conjunction with optimisation techniques such as genetic algorithms. The later may also utilise existing results to seed initial populations and inform fitness functions.

List of references.

Albright, T. & Stoner, G. (1995), 'Visual motion perception.', *Proceedings of the National Academy of Sciences of the United States of America* **92**, 2433–2440.

Albus, K. & Beckmann, R. (1980), 'Second and third visual areas of the cat: Interindividual variability in retinotopic arrangement and cortical location.', *The Journal of Physiology* **299**, 247–276.

Alitto, H. & Usrey, W. (2003), 'Corticothalamic feedback and sensory processing.', *Current Opinion in Neurobiology* **13**(4), 440–445.

Allison, J., Kabara, J., Snider, R. & Casagrande, V. (1996), 'Gabab-receptor-mediated inhibition reduces the orientation selectivity of the sustained response of striate cortical neurons in cats.', *Visual Neuroscience* **13**(3), 559–566.

Anderson, P., Olavarria, J. & Sluyters, R. V. (1988), 'The overall pattern of ocular dominance bands in cat visual cortex.', *The Journal of Neuroscience* **8**(6), 2183–2200.

Arieli, A., Shoham, D., Hildesheim, R. & Grinvald, A. (1995), 'Coherent spatiotemporal patterns of ongoing activity revealed by real-time optical imaging coupled with single-unit recording in the cat visual cortex.', *Journal of Neurophysiology* **73**(5), 2072–2093.

Arieli, A., Sterkin, A., Grinvald, A. & Aertsen, A. (1996), 'Dynamics of ongoing activity: Explanation of the large variability in evoked cortical responses', *Science* **273**(5283), 1868–1871.

Barlow, H., Fitzhugh, R. & Kuffler, S. (1957), 'Change of organization in the receptive fields of the cat's retina during dark adaptation', *The Journal of Physiology* **137**(3), 338–354.

Barlow, H. & Levick, W. (1969), 'Changes in the maintained discharge with adaptation level in the cat retina.', *The Journal of Physiology* **202**(3), 699–718.

Bear, M., Connors, B. & Paradiso, M. (2000), *Neuroscience: Exploring the brain.*, Lippincott Williams and Wilkins.

Bender, K., Rangel, J. & Feldman, D. (2003), 'Development of columnar topography in the excitatory layer 4 to layer 2/3 projection in rat barrel cortex.', *The Journal of Neuroscience* **23**(25), 8759–8770.

Binzegger, T., Douglas, R. & Martin, K. (2004), 'A quantitative map of the circuit of cat primary visual cortex', *The Journal of Neuroscience* **24**, 8441–8453.

Bishop, P., Kozak, W. & Vakkur, G. (1962), 'Some quantitative aspects of the cat's eye: Axis and plane of reference, visual field co-ordinates and optics.', *The Journal of Physiology* **163**(3), 466–502.

Booch, G. (1993), *Object oriented analysis and design with applications.*, Benjamin-Cummings Publishing Company, Subs of Addison Wesley Longman, Inc.

Born, R. & Bradley, D. (2005), 'Structure and function of visual area mt.', *Annual Review of Neuroscience* **28**, 157–189.

Bosking, W., Zhang, Y., Schofield, B. & Fitzpatrick, D. (1997), 'Orientation selectivity and the arrangement of horizontal connections in tree shrew striate cortex', *The Journal of Neuroscience* **17**, 2112–2127.

Bringuier, V., Chavane, F., Glaeser, L., Y. & Frégnac (1999), 'Horizontal propagation of visual activity in the synaptic integration field of area 17 neurons', *Science* **283**, 695–699.

Burr, D. (2000), 'Motion vision: Are 'speed lines' used in human visual motion?', *Current Biology* **10**(12), R440–R443.

Buzás, P., Kovács, K., Ferecskó, A., Budd, J., Eysel, U. & Kisvárday, Z. (2006), 'Model-based analysis of excitatory lateral connections in the visual cortex', *The Journal of Comparative Neurology* **499**, 861–881.

Cai, D., DeAngelis, G. & Freeman, R. (1997), 'Spatiotemporal receptive field organization in the lateral geniculate nucleus of cats and kittens.', *The Journal of Neurophysiology* **78**(2), 1045–1061.

Cai, D., Rangan, A., & McLaughlin, D. (2005), 'Architectural and synaptic mechanisms underlying coherent spontaneous activity in V1.', *Proceedings of the National Academy of Sciences of the United States of America* **102**(16), 5868–5873.

Callaway, E. (1998), 'Local circuits in primary visual cortex of the macaque monkey.', *Annual Review of Neuroscience* **21**, 47–74.

Carandini, M. & Ferster, D. (2000), 'Membrane potential and firing rate in cat primary isual cortex', *The Journal of Neuroscience* **20**, 470–484.

Casagrande, V., Guillery, R. & Sherman, S. (2005), *Cortical function a view from the thalamus.*, Elsevier.

Casagrande, V. & Ichida, J. (2002), The lateral geniculate nucleus., *in* P. Kaufman & A. Alm, eds, 'Alder's physiology of the eye.', C. V. Mosby, St. Louis, MO, pp. 655–668.

Casti, A., Hayot, F., Xiao, Y. & Kaplan, E. (2008), 'A simple model of retina-lgn transmission.', *Journal of Computational Neuroscience* **24**(24), 235–252.

Cheney, W. & Kincaid, D. (2003), *Numerical mathematics and computing.*, Brooks Cole.

Cleland, B., Harding, T. & Tulunay-Keesey, U. (1979), 'Visual resolution and receptive field size: Examination of two kinds of cat retinal ganglion cell.', *Science* **205**(4410), 1015–1017.

Cleland, B. & Lee, B. (1985), 'A comparison of visual responses of cat lateral geniculate nucleus neurones with those of ganglion cells afferent to them.', *The Journal of Physiology* **369**, 249–268.

Cleland, B., Levick, W. & Sanderson, K. (1973), 'Properties of sustained and transient ganglion cells in the cat retina.', *The Journal of Physiology* **228**(3), 649–680.

Cohen, E. & Sterling, P. (1992), 'Parallel circuits from cones to the on-beta ganglion cell.', *European Journal of Neuroscience* **4**(6), 459–593.

Coppola, D., Purves, H., McCoy, A. & Purves, D. (1998), 'The distribution of oriented contours in the real world.', *Proceedings of the National Academy of Sciences of the United States of America* **95**(7), 4002–4006.

Cossart, R., Aronov, D. & Yuste, R. (2003), 'Attractor dynamics of network up states in the neocortex.', *Nature* **423**(6937), 283–288.

Crocker, R., Ringo, J., Wolbarsht, M. & Wagner, H. (1980), 'Cone contributions to cat retinal ganglion cell receptive fields.', *The Journal of General Physiology* **76**(6), 763–785.

Dacey, D., Packer, O., Diller, L., Brainard, D., Peterson, B. & Lee, B. (2000), 'Center surround receptive field structure of cone bipolar cells in primate retina.', *Vision Research* **40**(14), 1801–1811.

Dayan, P. & Abbott, L. (2005), *Theoretical neuroscience: Computational and mathematical modeling of neural systems.*, The MIT Press.

DeAngelis, G., Ohzawa, I. & Freeman, R. (1995), 'Receptive-field dynamics in the central visual pathways.', *Trends in Neuroscience* **18**(10), 451–458.

Douglas, R. & Martin, K. (1991), 'A functional microcircuit for cat visual cortex.', *The Journal of Physiology* **440**, 735–769.

Ebner, T. & Chen, G. (1995), 'Use of voltage-sensitive dyes and optical recordings in the central nervous system', *Progress in Neurobiology* **46**, 463–506.

Enroth-Cugell, C. & Robson, J. (1966), 'The contrast sensitivity of retinal ganglion cells of the cat', *The Journal of Physiology* **187**(3), 517–552.

Fain, G., Mathews, H., Cornwall, M. & Koutalos, Y. (2001), 'Adaptation in vertebrate photreceptors.', *Physiological Reviews* **81**(1), 117–151.

Ferster, D. & Miller, K. (2000), 'Neural mechanisms of orientation selectivity in the visual cortex', *Annual Review of Neuroscience* **23**, 441–471.

Fiser, J., Chiu, C. & Weliky, M. (2004), 'Small modulation of ongoing cortical dynamics by sensory input during natural vision.', *Nature* **431**(7008), 573–578.

Fitzpatrick, D. (2000), 'Cortical imaging: Capturing the moment', *Current Biology* **10**, R187–R190.

Fox, K., Sato, H. & Daw, N. (1989), 'The location and function of NMDA receptors in cat and kitten visual cortex.', *The Journal of Neuroscience* **9**(7), 2443–2454.

Geisler, W. (1999), 'Motion streaks provide a spatial code for motion direction.', *Nature* **400**(6739), 65–69.

Geisler, W., Albrecht, D., Crane, A. & Stern, L. (2001), 'Motion direction signals in the primary visual cortex of cat and monkey.', *Visual Neuroscience* **18**(4), 501–516.

Gerstner, W. & Kistler, W. (2002), *Spiking Neuron Models: Single Neurons, Populations, Plasticity*, Cambridge University Press, New York.

Gibber, M., Chen, B. & Roerig, B. (2001), 'Direction selectivity of excitatory and inhibitory neurons in ferret visual cortex.', *Neuroreport* **12**(10), 2293–2296.

Gilbert, C., Das, A., Ito, M., Kapadia, M. & Westheimer, G. (1996), 'Spatial integration and cortical dynamics.', *Proceedings of the National Academy of Sciences of the United States of America* **93**(2), 615–622.

Gilbert, C. & Wiesel, T. (1983), 'Clustered intrinsic connections in cat visual cortex', *The Journal of Neuroscience* **3**, 1116–1133.

Grand, Y. L. (1968), *Light, colour and vision.*, Chapman & Hall.

Grinvald, A., Lieke, E., Frostig, R. & Hildesheim, R. (1994), 'Cortical point-spread function and long-range lateral interactions revealed by real-time optical imaging of macaque monkey primary visual cortex', *The Journal of Neuroscience* **14**, 2545–2568.

Guillery, R. (1995), 'Anatomical evidence concerning the role of the thalamus in corticocortical communication: A brief review.', *Journal of Anatomy* **187**(3), 583–592.

Guillery, R. & Sherman, S. (2002), 'Thalamic relay functions and their role in corticocortical communication: Generalizations from the visual system.', *Neuron* **33**(2), 163–175.

Harvey, I. (2001), Artificial evolution: A continuing saga., *in* T. Gomi, ed., 'Evolutionary robotics from intelligent robotics to artificial life', Springer, Berlin , Heidelberg, p. pp139.

Hennig, M., Funke, K. & Wörgötter, F. (2002), 'The influence of different retinal subcircuits on the nonlinearity of ganglion cell behavior', *The Journal of Neuroscience* **22**(19), 8726–8738.

Hirsch, J. & Gilbert, C. (1991), 'Synaptic physiology of horizontal connections in the cat's visual cortex', *The Journal of Neuroscience* **11**, 1800–1809.

Hirsch, J., Martinez, L., Alonso, J.-M., Desai, K., Pillai, C. & Pierre, C. (2002), 'Synaptic physiology of the flow of information in the cat's visual cortex in vivo.', *The Journal of Physiology* **540**, 335–350.

Hubel, D. (1995), 'Eye, brain and vision.', *Scientific American Library* p. 240 pp.

Humphrey, A., Sur, M., Uhlrich, D. & Sherman, S. (1985), 'Projection patterns of individual x- and y-cell axons from the lateral geniculate nucleus to cortical area 17 in the cat.', *The Journal of Comparative Neurology* **233**(2), 159–189.

Issa, N., Trepel, C. & Stryker, M. (2000), 'Spatial frequency maps in cat visual cortex.', *The Journal of Neuroscience* **20**(22), 8504–8514.

Jakiela, H., Enroth-Cugell, C. & Shapley, B. (1976), 'Adaptation and dynamics in X-cells and Y-cells of the cat retina.', *Experimental Brain Research* **24**(4), 335–342.

Jancke, D. (2000), 'Orientation formed by a spot's trajectory: A two-dimensional population approach in primary visual cortex.', *The Journal of Neuroscience* **20**(RC86), 1–6.

Jones, J. & Palmer, L. (1987), 'The two-dimensional spatial structure of simple receptive fields in cat striate cortex.', *The Journal of Neurophysiology* **58**(6), 1187–1211.

Josuttis, N. (2002), *Object oriented programming in C++.*, John Wiley and Sons Ltd.

Kandel, E., Schwartz, J. & Jessell, T. (2000), *Principles of neural science*, McGraw-Hill, New York.

Kaplan, E., Purpura, K. & Shapley, R. (1987), 'Contrast affects the transmission of visual information through the mammalian lateral geniculate nucleus.', *The Journal of Physiology* **391**, 267–288.

Kara, P. & Reid, R. (2003), 'Efficacy of retinal spikes in driving cortical responses.', *The Journal of Neuroscience* **23**(24), 8547–8557.

Kara, P., Reinagel, P. & Reid, R. (2000), 'Low response variability in simultaneously recorded retinal, thalamic, and cortical neurons.', *Neuron* **27**(3), 635–646.

Kenet, T., Bibitchkov, D., Tsodyks, M., Grinvald, A. & Arieli, A. (2003), 'Spontaneously emerging cortical representations of visual attributes.', *Nature* **425**(6961), 954–956.

Kenyon, G., Moore, B., Jeffs, J., Denning, K., Stephens, G., Travis, B., George, J., Theiler, J. & Marshak, D. (2003), 'A model of high-frequency oscillatory potentials in retinal ganglion cells.', *Visual Neuroscience* **20**(5), 465–480.

Kisvárday, Z., Tóth, E., Rausch, M. & Eysel, U. (1997), 'Orientation-specific relationship between populations of excitatory and inhibitory lateral connections in the visual cortex of the cat', *Cerebral Cortex* **7**, 605–618.

Knox, B. & Solessio, E. (2006), 'Shedding light on cones.', *The Journal of General Physiology* **127**(4), 355–358.

Kolb, H., Nelson, R. & Mariani, A. (1981), 'Amacrine cells, bipolar cells and ganglion cells of the cat retina: A golgi study.', *Vision Research* **21**(7), 1081–1114.

Kuffler, S., Fitzhugh, R. & Barlow, H. (1957), 'Maintained activity in the cat's retina in light and darkness.', *The Journal of General Physiology* **40**(5), 683–702.

Lamb, T. & Pugh, E. (2004), 'Dark adaptation and the retinoid cycle of vision.', *Progress in Retinal and Eye Research* **23**(3), 307–380.

Lankheet, M., Rowe, M., Wezel, R. V. & van de Grind, W. (1996), 'Spatial and temporal properties of cat horizontal cells after prolonged dark adaptation.', *Vision Research* **36**(24), 3955–3967.

Lennie, P., Hertz, G. & Enroth-Cugell, C. (1976), 'Saturation of rod pools in cat.', *Vision Research* **16**(9), 935–940.

Lev-Ram, V. & Grinvald, A. (1986), 'Ca^{2+}- and K^{+}-dependent communication between central nervous system myelinated axons and oligodendrocytes revealed by voltage-sensitive dyes.', *Proceedings of the National Academy of Sciences of the United States of America* **83**(17), 6651–6655.

LeVay, S., Connolly, M., Houde, J. & Essen, D. V. (1985), 'The complete pattern of ocular dominance stripes in the striate cortex and visual field of the macaque monkey.', *The Journal of Neuroscience* **5**(2), 486–501.

Levick, W. & Williams, W. (1964), 'Maintained activity of lateral geniculate neurones in darkness.', *The Journal of Physiology* **170**(3), 582–597.

Levick, W. & Zacks, J. (1970), 'Responses of cat retinal ganglion cells to brief flashes of light.', *The Journal of Physiology* **206**(3), 677–700.

Levine, M. & Troy, J. (1986), 'The variability of the maintained discharge of cat dorsal lateral geniculate cells.', *The Journal of Physiology* **375**(1), 339–359.

Livingstone, M. (1998), 'Mechanisms of direction selectivity in macaque V1.', *Neuron* **20**, 509–526.

Lund, J., Henry, G., MacQueen, C. & Harvey, A. (1979), 'Anatomical organization of the primary visual cortex (area 17) of the cat. a comparison with area 17 of the macaque monkey.', *The Journal of Comparative Neurology* **184**(4), 599–618.

MacLean, J., Watson, B., Aaron, G. & Yuste, R. (2005), 'Internal dynamics determine the cortical response to thalamic stimulation.', *Neuron* **48**(5), 811–823.

Malach, R., Amir, Y., Harel, M. & Grinvald, A. (1993), 'Relationship between intrinsic connections and functional architecture revealed by optical imaging and in vivo targeted biocytin injections in primate striate cortex', *Proceedings of the National Academy of Sciences of the United States of America* **90**, 10460–10473.

Mante, V., Frazor, R., Bonin, V., Geisler, W. & Carandini, M. (2005), 'Independence of luminance and contrast in natural scenes and in the early visual system.', *Nature Neuroscience* **8**(12), 1690–1697.

Martinez, L. & Alonso, J.-M. (2003), 'Complex receptive fields in primary visual cortex.', *The Neuroscientist* **9**(5), 317–331.

Martinez, L., Wang, Q., Reid, R., Pillai, C., Alonso, J.-M. & Sommer, F. (2005), 'Receptive field structure varies with layer in the primary visual cortex.', *Nature Neuroscience* **8**(3), 372–379.

Masland, R. (2001), 'The fundamental plan of the retina.', *Nature Neuroscience* **4**(9), 877–886.

Muckli, L., Kohler, A., Kriegeskorte, N. & Singer, W. (2005), 'Primary visual cortex activity along the apparent-motion trace reflects illusory perception.', *PLoS Biology* **3**(8), 1501–1510.

Mullikin, W., Jones, J. & Palmer, L. (1984), 'Receptive-field properties and laminar distribution of x-like and y-like simple cells in cat area 17.', *The Journal of Neurophysiology* **52**(2), 350–371.

Nakatani, K., Tamura, T. & Yau, K. (1991), 'Light adaptation in retinal rods of the rabbit and two other nonprimate mammals.', *The Journal of General Physiology* **97**(3), 413–435.

Nelson, R. (1977), 'Cat cones have rod input: A comparison of the response properties of cones and horizontal cell bodies in the retina of the cat.', *The Journal of Comparative Neurology* **172**(1), 109–135.

Newsome, W. & Salzman, C. (1993), 'The neuronal basis of motion perception.', *Ciba foundation symposium* **174**, 217–230.

Nowak, L., Azouz, R., Sanchez-Vives, M., Gray, C. & McCormick, D. (2003), 'Electrophysiological classes of cat primary visual cortical neurons in vivo as revealed by quantitative analyses', *Journal of Neurophysiology* **89**, 1541–1566.

O'Brien, B., Isayama, T., Richardson, R. & Berson, D. (2002), 'Intrinsic physiological properties of cat retinal ganglion cells.', *Journal of Physiology* **538**(3), 787–802.

Palm, W. I. (2005), *Introduction to MATLAB 7 for engineers.*, McGraw-Hill.

Payne, B. (1993), 'Evidence for visual cortical area homologs in cat and macaque monkey.', *Cerebral Cortex* **3**(1), 1–25.

Payne, B. & Peters, A. (2001), *The cat primary visual cortex.*, Academic Press Inc.

Peichl, L. & Wässle, H. (1979), 'Size, scatter and coverage of ganglion cell receptive field centres in the cat retina.', *The Journal of Physiology* **291**, 117–141.

Peters, A. & Payne, B. (1993), 'Numerical relationships between geniculocortical afferents and pyramidal cell modules in cat primary visual cortex.', *Cerebral Cortex* **3**(1), 69–78.

Peters, A. & Yilmaz, E. (1993), 'Neuronal organization in area 17 of cat visual cortex.', *Cerebral Cortex* **3**(1), 49–68.

Peterson, M., Li, B. & Freeman, R. (2004), 'The derivation of direction selectivity in the striate cortex.', *The Journal of Neuroscience* **24**(14), 3583–3591.

Rodieck, R. (1965), 'Quantitative analysis of cat retinal ganglion cell response to visual stimuli.', *Vision Research* **5**(12), 583–601.

Rodieck, R. & Stone, J. (1965), 'Analysis of receptive fields of cat retinal ganglion cells.', *Journal of Neurophysiology* **28**(5), 833–849.

Roerig, B. & Kao, J. (1999), 'Organization of intracortical circuits in relation to direction preference maps in ferret visual cortex', *The Journal of Neuroscience* **19**, 1–5.

Rosa, M., Schmid, L. & Calford, M. (1995), 'Responsiveness of cat area 17 after monocular inactivation: Limitation of topographic plasticity in adult cortex.', *The Journal of Physiology* **482**(3), 589–608.

Rosier, A., Arckens, L., Orban, G. & Vandesande, F. (1993), 'Laminar distribution of NMDA receptors in cat and monkey visual cortex visualized by [3h]-mk-801 binding.', *The Journal of Comparative Neurology* **335**(3), 369–380.

Sakmann, B. & Creutzfeldt, O. D. (1969), 'Scotopic and mesopic light adaptation in the cat's retina.', *Pflügers Archiv European Journal of Physiology* **313**(2), 168–185.

Sanseverino, E., Galletti, C. & Maioli, M. (1977), 'Maintained activity of single neurons in the cat visual cortex at different levels of retinal adaptation', *Brain Research* **124**(2), 251–261.

Sato, H., Hata, Y. & Tsumoto, T. (1999), 'Effects of blocking non-n-methyl-d-aspartate receptors on visual responses of neurons in the cat visual cortex.', *Neuroscience* **94**(3), 697–703.

Schmidt, K., Goebel, R., Löwel, S. & Singer, W. (1997), 'The perceptual grouping criterion of colinearity is reflected by anisotropies of connections in the primary visual cortex', *The European Journal of Neuroscience* **9**, 1083–1089.

Schmolesky, M., Wang, Y., Hanes, D., Thompson, K., Leutgeb, S., Schall, J. & Leventhal, A. (1998), 'Signal timing across the macaque visual system.', *Journal of Neurophysiology* **79**(6), 3272–3278.

Seriés, P., Lorenceau, J. & Frégnac, Y. (2003), 'The "silent" surround of v1 receptive fields: theory and experiments', *Journal of Physiology, Paris* **97**, 453–474.

Shapley, R. & C. Enroth-Cugell, C. (1984), Visual adaptation and retinal gain controls., *in* N. Osborne & G. Chader, eds, 'Progress in retinal research.', Pergamon, London., pp. 263–346.

Sharon, D., Jancke, D., Chavane, F., Na'aman, S. & Grinvald, A. (2007), 'Cortical response field dynamics in cat visual cortex.', *Cerebral Cortex* **17**, 2866–2877.

Sherman, S. (2005), Thalamic relays and cortical functioning., *in* V. Casagrande, R. Guillery & S. Sherman, eds, 'Cortical function a view from the thalamus.', Elsevier, pp. 107–126.

Sherman, S. & Guillery, R. (2002), 'The role of the thalamus in the flow of information to the cortex.', *Philosophical Transactions of the Royal Society of London. Series B, Biological Sciences* **357**(1428), 1695–1708.

Sillito, A. & Jones, H. (2002), 'Corticothalamic interactions in the transfer of visual information.', *Philosophical Transactions of the Royal Society of London. Series B, Biological Sciences* **357**(1428), 1739–1752.

Sincich, L. & Blasdel, G. (2001), 'Oriented axon projections in primary visual cortex of the monkey', *The Journal of Neuroscience* **21**, 4416–4426.

Sincich, L. & Horton, J. (2005), 'The circuitry of v1 and v2: Integration of color, form, and motion.', *Annual Review of Neuroscience* **28**, 303–326.

Smirnakis, S., Berry, M., Warland, D., Bialek, W. & Meister, M. (1997), 'Adaptation of retinal processing to image contrast and spatial scale.', *Nature* **386**(6620), 69–73.

Smith, R. & Sterling, P. (1990), 'Cone receptive field in cat retina computed from microcircuitry.', *Visual Neuroscience* **5**(5), 453–461.

Snodderly, D. & Gur, M. (1995), 'Organization of striate cortex of alert, trained monkeys (macaca fascicularis): Ongoing activity, stimulus selectivity, and widths of receptive field activating regions.', *Journal of Neurophysiology* **74**(5), 2100–2125.

Somogyi, P., Kisvárday, Z., Martin, K. & Whitteridge, D. (1983), 'Synaptic connections of morphologically identified and physiologically characterized large basket cells in the striate cortex of cat', *Neuroscience* **10**, 261–294.

Song, S., Miller, K. & Abbott, L. (2000), 'Competitive hebbian learning through spike-timing-dependent synaptic plasticity', *Nature Neuroscience* **3**, 919–926.

Stein, J., Johnson, S. & Berson, D. (1996), 'Distribution and coverage of beta cells in the cat retina.', *The Journal of Comparative Neurology* **372**(4), 597–617.

Steinberg, R. (1971), 'Incremental responses to light recorded from pigment epithelial cells and horizontal cells of the cat retina', *The Journal of Physiology* **217**(1), 93–110.

Stepanyants, A. & Chklovskii, D. (2005), 'Neurogeometry and potential synaptic connectivity', *Trends in Neuroscience* **28**, 387–394.

Stepanyants, A., Hirsch, J., Martinez, L., Kisvárday, Z., Ferecskó, A. & Chklovskii, D. (2008), 'Local potential connectivity in cat primary visual cortex', *Cerebral Cortex* **18**, 13–28.

Sterling, P. (1999), 'Deciphering the retina's wiring diagram.', *Nature Neuroscience* **2**(10), 851–853.

Stone, J. (1978), 'The number and distribution of ganglion cells in the cat's retina.', *The Journal of Comparative Neurology* **180**(4), 753–771.

Stone, J. & Keens, J. (1980), 'Distribution of small and medium-sized ganglion cells in the cat's retina.', *The Journal of Comparative Neurology* **192**(2), 235–246.

Symes, A. & Wennekers, T. (2009), 'Spatiotemporal dynamics in the cortical microcircuit: a modelling study of primary visual cortex layer 2/3.', *Neural Networks* **22**, 1079–1092.

Symonds, L. & Rosenquist, A. (1984), 'Laminar origins of visual corticocortical connections in the cat.', *The Journal of Comparative Neurology* **229**(1), 39–47.

Tamura, T., Nakatani, K. & Yau, K. (1989), 'Light adaptation in cat retinal rods.', *Science* **245**(4919), 755–758.

Tanigawa, H., Wang, Q. & Fujita, I. (2005), 'Organization of horizontal axons in the inferior temporal cortex and primary visual cortex of the macaque monkey', *Cerebral Cortex* **15**, 1887–1899.

Thomson, A. & Bannister, A. (2003), 'Interlaminar connections in the neocortex.', *Cerebral Cortex* **13**(1), 5–14.

Tsodyks, M., Kenet, A., Grinvald, A. & Arieli, A. (1999), 'Linking spontaneous activity of single cortical neurons and the underlying functional architecture.', *Science* **286**(5446), 1943–1946.

Tucker, T. & Katz, L. (2003), 'Spatiotemporal patterns of excitation and inhibition evoked by the horizontal network in layer 2/3 of ferret visual cortex', *The Journal of Neurophysiology* **89**, 488–500.

Tumosa, N., McCall, M., Guido, W. & Spear, P. (1989), 'Responses of lateral geniculate neurons that survive long-term visual cortex damage in kittens and adult cats.', *The Journal of Neuroscience* **9**(1), 280–298.

Tusa, R., Palmer, L. & Rosenquist, A. (1978), 'The retinotopic organization of area 17 (striate cortex) in the cat.', *The Journal of Comparative Neurology* **177**(2), 213–235.

Usrey, W., Reppas, J. & Reid, R. (1999), 'Specificity and strength of retinogeniculate connections.', *Journal of Neurophysiology* **82**(6), 3527–3540.

Vakkur, G. J. & Bishop, P. O. (1963), 'The schematic eye in the cat.', *Vision Research* **3**(7-8), 357–381.

Valeton, J. & Norren, D. V. (1983), 'Light adaptation of primate cones: An analysis based on extracellular data', *Vision Research* **23**(12), 1539–1547.

Valois, R. D. & Cottaris, N. (1998), 'Inputs to directionally selective simple cells in macaque striate cortex.', *Proceedings of the National Academy of Sciences of the United States of America* **95**(24), 14488–14493.

Valois, R. D., Cottaris, N., Mahon, L., Elfar, S. & Wilson, J. (2000), 'Spatial and temporal receptive fields of geniculate and cortical cells and directional selectivity.', *Vision Research* **40**, 3685–3702.

van der Togt, C., Spekreijse, H. & Supér, H. (2005), 'Neural responses in cat visual cortex reflect state changes in correlated activity.', *European Journal of Neuroscience* **22**(2), 465–475.

Wässle, H., Boycott, F. & Illing, R. (1981), 'Morphology and mosaic of on- and off-beta cells in the cat retina and some functional considerations.', *Proceedings of the Royal Society of London. Series B, Biological Sciences* **212**(1187), 177–195.

Wohrer, A., Kornprobst, P. & Viéville, T. (2006), 'Contrast gain control through a feedback in the retina.', *Neurocomp 2006. Premiere conference francophone de Neurosciences Computationelles* .

Wörgötter, F., Eyding, D., Macklis, J. & Funke, K. (2002), 'The influence of the corticothalamic projection on responses in thalamus and cortex.', *Philosophical Transactions of the Royal Society of London. Series B, Biological Sciences* **357**(1428), 1823–1834.

Wörgötter, F. & Eysel, U. (1989), 'Axis of preferred motion is a function of bar length in visual cortical receptive fields.', *Experimental Brain Research* **76**(2), 307–314.

Wyszecki, G. & Stiles, W. (1967), *Colour science: Concepts and methods, quantitative data and formulas.*, John Wiley & Sons Inc.

Yoshimura, Y., Sato, H., Imamura, K. & Watanabe, Y. (2000), 'Properties of horizontal and vertical inputs to pyramidal cells in the superficial layers of the cat visual cortex.', *The Journal of Neuroscience* **20**(5), 1931–1940.

LIST OF REFERENCES.

Chapter 6

Bound copies of published papers.

Neural Networks 22 (2009) 1079–1092

Contents lists available at ScienceDirect

Neural Networks

journal homepage: www.elsevier.com/locate/neunet

2009 Special Issue

Spatiotemporal dynamics in the cortical microcircuit: A modelling study of primary visual cortex layer 2/3

Andrew Symes, Thomas Wennekers *

Centre for Theoretical and Computational Neuroscience, Portland Square Building, Room A218, University of Plymouth, PL4 8AA Plymouth, Devon, United Kingdom

ARTICLE INFO

Article history:
Received 3 February 2009
Received in revised form 20 May 2009
Accepted 14 July 2009

Keywords:
Lateral connections
Voltage sensitive dye
Mean field model
Extracellular stimulation
Inhibition

ABSTRACT

The plexus of long and short range lateral connections is a prominent feature of the layer 2/3 microcircuit in the primary visual cortex. Despite the scope for possible functionality, the interdependence of local and long range circuits is still unclear. Spatiotemporal patterns of activity appear to be shaped by the underlying connectivity architecture and strong inhibition. A modelling study has been conducted to capture population activity that has been observed in vitro using voltage sensitive dyes. The model demonstrates that the precise spatiotemporal spread of activity seen in the cortical slice results from long range connections that target specific orientation domains whilst distinct regions of suppressed activity are shown to arise from local isotropic axonal projections. Distal excitatory activity resulting from long range axons is shaped by local interneurons similarly targeted by such connections. It is shown that response latencies of distal excitation are strongly influenced by frequency dependent facilitation and low threshold characteristics of interneurons. Together, these results support hypotheses made following experimental observations in vitro and clearly illustrate the underlying mechanisms. However, predictions by the model suggest that in vivo conditions give rise to markedly different spatiotemporal activity. Furthermore, opposing data in the literature regarding inter-laminar connectivity give rise to profoundly different spatiotemporal patterns of activity in the cortex.

1. Introduction

Lateral connections are a prominent feature of the visual cortex and comprise the dominant synaptic input to layer 2/3 cortical cells (Binzegger, Douglas, & Martin, 2004). Such projections exhibit striking specificity in their patterns of connectivity (Bosking, Zhang, Schofield, & Fitzpatrick, 1997; Buzás et al., 2006; Gilbert & Wiesel, 1983; Kisvárday, Tóth, Rausch, & Eysel, 1997; Malach, Amir, Harel, & Grinvald, 1993; Schmidt, Goebel, Löwel, & Singer, 1997; Sincich & Blasdel, 2001; Tanigawa, Wang, & Fujita, 2005). Within layer 2/3, glutamatergic lateral connections appear to form two distinct circuits. Local axonal projections extend in an isotropic pattern over several hundred microns and synapse on cells of all orientation tunings. Long range connections can extend many times further. Evidence also shows that these connections tend to project anisotropically in directions that are coaxial with the orientation tuning of the presynaptic cell (Bosking et al., 1997; Schmidt et al., 1997; Sincich & Blasdel, 2001). In addition, such projections target postsynaptic cells that have a similar orientation tuning to the presynaptic cell. In contrast the inhibitory lateral circuitry of layer 2/3 appears far less extensive (Kisvárday et al., 1997). Such a proliferation of highly specific axonal projections suggests that they play an important role in cortical behaviour. As such, horizontal connections have been associated with a number of cortical functions; non-classical receptive fields (Seriés, Lorenceau, & Frégnac, 2003); orientation tuning (Ferster & Miller, 2000); motion selectivity (Seriés, George, Lorenceau, & Frégnac, 2002). To better understand the implications of such hypotheses we consider the spatiotemporal dynamics of both the local and long range microcircuits, and their interdependence.

In vitro focal extracellular stimulation of ferret layer 2/3 slices produces very specific spatiotemporal patterns of activity (Tucker & Katz, 2003a, 2003b). Voltage sensitive dye (VSD) techniques (Fitzpatrick, 2000) allowed the authors to image activity in vitro at the population level. Clear distinctions can be made in the patterns of activity proximal or distal to the stimulus site. Local activity is extensive and diffuse whilst distal activity is more discrete and correlated with iso-orientation domains. Inhibition plays a prominent role in activity observed both locally and distally. The authors hypothesised that various mechanisms such as frequency dependent facilitation and plasticity might underlie these observations. It is proposed here that these spatiotemporal patterns of excitatory and inhibitory activity result directly from the specific underlying microcircuitry and in particular the dichotomy of local and long range connection architectures. We present a mod-

* Corresponding author. Tel.: +44 1752 23 3593; fax: +44 1752 23 3349.
E-mail address: thomas.wennekers@plymouth.ac.uk (T. Wennekers).

0893-6080/$ – see front matter © 2009 Elsevier Ltd. All rights reserved.
doi:10.1016/j.neunet.2009.07.017

elling study which clearly demonstrates such behaviour through a combination of characteristic axonal projections and electrophysiological properties of cortical cells. Furthermore, the specific underlying mechanisms responsible for the observed data are clarified. In addition, the work presented here provides additional evidence regarding which elements are activated by extracellular stimulation, and the interpretation of VSD signals. Finally, predictions were made of the expected activity in the layer 2/3 lateral microcircuitry in vivo. Driving the layer 2/3 microcircuit by extralaminar input results in profoundly different spatiotemporal patterns of activity. Distal activity is significantly attenuated whilst proximal activity is more localised and does not regenerate the same spatiotemporal patterns during repeated stimulation.

A computational model has been developed based on a mean field premise representing a patch of layer 2/3 visual cortex. Detailed patterns of connectivity specific to excitatory and inhibitory cells are represented including both local and long range paradigms. The model also captures the differences in temporal characteristics exhibited by excitatory and inhibitory cells, and their associated synapses. Propagation delays are incorporated reflecting the different synaptic pathways.

2. Methods

A coarse grain modelling approach has been adopted with activity represented using a mean field model that describes the time dependent activity of cortical cells. The model represents a small patch of layer 2/3 of the primary visual cortex approximately 3 mm^2, using two arrays of cells, one excitatory the other inhibitory. Each set is arranged in a 51×51 grid, a cell at position (x, y) representing the activity at a corresponding spatial position on the cortical patch. Thus for 2601 evenly distributed locations on the cortical patch there is an excitatory and inhibitory model cell representing the average local activity of a small population of excitatory and inhibitory neurons. The time dependent activity of model cells is expressed as a series of ordinary differential equations that are numerically solved by iteration of Euler's method. Representation of both cells and synapses are influenced by Gerstner and Kistler (2002), Lumer, Edelman, and Tononi (1997) and Song, Miller, and Abbott (2000). The membrane potential, $V(x, y)$, of a model cell at location (x, y), is governed by

$$\tau \frac{dV(x,y,t)}{dt} = -(V(x,y,t) - V_r) - g_{ex}(V(x,y,t) - E_{ex}) - g_{in}(V(x,y,t) - E_{in}). \quad (1)$$

The resting potential of the cell is determined by V_r, and was set to -70 mV from the observation of the in vitro data that the population resting potential was close to the $GABA_A$ reversal potential (Tucker & Katz, 2003b). The passive membrane time constant, τ, for excitatory and inhibitory cells were representative of regular and fast spiking cells in the cat and took values of 10.4 ms and 7.6 ms respectively (Nowak, Azouz, Sanchez-Vives, Gray, & McCormick, 2003). The excitatory and inhibitory synaptic inputs to a cell, representing AMPA and $GABA_A$, are given by g_{ex} and g_{in}, respectively, with associated reversal potentials E_{ex} and E_{in}. AMPA and $GABA_A$ reversal potentials were set at 0 mV and -70 mV (Lumer et al., 1997).

As the phenomena under investigation have relatively brief temporal dynamics, only AMPA and $GABA_A$, with their comparatively rapid kinetics, are considered. In keeping with the notion that each model cell represents a number of individual neurons, connections between model cells similarly represent a collection of neurites and synapses. Connectivity is simplified further by modelling all synaptic input of a given type, i.e., AMPA or $GABA_A$, to a cell by a two-stage low-pass filter of the form

$$\tau_r \frac{dg}{dt} = -g + h \quad (2)$$

$$\tau_f \frac{dh}{dt} = -h + w \sum_{x,y} \phi(d) f(V(x,y,t - \Delta t)). \quad (3)$$

This represents essentially a difference of exponentials with τ_r and τ_f the rise and fall time constants for conductance changes in response to spikes. Rise and decay time constants were 0.5 ms and 2.4 ms for AMPA synapses; 1 ms and 7 ms for $GABA_A$ synapses (Lumer et al., 1997). The summation term of Eq. (3) is over all locations, (x, y), of cells that provide synaptic input. Thus for AMPA synaptic input this summation is over all excitatory cell locations, and for $GABA_A$ over all inhibitory cell locations. The distance between each of these cells and the cell that they provide synaptic input to is given by d. Synaptic efficacy is considered to decrease as the separation between pre- and postsynaptic cells increases and is reflected by the term $\phi(d)$. $f(V(x, y, t - \Delta t))$ is an activation function that determines the firing rate of cell at location (x, y) at time $t - \Delta t$ where t is the current time and Δt a propagation delay determined by d. Propagation delays were based on a conduction velocity of 0.2m/s in keeping with experimental data (Bringuier, Chavane, Glaeser, & Frégnac, 1999; Grinvald, Lieke, Frostig, & Hildesheim, 1994; Tucker & Katz, 2003b). The activation function is essentially the rectification model of Carandini and Ferster (2000). Spike threshold was the same for both excitatory and inhibitory cells at -54 mV (Carandini & Ferster, 2000). Gain in terms of spikes per mV had values of 2.5 spikes/mV and 10.0 spikes/mV for excitatory and inhibitory cells respectively. The value of w is determined by the type, excitatory or inhibitory, of pre- and post synaptic cells. It is a tuneable parameter that controls the relative strengths of the four connection types; excitatory to excitatory; excitatory to inhibitory; inhibitory to excitatory; and inhibitory to inhibitory. This makes the selection of gain parameters for the activation function somewhat arbitrary.

Modelling studies suggest that the number of synapses made between cells is a function of their separation (Stepanyants & Chklovskii, 2005; Stepanyants et al., 2008). It is assumed here that the number of synapses made between two cells reflects a putative connection strength. To reflect this connection strength, the efficacy of connections between cells is determined by a simple Gaussian function. Locally within layer 2/3, lateral connectivity is isotropic (Bosking et al., 1997; Buzás et al., 2006; Kisvárday et al., 1997; Malach et al., 1993; Roerig & Kao, 1999; Schmidt et al., 1997; Sincich & Blasdel, 2001; Tanigawa et al., 2005; Tucker & Katz, 2003b), with excitatory and inhibitory model cells making projections in a radially symmetric halo (Kisvárday et al., 1997). For local isotropic connections the connection efficacy, $\phi(d)$, is given by

$$\phi(d) = e^{-\frac{d^2}{2\sigma^2}}. \quad (4)$$

Data from Kisvárday et al. (1997) suggests that the density and extent of lateral excitatory connections in cat layer 2/3 is significantly greater than that of inhibitory connections. This characteristic is captured in the model by using different values of σ for connections from excitatory and connections from inhibitory cells. Whilst biological data suggests excitatory connections are 2–3 times more extensive than inhibitory connections (Kisvárday et al., 1997), results derived from modelling software (Stepanyants et al., 2008) would imply the two networks are more similar in extent. Here, connections from excitatory cells assume $\sigma = 300\ \mu m$ and those from inhibitory cells that $\sigma = 200\ \mu m$.

From Eq. (4), the efficacy of a connection from a presynaptic cell located at (x, y) to postsynaptic cell located at (x_j, y_j) is

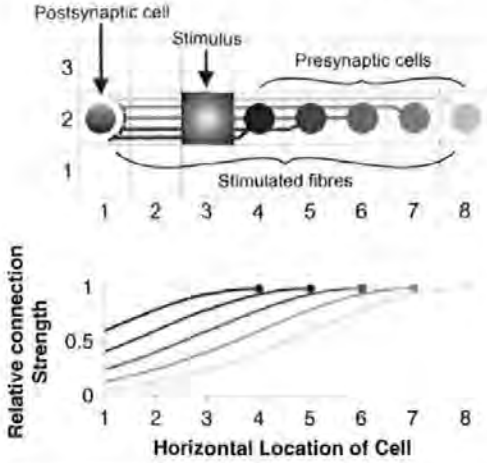

Fig. 1. Model of extracellular stimulation of axons. The upper panel depicts an 8×3 grid of model cells. An extracellular stimulus is applied at the shaded square location (3, 2). The 5 solid shaded circles to the right of the stimulus site indicate presynaptic cells and the shaded lines their axonal projections; circles and lines of the same shade denote a model cell and its axonal projection. The gradient shaded circle to the left of the stimulus site at location (1, 2) marks a postsynaptic cell. Axonal projections are considered to follow a straight line from pre- to postsynaptic cell. For this postsynaptic cell only those afferent axons shown will be activated by the stimulus as no other afferent axons lie on a straight line through the stimulus site. For modelling purposes an axon passes through the stimulus site if the (x, y) location of the stimulus cell lies on the line connection the (x, y) locations of pre- and postsynaptic cells. The lower panel shows the efficacy of connections between pre- and postsynaptic cells. Each circle corresponds to the horizontal location of a presynaptic cell in the upper panel. For each circle, the line of the same shade shows the connection efficacy of projections to progressively more distant horizontal locations. The value of each line where it crosses the y-axis (i.e., at horizontal location 1) shows the efficacy of the corresponding axonal projection at the postsynaptic cell.

$\exp(-0.5((x-x_j)^2+(y-y_j)^2)/\sigma^2)$. Model cells are also assumed to make long range connections to a number, n, of distal patches each of which has a centre located at (x_i, y_i), $i = 1, \ldots, n$. For local and long range connections, the combined efficacy for a connection from presynaptic cell at (x, y) to postsynaptic cell at (x_j, y_j) is

$$C(x, y, x_j, y_j) = \max_{i=1,\ldots,n} \left(e^{\frac{(x-x_j)^2+(y-y_j)^2}{2\sigma^2}}, a_i e^{\frac{(x_i-x_j)^2+(y_i-y_j)^2}{2\sigma_i^2}} \right). \quad (5)$$

The parameter a_i enables weighting of distal patchy connection strengths relative to each other and the local isotropic connections. The spatial extent, σ_i, of each patch was identical, with value 135 μm (Tucker & Katz, 2003b). As the current study is not specifically concerned with the relationship between long range patches and orientation tuning, their number, n, and location, (x_i, y_i) was arbitrarily chosen.

Both experimental (Nowak & Bullier, 1998a, 1998b) and theoretical evidence (McIntyre & Grill, 1999) indicate activity evoked by extracellular stimulation originates in axons rather than somata. Modelling the excitation of such fibres by extracellular stimulation is kept very simple. Consider the 8×3 grid of model cells in the upper panel of Fig. 1 where an extracellular stimulation is applied to location (3, 2), and is indicated by the diffusely shaded square. Lateral connections are considered to project in a straight line. Thus the postsynaptic model cell at location (1, 2), indicated by the gradient shaded circle (left most circle), will receive input from stimulated fibres that lie in a straight line between itself and the stimulus location. The presynaptic cells that project these fibres (the 5 solid shaded circles to the right of the stimulus site) are seen to be those cells that lie on a straight line that passes through the stimulus site to the postsynaptic cell.

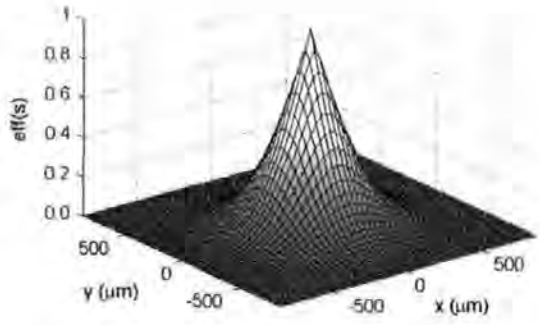

Fig. 2. Input from extracellular stimulation of axons. A 1.76 mm × 1.76 mm patch of cortex is modelled and an extracellular stimulus applied to the central location. The normalized efficacy of stimulated afferents for each location is shown. Efficacy is greatest for cells located at the stimulus site and drops of sharply for more distant cells.

From Fig. 1 the total efficacy of afferent projections to the postsynaptic cell is

$$\sum_{i=s+1}^{\infty} e^{-\frac{a_i^2}{2\sigma^2}}. \quad (6)$$

This is given the connection efficacy specified by Eq. (4). The horizontal location of the stimulus is given by s whilst a is the cortical distance between model cells. Using a continuous sum over all possible presynaptic cells, including the stimulus site, Eq. (6) can be rewritten as

$$\int_s^{\infty} e^{-\frac{x^2}{2\sigma^2}} dx. \quad (7)$$

Here x is the distance between pre- and postsynaptic cells and s the distance between postsynaptic cell and stimulus. Normalising, the efficacy function, $eff(s)$, is given by

$$eff(s) = 1 - erf\left(\frac{s}{\sqrt{2}\sigma}\right). \quad (8)$$

Fig. 2 shows the efficacy of afferents for a 1.76×1.76 mm cortical patch when a stimulus is applied at the centre of the grid. For postsynaptic cells at location (x, y), the z axis gives the efficacy of stimulated afferent axons. Axons are considered to project from excitatory cells with $\sigma = 300$ μm (see Eq. (4)). This model only captures orthodromic input and not antidromic propagation. Inclusion of antidromic activation would simply lead to a fractional elevation of all cell membrane potentials. Further, this may be dwarfed by potential amplification of axonal activity by chemical synapses (Kandel, Schwartz, & Jessell, 2000).

The afferent efficacy $eff(s)$ only considers local isotropic connections and so must be augmented to include contributions from long range anisotropic connections. However, such connections are very specific regarding pre- and postsynaptic cells. Of those anisotropic afferents that might augment $eff(s)$, contribution from axons of presynaptic cells at the stimulus site will dominate. Thus for a cell at location (x, y), including anisotropic afferents, gives the new definition

$$eff(x, y, x_s, y_s) = \max_{i=1,\ldots,n} \left(1 - erf\left(\frac{\sqrt{(x-x_s)^2+(y-y_s)^2}}{\sqrt{2}\sigma}\right), a_i e^{-\frac{\sqrt{(x-x_i)^2+(y-y_i)^2}}{\sqrt{2}\sigma_i}} \right). \quad (9)$$

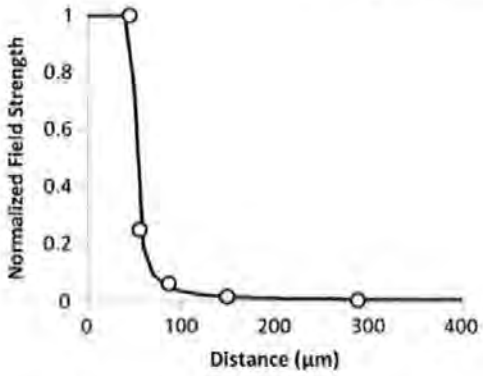

Fig. 3. Decay in field strength. The decay in electric field strength is plotted against horizontal distance from the electrode tip. The circles show normalised data taken directly from Figure 3 of Gimsa et al. (2006). The solid line shows the fitted estimate of field strength.

Here, (x_s, y_s) denotes the location of the extracellular stimulus; n specifies the number of distal patches that cells located at (x_s, y_s) make long range anisotropic projections to; (x_i, y_i) are the corresponding centres of each patch, $i = 1, \ldots, n$; and a_i controls the relative weighting of each patch.

Modelling studies suggest that extracellular stimulation with bipolar electrodes produces a very localised electric field (Gimsa, Schreiber, Habel, Flehr, van Rienen, & Gimsa, 2006). These predicted electric fields were used to estimate the decay in strength with horizontal distance. Fig. 3 shows the results for a round tipped electrode with an outer pole diameter of 125 μm as used for in vitro stimulation (Tucker & Katz, 2003b) (personal communication with author).

From Fig. 3 it can be seen that the spatial extent of the electric field may cover an area representing a number of model cells, rather than just one as in Fig. 1. To maintain simplicity, each model location stimulated by the field is treated independently. Thus an addition grid of model cells is created representing excitatory afferent axons. Each of these cells is governed by

$$\tau \frac{dV(x, y, t)}{dt} = -(V(x, y, t) - V_r) + wI(x, y). \tag{10}$$

This model is similar to Eq. (1), with $V(x, y, t)$ the axon membrane potential of axonal afferents at location (x, y), V_r the resting potential equal to −65 mV, τ the passive membrane time constant with value 1.5 ms (Beecroft, Alkhateeb, & Gaumond, 1994; Nowak & Bullier, 1998a) and $I(x, y)$ the field strength at location (x, y). The weight parameter, w, is adjusted to represent different stimulus strengths. From Eq. (10) a firing rate, $F(x, y, t - \Delta t)$, is determined using an activation function as in Eq. (3), with threshold −54 mV and gain 10 spikes/mV. From Eqs. (9) and (10), the input to a cell at location (x_i, y_i) from afferents stimulated at location (x_j, y_j) is

$$G(x_i, y_i, x_j, y_j) = eff(x_i, y_i, x_j, y_j)F(x_j, y_j, t - \Delta t). \tag{11}$$

A second set of afferent axon cells is created to represent stimulation of afferents from GABAergic cells. Eq. (3) can then be rewritten to include input from extracellular stimulation of afferents. $GABA_A$ synapses receive input from GABAergic afferents whilst AMPA synapses receive input from glutamatergic afferents. Given a cell at location (p, q), the general form of Eq. (3) for either type of synapse is then

$$\tau_f \frac{dh}{dt} = -h + w \sum_{x,y} \phi(d) f(V(x, y, t - \Delta t)) + w \sum_{x,y} G(p, q, x, y). \tag{12}$$

Interpreting signals from voltage sensitive dye experiments is not straightforward. The signal results from the combined activity of all membrane surfaces stained by the dye (Ebner & Chen, 1995; Grinvald et al., 1999). In terms of excitatory and inhibitory cell activity, the signal is biased by activity in the dendritic tree (Grinvald et al., 1994). To reflect the observation that the synaptic potential is slower than the current (Kandel et al., 2000) and that averaging across an area of cortex will temporally spread dendritic activity, synaptic input to a cell is low pass filtered to give the voltage sensitive dye signal

$$\tau \frac{dS(x, y)}{dt} = -S(x, y) + K(x, y). \tag{13}$$

Here $S(x, y)$ is the voltage sensitive dye signal generated by a model cell at location (x, y). $K(x, y)$ is the sum of synaptic inputs to the model cell located at (x, y), i.e., $g_{ex}(E_{ex} - V(x, y)) + g_{in}(E_{in} - V(x, y))$ of Eq. (1), whilst $\tau = 5$ ms. Recall that the model represents both excitatory and inhibitory cells. As such at each location (x, y) there is an inhibitory and excitatory model cell. To reflect the relative contribution of both excitatory and inhibitory cells to the voltage sensitive dye signal, the final signal at location (x, y), is given by

$$VSD(x, y) = pS_{ex}(x, y) + (1 - p)S_{in}(x, y). \tag{14}$$

The values $S_{ex}(x, y)$ and $S_{in}(x, y)$ are the excitatory and inhibitory cell voltage sensitive dye signals at (x, y) as defined by Eq. (13). The relative contribution of the two cell types to the VSD signal is controlled by p. As the combined surface area of excitatory dendritic trees is expected to be significantly larger than that attributable to inhibitory dendrites p was set to 0.8. Running simulations with $p = 0.7$ and 0.9 did not give rise to significantly different results.

3. Results

A mean field computational model representing the extensive lateral microcircuitry of primary visual cortex layer 2/3 has been constructed, including both local and long range lateral connectivity (Bosking et al., 1997; Buzás et al., 2006; Gilbert & Wiesel, 1983; Grinvald et al., 1994; Hirsch & Gilbert, 1991; Kisvárday et al., 1997; Malach et al., 1993; Schmidt et al., 1997; Sincich & Blasdel, 2001; Stepanyants et al., 2008; Tanigawa et al., 2005; Tucker & Katz, 2003b). This model has subsequently been used to determine the mechanisms that underlie specific patterns of spatiotemporal activity observed in vitro in layer 2/3 of ferret primary visual cortex (Tucker & Katz, 2003b). These authors present data largely at the population level in the form of optical signals from voltage sensitive dyes (Ebner & Chen, 1995; Fitzpatrick, 2000). A qualitative rather than quantitative comparison is only possible due to a number of uncertainties including; precisely what voltage sensitive dye (VSD) signals reflect (Grinvald et al., 1999); the exact stimulus parameters associated with observed data; and which neural elements are stimulated (McIntyre & Grill, 1999; Nowak & Bullier, 1998a, 1998b). In addition to the VSD data, simultaneous single cell intracellular recordings were made. Such combined recording techniques have demonstrated that optical signals from voltage sensitive dyes at the population level serve as a good predictor of subthreshold membrane activity observed in individual cells (Grinvald et al., 1999; Petersen, Grinvald, & Sakmann, 2003; Tucker & Katz, 2003b). Whilst the in vitro data revealed a number of different characteristic behaviours this study focuses on three; the spatiotemporal spread of activity; local inhibition; and reduction in time to peak of distal activity patches.

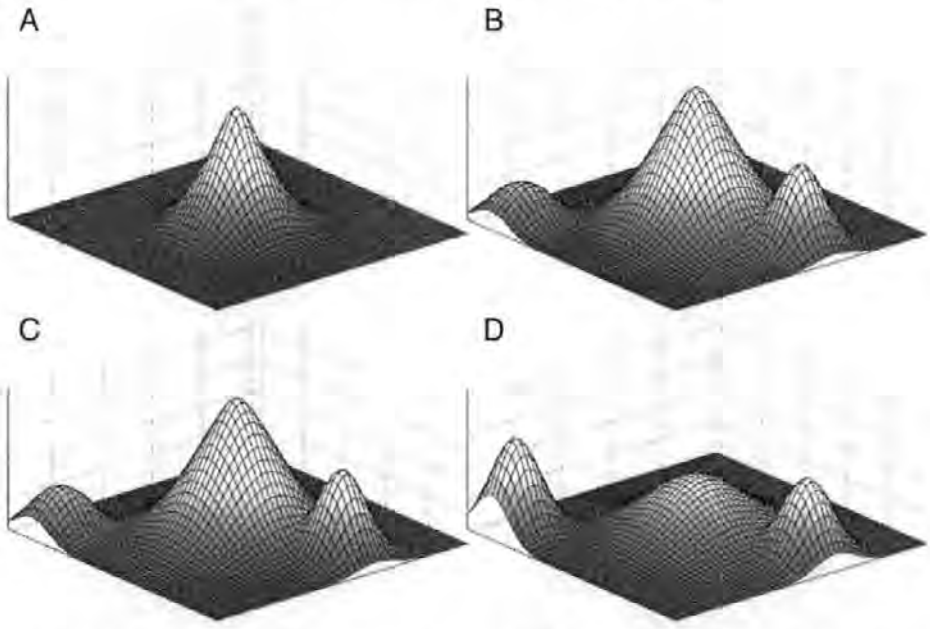

Fig. 4. Model spatiotemporal activity. Four weak focal pulses of an extracellular stimulus at 100 Hz were modelled at the centre of the grid. The plots A, B, C and D show the induced activity 3, 15, 25 and 40 ms after the initial pulse. As with the results of Tucker and Katz, an initial diffuse zone of activity centred on the stimulation site is followed by more distal patches of activity that emerge in panel B and are fully established in panel D. Lighter shades indicate higher activity.

3.1. Spatiotemporal activity

Tucker and Katz observed that in vitro 4 weak focal extracellular pulses at 100 Hz elicited a diffuse spreading zone of activity centred on the stimulus site. A number of discrete distal zones of activity, termed "optical clusters", were also produced. In the model, weak focal stimulation was applied to the central position of a 51×51 grid of cells representing a patch of layer 2/3 cortex ~ 3 mm^2. A distinct spatiotemporal pattern of activity similar to the in vitro data was produced and can be seen in Fig. 4. A large, spreading zone of activity is centred on the stimulus site, with two distal zones of activity beginning to emerge approximately 5 ms after the initial stimulus. These distal zones become more fully established by 40 ms as the diffuse zone is decaying. Activation spread follows specific excitatory pathways, but propagation delays induce typical temporal response dispersal. The emergence of distinct distal regions of activity is mediated by the precise targeting of long range connections. The spatial characteristics of a local diffuse zone and distal optical clusters are regenerated after each stimulus pulse. The diffuse zone 15 ms after the initial pulse has a full width at half maximum (FWHM) of approximately 527 μm, whilst the mean FWHM for the optical clusters is 342 μm. A closer inspection revealed that all cell activity was subthreshold. Hence the VSD signal shown in Fig. 4 results entirely from dendritic activity driven by excitation of lateral axons. The model makes two significant assumptions regarding extracellular stimulation. The first of these is that axons, rather than somata are activated by extracellular stimulation. The second is the efficacy with which this activity is propagated laterally. To test their validity, these two assumptions were tested with additional simulations. Testing the first assumption simply required activation of somata by the stimulus. The second required employing a different distribution for the efficacy of laterally propagated activity. In this case it was decided to use a Gaussian function. In the first validation simulation, activation of somata by extracellular stimulation was achieved by replacing Eq. (1) with

$$\tau \frac{dV(x,y,t)}{dt} = -(V(x,y,t) - V_r) - g_{ex}(V(x,y,t) - E_{ex}) - g_{in}(V(x,y,t) - E_{in}) + I(x,y). \quad (15)$$

The term $I(x, y)$ denotes the field strength at location (x, y). Furthermore, synaptic equation (3) rather than (12) is used. Adopting this stimulation protocol resulted in anomalous patterns of activity not observed in vitro, consisting of a deep crater situated at the electrode position that appeared immediately following stimulation (data not shown). This reduction in VSD signal was not due to inhibition but resulted from elevated membrane potentials of cells at this location. When the stimulus only activates axons, membrane potentials remain very low and similar for neighbouring cells. When only somata are activated, the membrane potential of such cells, V_a, must be suprathreshold in order to observe laterally propagating activity. However, as the stimulus is extremely localised (see Fig. 3) the membrane potential of neighbouring cells, V_n, is initially much lower and near the resting potential. Immediately following a stimulus pulse AMPA dominates synaptic activity. Since $V_a \gg V_n$ then $g_{ex}(E_{ex} - Va) \ll g_{ex}(E_{ex} - V_n)$ and so from Eqs. (13) and (14) the model voltage sensitive dye signal for cells neighbouring the stimulus site is much greater than that of cells activated by the stimulus. This result supports the proposition that axons rather than somata are excited by extracellular stimulation (McIntyre & Grill, 1999; Nowak & Bullier, 1998a, 1998b). For the second validation experiment, simulations were also conducted that replaced Eq. (8) by a Gaussian function as in Eq. (4). Under these conditions, a combination of the less peaked Gaussian function and propagation velocity resulted in a noticeable expanding ring of activity following stimulus pulses which gave the appearance of an inhibitory region (data not shown). This disparity of the validation results with the in vitro data supports the model for extracellular stimulation adopted here.

3.2. Local inhibition

A distinctive characteristic of the optical signals recorded by Tucker and Katz was a region of suppression centred on the stimulus site. Following each stimulus pulse activity in this inhibitory region was observed to deepen and expand. In some cases this appeared to form a ring around the stimulus site (Figure 7 in Tucker and Katz (2003b)) whilst in another instance

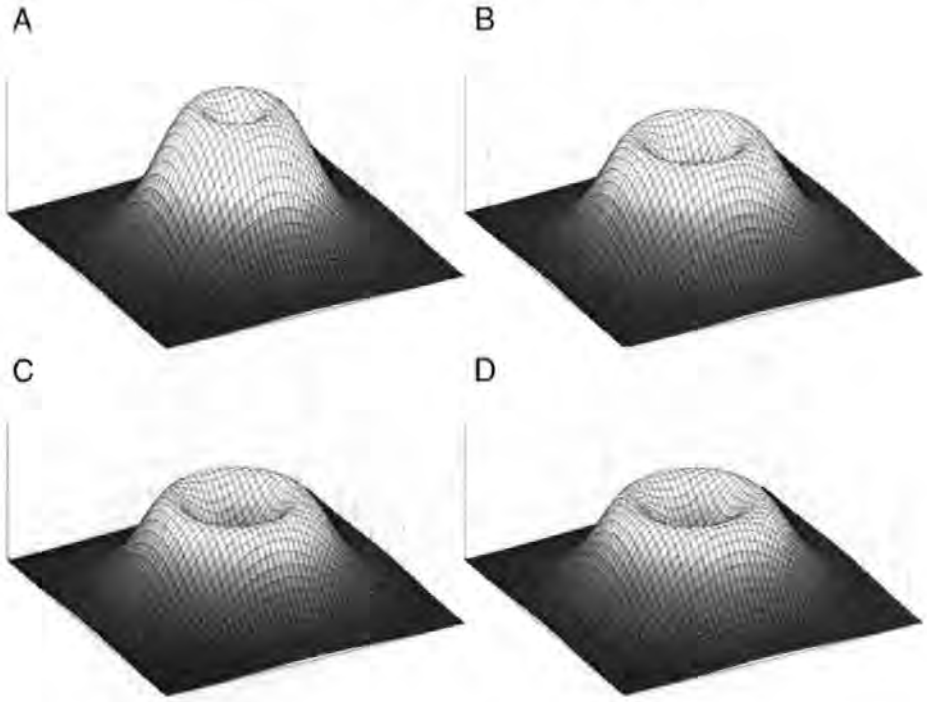

Fig. 5. Expanding region of inhibition. Four focal pulses of an extracellular stimulus at 100 Hz were modelled at the centre of the grid. The plots A, B, C and D show the induced activity 10, 20, 30 and 40 ms after the initial pulse. An expanding and deepening region of inhibition is centred on the stimulus site. Lighter shades indicate higher activity.

activity at the stimulus site was also suppressed forming more of a crater than a ring (their Fig. 5[1]). A similar crater region of suppression was also observed in the simulations. Increasing the pulse strength of stimuli from that used to generate Fig. 4 resulted in pronounced inhibition as seen in Fig. 5. Note that the long range connections have been excluded from this simulation in order to focus on the local inhibition. Since the distal patches lay beyond the suppression region they did not affect it in any way and could safely be excluded from this particular simulation. The diameter of the inhibited region expanded from 414 μm at 10 ms after the first stimulus (panel A of Fig. 5) to 621 μm at 40 ms after the first stimulus (panel D of Fig. 5). This region of inhibition was still expanding when the simulation stopped, 45 ms after the initial pulse, by which time it had reached a diameter of 759 μm. Inspection of cell activity revealed that suprathreshold activity occurred in the inhibitory population at the stimulus site. However, this only occurred following the second stimulus pulse and thus the inhibition observed in panel A of Fig. 5 is independent of suprathreshold interneuron activity. No such suprathreshold activity was observed in the excitatory population. In order to determine the contribution of suprathreshold inhibitory cell activity to the inhibition of Fig. 5, the gain term for the inhibitory cell activation function (Eq. (3)) was changed from 10 spikes/mV to 0 spikes/mV. Even with no contribution from inhibitory cells, a similar pattern of inhibition was observed to that of Fig. 5. For the same stimulus, between 10 ms and 40 ms following the first pulse the inhibitory region expanded from 414 μm to 552 μm, and reached a maximum of 690 μm when the simulation stopped at 45 ms. This corresponds to a reduction in the extent of the inhibitory region of 69 μm at both 40 ms and 45 ms, or 11% and 9% respectively. Hence the contribution of suprathreshold interneuron activity to the observed inhibitory region is very small. Rather, the strong inhibition shown in Fig. 5 is a consequence of direct stimulation of GABAergic axons and the resultant suppression of excitatory cells they target.

All activity in Fig. 5 is above the baseline signal observed at rest before stimulation. This is in contrast to in vitro results where VSD signals were observed to fall below resting values on occasions. The model VSD results remained positive largely due to; the proximity of the resting potential to the $GABA_A$ reversal potential; and inhibitory to excitatory connection weights. Elevating both parameters resulted in negative VSD signals in the inhibitory region (data not shown).

A search of the parameter space specifying w in Eq. (3) did not produce a ring of inhibition as observed by Tucker and Katz (2003b) and illustrated in their Fig. 7. However, the search was not exhaustive and employing an optimisation technique such a genetic algorithm might prove more successful. As an alternative hypothesis to retuning the w parameter it was hypothesised that the ring of inhibition may be an artefact of stimulated long range connections. Recall from Eq. (9) that stimulated long range fibres only contribute to the spatiotemporal activity of distal patches and not activity close to the stimulus site. To more accurately determine the contribution of long range fibres during extracellular stimulation the model of bouton density proposed by Buzás et al. (2006) was considered. Their model predicts the bouton density that the axonal projections of a presynaptic cell will give rise to at a given cortical location. For simplicity, it is assumed here that the bouton density at a given cortical location is analogous to connection strength of axonal projections to postsynaptic cells at the same location. The bouton density model has two components, a long range orientation tuned term and a local untuned term. For the long range connections investigated here, only the tuned component is considered which is defined by

$$G(x, y, \sigma)V(\phi, \kappa, \mu). \tag{16}$$

[1] This is more apparent in the complete set of time series data pertaining to this figure as kindly supplied by the author in the form of an animated movie.

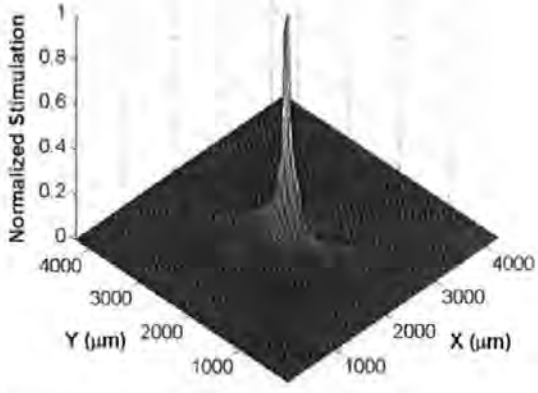

Fig. 6. Stimulation of long range fibres by extracellular stimulus. A focal extracellular stimulus is applied to the centre of a 100 × 100 grid of model cells. For each cell the normalised total of stimulated afferent long range axons is shown on the z-axis. Strongest stimulation occurs in afferents to cells coincident with the stimulus. Stimulation of afferents to regions neighbouring the stimulus site is significantly attenuated. This region of attenuation extends further in directions parallel with the orientation tuning observed at the stimulus site than in orthogonal directions.

The first term, $G(x, y, \sigma)$, is an isotropic Gaussian function that governs the spatial extent of the bouton distribution. The cortical location of interest is given by (x, y), whilst σ controls the spatial extent, The second term, $V(\phi, \kappa, \mu)$, is a von Mises distribution that controls bouton density orientation tuning. The orientation at location (x, y) relative to presynaptic tuning is given by ϕ; μ is the mean orientation at all bouton locations; and κ is the concentration parameter of the von Mises distribution. Averaging the population data of Buzás et al. (2006) gives μ and κ values of 0.05 and 0.935 respectively. To capture the anisotropy observed in long range layer 2/3 connections (Bosking et al., 1997; Kisvárday et al., 1997; Schmidt et al., 1997; Sincich & Blasdel, 2001; Tanigawa et al., 2005) $G(x, y, \sigma)$ was replaced by the Gaussian function $G(x, y, \sigma_=, \sigma_\perp, \theta)$ defined by

$$G(x, y, \sigma_=, \sigma_\perp, \theta) = \exp(-(ax^2 + bxy + cy^2)) \tag{17}$$

$$a = \left(\frac{\cos(\theta)}{\sigma_=}\right)^2 + \left(\frac{\sin(\theta)}{\sigma_\perp}\right)^2$$

$$b = \frac{\sin(2\theta)}{\sigma_=} - \frac{\sin(2\theta)}{\sigma_\perp}$$

$$c = \left(\frac{\sin(\theta)}{\sigma_=}\right)^2 + \left(\frac{\cos(\theta)}{\sigma_\perp}\right)^2.$$

For a presynaptic cell with orientation tuning θ, $\sigma_=$ and $\sigma_\perp$ control the spatial extent in directions parallel with and orthogonal to θ respectively. The spatial extent, σ, of long range connections of populations in layer 2/3 are 1105 μm and 889 μm (Buzás et al., 2006). For the model here the spatial extent of connections parallel with orientation tuning, $\sigma_=$, was set to 997 μm. In layer 2/3 of tree shrew primary visual cortex, the number of boutons in directions parallel with orientation tuning, $n_=$, is four times greater than the number, $n_\perp$, in orthogonal directions (Bosking et al., 1997). For the model, values of $\sigma_=$ and $\sigma_\perp$ satisfying this relationship are determined by

$$\frac{n_=}{n_\perp} = \frac{\int_{-\infty}^{\infty} e^{-\frac{p^2}{2\sigma_=^2}} dp}{\int_{-\infty}^{\infty} e^{-\frac{p^2}{2\sigma_\perp^2}} dp} = 4. \tag{18}$$

This condition leads to $\sigma_= = 4\sigma_\perp$ and so $\sigma_\perp = 249.25$ μm. As with the simplified model for extracellular stimulation presented earlier, long range axons are considered to project in a straight line. It is assumed that the contribution of long range fibres during extracellular stimulation is proportional to that part of the electric field in which they lie. To determine this first consider an axon from a presynaptic cell at location (x_{pre}, y_{pre}) to a postsynaptic cell located at (x_{post}, y_{post}). This axon can be defined by the line segment $ax + by + c = 0$ between (x_{pre}, y_{pre}) and (x_{post}, y_{post}). For each point $p = (x_a, y_a)$ satisfying $ax + by + c = 0$ between (x_{pre}, y_{pre}) and (x_{post}, y_{post}) there is a value $S(p)$ corresponding to the strength of the extracellular stimulus field at that location. The stimulation of a single long range fibre for an extracellular stimulus is then proportional to

$$H(x_{pre}, y_{pre}, x_{post}, y_{post}) = \sum_p G(x_{post} - x_{pre}, y_{post} - y_{pre}, \sigma_=, \sigma_\perp, \theta) V(\phi, \kappa, \mu) S(p). \tag{19}$$

For a given cortical location (a, b), the stimulation of all afferent long range fibres is proportional to

$$\int_{-\infty}^{\infty} \int_{-\infty}^{\infty} H(x, y, a, b) dx dy. \tag{20}$$

Here a patch of cortex of approximately 18 mm^2 was considered. An orientation map of area 18 (supplied by Zoltán Kisvárday) was used to determine the orientation of a 100 × 100 grid of cells at a resolution of 42.56 μm/cell. The electric field was based on a round tipped concentric bipolar electrode with outer pole radius of 125 μm positioned at the centre of the patch. The stimulation of afferent long range fibres was normalised and is presented in Fig. 6. The results of the model demonstrate that extracellular stimulation has the greatest influence on those long range fibres afferent to cells coincident with the stimulus. Stimulation of afferents to neighbouring cells is significantly reduced. This region is more extensive in directions parallel with the orientation tuning of cells coincident with the stimulating electrode than in orthogonal directions.

The combined stimulation of all afferents to a cell, local and long range, is used as an indicator of expected VSD activity. The stimulation of local excitatory afferents, A, and local inhibitory afferents, B, has been detailed previously in the methodology (e.g. Fig. 2). These can be combined with the stimulation of long range fibres, C, by $w_1A - w_2B + w_3C$ where w_1, w_2 and w_3 determine the relative contribution of each type of fibre. Fig. 7 shows a possible combination of local excitatory, local inhibitory and long range excitatory afferents. Using stimulation of afferents as an indicator of VSD signal reveals the customary diffuse isotropic region of activity centred on the stimulus site. However, now inhibition forms a distinct ring also centred on the stimulus site with a central region of elevated activity.

The simulated VSD signal and its first derivative at a point (x, y) close (207 μm) to the stimulus site are presented in Fig. 8. The derivative at time t is determined by $0.5(VSD(x, y, t + dt) - VSD(x, y, t - dt))/dt$ where $VSD(x, y, t)$ is the VSD signal at position (x, y) at time t and Δt is the simulation integration period. Maximum rate of decay of the VSD, indicated by the minimum of the derivative signal, was on average 7 ms after each stimulus pulse, coincident with the 7 ms figure observed in vitro. From Fig. 8 it can also be seen that the maximum and minimum of the VSD signal decreases following each stimulus pulse. For all points, (x, y), on the simulation grid, the rate of change of the VSD signal, $dVSD(x, y)$, was also calculated. At 7 ms after each stimulus pulse positive values of $dVSD(x, y)$ formed a circular region centred on the stimulus site. The diameter of this region progressively expanded from 1035 μm to 1311 μm with successive pulses. Again, a similar characteristic was observed in vitro where the region expanded from 302 ± 147 to 631 ± 164 μm (Tucker & Katz, 2003b).

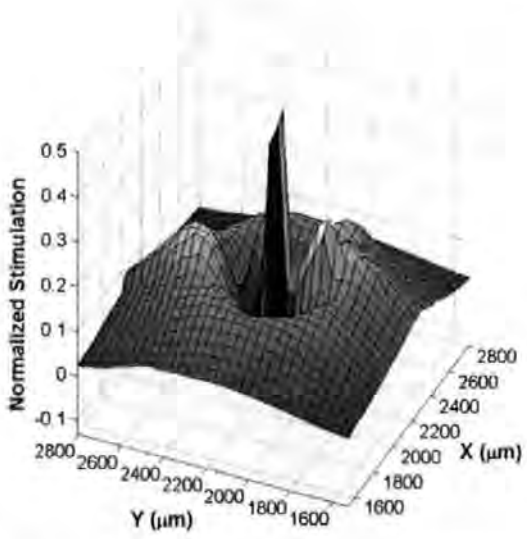

Fig. 7. Combined stimulated afferents from local and long range connections. The stimulation of local excitatory, local inhibitory and long range excitatory afferents is determined for a focal extracellular stimulation applied to the centre of a 100 × 100 grid of model cells. The stimulation of local inhibitory afferents is subtracted from the sum of local and long range stimulated afferents. A distinct ring of inhibition is observed in a more diffuse isotropic region of stimulation. The central 30 × 30 cells have been shown for clarity.

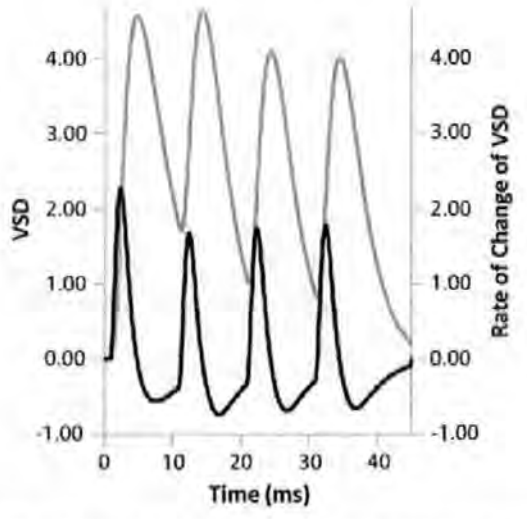

Fig. 8. VSD signal and first derivative near stimulus site. The light grey line presents the change in VSD signal with time for a point 207 μm from the stimulus site. The corresponding rate of change of this signal with time is indicated by the darker line.

3.3. *Extra-laminar stimulation*

The spatiotemporal patterns of activity presented thus far have resulted from extracellular stimulation of horizontal axons. It is unlikely that activity in vivo will originate exclusively from such processes. Rather activity observed in the horizontal microcircuitry of layer 2/3 will more likely be driven by spiking activity originating from other layers. To this end further studies were conducted in order to determine whether the same spatiotemporal patterns of activity presented in Fig. 4, and in particular in Fig. 5, would be expected in vivo. Maps generated by the neurogeometry model (Stepanyants et al., 2008) were used to estimate the number of synapses made between layer 4 and layer 2/3 cells. A Gaussian estimate of each map was determined from FWHM values. The resultant Gaussian parameter values used were $\sigma \approx 152$ μm, 134 μm, 115 μm, 101 μm for excitatory to excitatory; excitatory to inhibitory; inhibitory to excitatory; and inhibitory to inhibitory connections. Thus Eq. (9) was replaced by

$$eff(x, y, x_s, y_s) = e^{-\frac{(x-x_s)^2+(y-y_s)^2}{2\sigma^2}}. \tag{21}$$

The first point of note is that the spatial extent of vertical projection from layer 4 to layer 2/3 is smaller than that of lateral connections in layer 2/3. The second point of note is that unlike Eq. (9), Eq. (21) does not incorporate long range patchy connections. As a consequence only disynaptic routes exist from stimulus to distal patches. For the very strong stimulus values presented in Figs. 10 and 11, long range connections were not included as such stimuli may induce suprathreshold activity in distal sites thus long range connections for model cells were not specified. When long range connections were included for these stimulus strengths only weak subthreshold activity was observed in distal patches under parameter regimes 1–4 and thus the inclusion or exclusion of long range connections is irrelevant with regard to local activity. Higher, suprathreshold, activity was observed in distal patches during strong direct stimulation of layer 2/3. However, these simulations did not incorporate facilitation of distal interneurons as discussed in the following section. Such a mechanism would have significantly attenuated any activity in distal patches of excitatory cells.

Four parameter regimes were considered. Under the first, the axonal inputs from layer 4 were weighted the same as the lateral connections within layer 2/3, i.e., the same w parameter values used in Eq. (3) were applied to axonal inputs from layer 4. The second parameter regime made the unbiased assumption that all inputs from stimulation of layer 4 projections to layer 2/3 were weighted the same. The value was selected such that extracellular stimulation could produce suprathreshold activity in cells. Data from the neurogeometry model (Stepanyants et al., 2008) suggests weighting the extra-laminar inputs roughly in the ratio 21:3:3:2 for excitatory to excitatory; excitatory to inhibitory; inhibitory to excitatory and inhibitory to inhibitory connections. This ratio was thus used to determine weights for the third regime. Other modelling studies (Binzegger et al., 2004) suggest that for these connection types the ratio of total number of synapses is 5.4:4.9:1.6:1.7. Suppose that the volume, V, below the surface defined by the connection weight of Eq. (4) ($V = 2\pi\sigma^2$) is proportional to the total number of synapses of that connection type, e.g. excitatory to excitatory. Using the values of σ for connections from layer 4 to layer 2/3 gives weight ratios of $\frac{5.4}{2\pi 38^2} : \frac{4.9}{2\pi 30^2} : \frac{1.6}{2\pi 28^2} : \frac{1.7}{2\pi 30^2}$ or approximately 15:22:8:8. These values were used to determine weights for the fourth regime. The w value for excitatory to excitatory connections within layer 2/3 was used for excitatory to excitatory axonal inputs from layer 4 for each parameter regime. The connection weights of all other layer 4 axonal inputs were scaled to conform to the specified weight ratio.

Stimulus strengths up to that used for Fig. 5 result in similar spatiotemporal patterns of activity under all four parameter regimes. Each parameter regime gives rise to more compact local activity than observed when layer 2/3 is stimulated directly. For the latter case the FWHM of local activity 13 ms after the initial pulse is 515 μm. The FWHM observed 13 ms after the initial pulse for parameter regimes 1–4, is 410, 340, 344 and 344 μm respectively. All local activity in layer 2/3 was subthreshold under all parameter regimes and thus no distal activity was observed. Examples of the observed activity can be seen in Fig. 9. The vertical axis represents simulation time, the horizontal axis is radial distance from the centre of the stimulus site, with lighter shades indicating higher activity. Hence, activity is a cross-section of the two dimensional VSD signal. The particular cross-section is

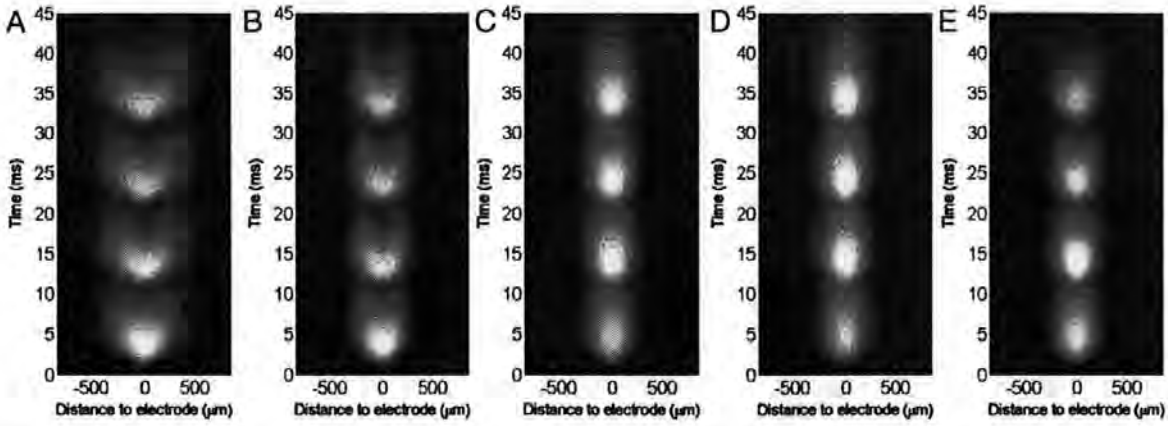

Fig. 9. Comparison of similarities between parameter regimes for extra-laminar input. For each panel the vertical axis is the simulation time; and the horizontal axis is the distance from the centre of the stimulus site with positive and negative distances indicating radial directions separated by 180 degree. The specific radial directions are unimportant due to the radial symmetry of the VSD signals about the stimulus site provided that optical clusters were not bisected. Brighter areas denote increased activity. Grey scales are specific to each panel, however zero activity is represented by the same shade in order to compare positive and negative regions. Panels B to E are from parameter regimes 1–4 whilst panel A shows activity when layer 2/3 is directly stimulated for comparison. The same stimulus as used for Fig. 5 was used for each panel.

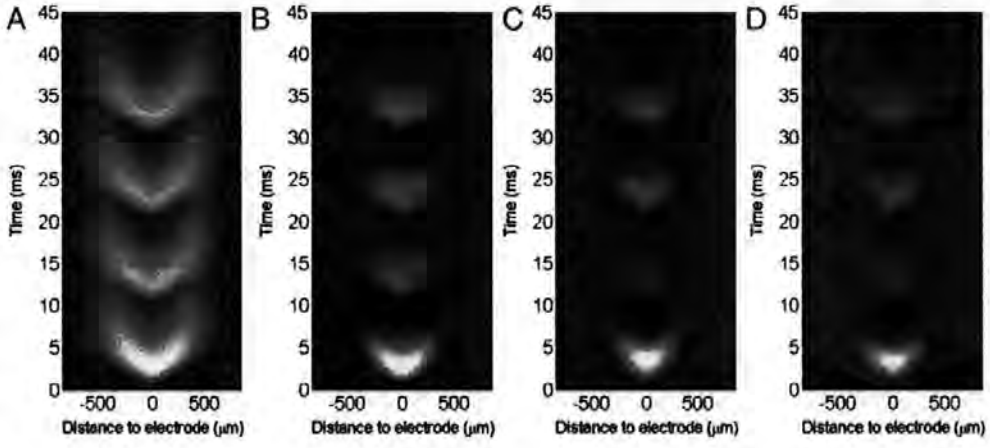

Fig. 10. Comparison of similarities between parameter regimes for strong extra-laminar input. Panels B to D show the activity generated by parameter regimes 1, 2 and 4 as a result of strong extra-laminar stimulation. For comparison, panel A shows activity when layer 2/3 is directly stimulated by the same strength stimulus. The grey scale conventions of Fig. 9 are adopted here. Direct stimulation of layer 2/3 results in similar activity being observed for weaker stimuli. Activity for parameter regimes 1, 2 and 4 are similar to each other and display significant attenuation of the optical signal for stimulus pulses 2–4. Activity below that observed at rest is indicated by the darkest regions and is only observed in panels B, C and D.

arbitrary as activity at a given instant has radial symmetry about the stimulus site provided an optical cluster is not bisected. Grey scales are relative to the range of values of each panel and thus quantitative comparisons should not be made between panels. However in all panels the same shade indicates zero activity, thus positive and negative regions can be distinguished. Panels B to E show the results from regimes 1–4 whilst panel A shows the activity observed during direct stimulation of layer 2/3 for comparison. The flattening of each ovoid region of activity and concomitant concaved upper edge indicates the appearance of an inhibitory region as observed in Fig. 5. From Fig. 9 it can be seen that inhibitory regions are present under regimes 1 and 4 (panels B and D) but are all but absent from regimes 2 and 3 (panels C and D).

Whilst Fig. 9 shows little difference in the activity observed under each parameter regime, a significant divergence in behaviour became apparent as stimulus strength was increased further. For stronger stimuli, local activity resulting from direct stimulation of layer 2/3 remains qualitatively similar to data recorded during weaker stimulation. This can be seen in panel A of Fig. 10 where the strongest stimulus produced activity characteristic of that seen in panel A of Fig. 9. Panels B, C and D of Fig. 10 show activity for parameter regimes 1, 2 and 4 using the same stimulus strength. Interestingly, under regime 1, which uses the same weights as in layer 2/3, increasing stimulus strength results in a significant attenuation of activity generated by stimulus pulses 2–4. Also of note are the regions where activity fell below that observed at rest (indicated by the darkest areas). Fig. 10 shows that parameter regimes 1, 2 and 4 result in qualitatively similar results under strong stimulation.

The most startling results are observed under regime 3. Panels A to D of Fig. 11 show activity observed for increasing stimulus strengths with panel D generated using the same stimulus strength as that for Fig. 10. As noted previously, inhibition was not initially observed under regime 3. Here it can be seen that inhibition is initially manifest as the abolition of activity following the final stimulus pulse. Stronger stimuli abolish activity increasingly earlier in the pulse train. Associated with the appearance of inhibition is a broadening of the local activity. From panel A of Fig. 11, the FWHM 33 ms after the first pulse is 616 μm compared with 354 μm from panel D of Fig. 9.

The VSD signal generated by the model was not always an accurate predictor of the concomitant membrane potential of model cells. Negligible VSD signals were observed in model cells when their corresponding membrane potentials deviated significantly from the resting potential. This is presumably because excitatory and inhibitory dendritic inputs cancel. To test the relationship between VSD and membrane potential the correlation coefficient was

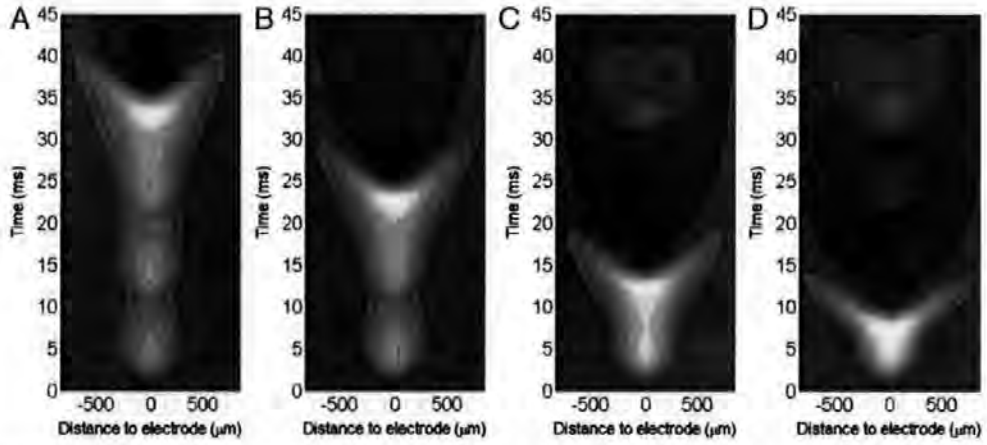

Fig. 11. Activity under parameter regime 3 for strong extra-laminar input. Panels A to D show the activity generated by parameter regime 3 as a result of increasing the strength of extra-laminar stimulation above that used for Fig. 10. The grey scale conventions of Fig. 9 are adopted here. The strongest stimulus strength, used for panel D, is the same as that used in Fig. 10. Under increasing stimulus strength inhibition becomes more apparent, attenuating the optical signal at earlier points in the pulse train. Regions of activity below that observed at rest are indicated by the dark areas. The region of local activity is also seen to broaden significantly in comparison with panel D of Fig. 9.

calculated between the two data sets $VSD(x, y, t)$ and $M(x, y, t)$, where $VSD(x, y, t)$ is the VSD signal at location (x, y) and time t; and $M(x, y, t)$ is the excitatory membrane potential at location (x, y) and time t. As model cells often displayed little or no activity, correlation coefficients were calculated for (x, y) values in the range $x = x_l, \ldots, x_u$ and $y = y_l, \ldots, y_u$. The value of t ranged over the entire duration of the simulation. Correlation coefficients were calculated for each parameter regime and for direct stimulation of layer 2/3 using stimulus strengths up to that used for Fig. 5. All correlation coefficients irrespective of parameter regime or range of (x, y) locations were very high, and lay in the range 0.81 to 0.99. Thus, whilst discrepancies were observed, in general the VSD signal is a good predictor of the excitatory membrane potential as observed in vitro (Tucker & Katz, 2003a, 2003b) and in vivo (Petersen et al., 2003).

3.4. Reduction in latency of distal activity

In vitro, the latency between extracellular stimulation and concomitant peak activity at distal patches decreased with successive pulses in a train of four at 100 Hz (Tucker & Katz, 2003b). The previous section has demonstrated that the activity of excitatory cells local to the stimulus site is always subthreshold. As excitatory cells are responsible for the long range patchy connectivity observed in layer 2/3 a simplified model was used to investigate the latency phenomenon. The model consisted of a number of axons driven by the extracellular stimulus and a single postsynaptic excitatory cell, and postsynaptic inhibitory cell. As the axons driven by the stimulus were separated by less than 70 μm, and only a single postsynaptic location was considered, synaptic efficacy as a function of pre- and postsynaptic cell separation, $\phi(d)$, was set to 1. Using the same parameters as specified in the methodology, the temporal pattern of activity at the distal site is shown in Fig. 12. Comparing the time of each peak in Fig. 12 with the time of the preceding stimulus pulse demonstrates a reduction with successive pulses, referred to as "acceleration" (Tucker & Katz, 2003b). For a range of weak stimulus strengths the mean reduction after each pulse is shown in Fig. 13 by circles. For comparison in vitro data is shown by crosses (taken directly from Figure 8 in Tucker and Katz (2003b)). Whilst the model data does show a reduction in latency it is clearly smaller than that observed in vitro. Investigation of the model revealed that a combination of interneuron membrane properties and synaptic time constants prohibited the rapid inhibitory effects observed in vitro.

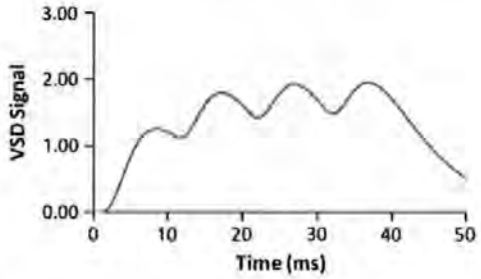

Fig. 12. Temporal response profile at a distal site. The activity recorded at the site of a distal patch is shown for the model.

A number of mechanisms might account for the discrepancy in latency reduction. Those initially considered in the model were spiking threshold; the temporal dynamics of synapses; and variation in conduction velocity. Each of these is now considered in turn. In vitro evidence suggests that lateral connections more readily induce a suprathreshold response in interneurons than excitatory cells (Hirsch & Gilbert, 1991). The relative depolarisation observed in some interneurons (Jonas, Bischofberger, Fricker, & Miles, 2004) would produce a similar behaviour in the model. Thus the resting potential of inhibitory cells was increased by 6 mV. Considering the second mechanism, the time course of synapses, experimental data shows significant variation. AMPA mediated postsynaptic currents can have considerably smaller time constants in hippocampal interneurons than their counterpart in excitatory cells (Jonas et al., 2004). In the rat, $GABA_A$ synapses show slightly smaller time constants than those used here (Szabadics, Tamás, & Soltesz, 2007) whilst in the mouse they show a large variation with a minimum decay time constants of 1.6 ms (Nusser, Naylor, & Mody, 2001). Furthermore the rise time and FWHM of postsynaptic potential can vary with postsynaptic cell type (Thomson, 1997). However, even significant reduction in the time constants of AMPA and $GABA_A$ synapses was insufficient to account for the reduction in latency observed in vitro. Even so, the rise and fall time constants of AMPA synapse on interneurons were reduced to 0.5 ms and 5 ms, whilst for $GABA_A$ synapses rise and fall time constants were reduced to 0.25 ms and 5 ms. The last of the three mechanisms, variation in conduction velocity is now considered. Any variation in the conduction velocity would be expected to disperse postsynaptic activity from a population of cells, as represented by a single model cell, over time. Furthermore, the extent of this dispersal would

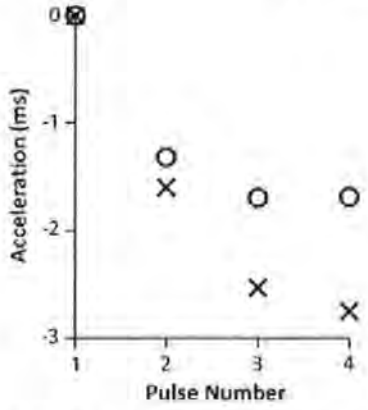

Fig. 13. Reduction in time to peak. The latency between a stimulus pulse and the corresponding peak activity (acceleration) is shown for a distal patch of activity. Successive stimulus pulses lead to a reduction in the latency. For comparison, model results are shown by circles and in vitro data by crosses. Model values represent the mean latency observed over a range of weak stimulus strengths.

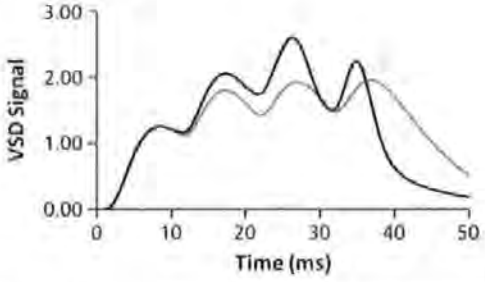

Fig. 14. Temporal response profile of distal site incorporating synaptic facilitation. The activity recorded at the site of a distal patch is shown for the model when facilitation is present and absent. The lighter grey line shows distal activity with no facilitation and is taken from Fig. 12. The darker line indicates activity at a distal site when EPSP facilitation of AMPA synapses with interneurons is incorporated. The result is a marked decrease in the latency at the distal site as seen in the sharpening of activity peaks.

be amplified with increasing distance between pre- and postsynaptic cells. Subsequent postsynaptic temporal integration of such distributed activity may result in a latency reduction between successive stimulus pulses. This is of particular interest given the quoted conduction velocity 0.24 ± 0.2 m/s (Tucker & Katz, 2003b) which suggests a large standard deviation of 0.2 m/s. Others also suggest a large variation in conduction velocity (Grinvald et al., 1994) and propagation delay (Hirsch & Gilbert, 1991). To capture this variation, conduction velocity, in μm/ms, was assumed to be normally distributed $N(\mu_v, \sigma_v)$ where μ_v is mean velocity and σ_v the standard deviation of the velocity. Maximum and minimum velocities, v_{max} and v_{min}, were constrained by

$$v_{max} = \mu_v + \sqrt{-2\ln(T)} \tag{22}$$

$$v_{min} = \max(1, \mu_v - \sqrt{-2\ln(T)}). \tag{23}$$

The threshold value T was set to 0.1. As a result the activation function, $f(V(x, y, t - \Delta t))$, of Eq. (3) was replaced by

$$\sum_{v=v_{min}}^{v_{max}} \frac{1}{\sqrt{2\pi}\sigma_v} e^{-\frac{1}{2}\left(\frac{v-\mu_v}{\sigma_v}\right)^2} f\left(V(x, y, t - d/v)\right). \tag{24}$$

As with Eq. (3), d is the distance between pre- and postsynaptic cells; and $V(x, y)$ is the membrane potential of presynaptic cell at location (x, y). Conduction velocity variation did indeed reduce the latency of distal activity, to the extent that a standard deviation of 0.095 m/s was sufficient alone to account for the average latency reduction observed in vitro (data not shown). However, in vitro, weak stimuli result in a maximum latency reduction of ≈1.4 ms. As such stimuli are not expected to produce inhibition it is reasonable to assume that the maximum reduction in latency is attributable to variation in conduction velocity is 1.4 ms. The model was adjusted such that the maximum latency attributable to conduction velocity variation was also ≈1.4 ms.

Depolarising inhibitory cells, reduction of synaptic time constants and inclusion of conduction velocity variation did reduce the latency of distal responses. However they were insufficient to account for the reduction in distal latency observed in vitro. From Fig. 13 it can be seen that the rate at which latency reduces is higher in vitro than observed in the model. This discrepancy remained after the introduction of the aforementioned mechanisms. The relatively constant acceleration values produced by the model for stimulus pulses 2–4 results from the observation that each of these stimulus pulses regenerated the same activity in distal inhibitory cells. Consequently the degree of inhibition of distal excitatory cells was constant following stimulus pulses 2–4. To produce the required inhibition, the efficacy of a stimulus in exciting distal interneurons must increase with successive pulses. Trains of presynaptic spikes from pyramidal cells have been shown to produce facilitation in excitatory postsynaptic potentials (EPSPs) of interneurons (Thomson, 1997). In a short series of EPSPs this facilitation is observed to increase with successive EPSPs. A simple facilitation model was incorporated into the synapses made by excitatory cells with distal interneurons. Based on the experimental observations of Thomson (1997), the AMPA input to interneurons was weighted by

$$h = 10^{0.22p - 0.22}. \tag{25}$$

Here h is the facilitation weighting, and p is the extracellular pulse number. This facilitation term resulted in a progressive increase in interneuron activity with successive stimulus pulses and a corresponding decrease in the distal latency. An example of the resultant distal VSD signal is shown in Fig. 14.

For low stimulus strengths where inhibition was subthreshold the latency reduction between the first and last stimulus pulse was ≈1.3 ms similar to the figure of 1.4 ms observed in vitro. For the model this value increased with stimulus strength up to moderate strengths after which it deceased. Again, this behaviour mirrors that reported for in vitro results. The mean latency between successive stimuli pulses was calculated over a range of strengths and is presented in Fig. 15 along with the data recorded in vitro. The mean latencies for successive stimuli pulses agree with in vitro data. For some stimulus strengths the latency did not monotonically decrease with successive pulses, rather the greatest decrease was observed following the second stimulus pulse.

To further verify the proposed mechanisms underlying activity at distal patches, the model was compared with in vitro data obtained under a stimulus protocol consisting of a single pulse of varying strength. For a single pulse qualitatively termed weak, moderate and strong, in vitro intracellular and optical recordings yielded distinct inhibitory signatures. Intracellular in vitro recordings showing inhibition in distal pyramidal cells were enhanced by depolarising the recorded cells through current injection. Such recordings showed that weak stimuli did not evoke inhibition in distal pyramidal cells, whilst progressively stronger stimuli induced greater inhibition. Strong stimuli induced significant hyperpolarisation of the cell below its depolarised resting potential. Regardless of stimulus strength, the optical signal did not fall below that observed at rest. However, evidence of inhibition was observed in the optical signal which developed a sharper peak with increasing stimulus strength. These in vitro observations in both intracellular and optical data can be seen in Fig. 11A–C. For weak, moderate and strong single pulse stimuli the model produced similar results which are presented in Fig. 16.

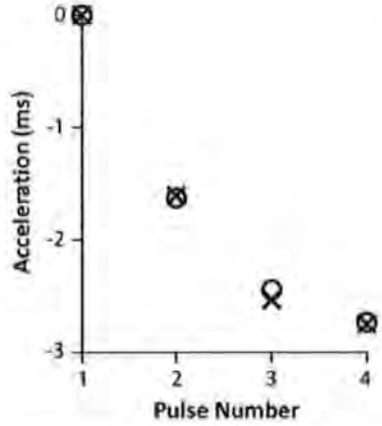

Fig. 15. Reduction in latency with synaptic facilitation. The mean latency over a range of weak stimulus strengths is shown for a distal patch of activity. Successive stimulus pulses lead to a significant reduction in the latency. For comparison, model results are shown by circles and in vitro data by crosses.

The upper three panels from left to right show model voltage sensitive dye signals for weak, moderate and strong single pulse stimuli. As with the in vitro data the model results did not fall below that observed at rest, whilst increasing stimulus strength produced a more peaked response. The lower three panels from left to right show the membrane potential of a distal excitatory cell which was been depolarised by 5 mV from a resting potential of −70 mV. Again the response developed a sharper peak with increased stimulus strength as a result of stronger inhibition, a feature also observed in vitro. The model also demonstrates that a strong stimulus induced significant hyperpolarising inhibition which was manifest as membrane potentials below −65 mV.

The qualitative observations of Fig. 16 can be quantified to some extent by the time to peak and FWHM. Both of these measures for intracellular and optical recording made in vitro are summarised in Table 1. For comparison, corresponding data produced by the model are also presented. The model time to peak data for both intracellular and optical recordings are representative of that observed in vitro. The only significant discrepancy between model and in vitro data is in the FWHM for weak stimuli. For weak stimuli the model produces FWHM values lower than that recorded in vitro. In the case of optical data this may be due to the observation that in vitro optical signals appear to persist for longer than in the model (c.f., Fig. 14 presented here with figures 8A and 9D in Tucker and Katz (2003b). Since the optical signal is less peaked for weak stimuli, the slower decay observed in vitro may increase the corresponding FWHM. The FWHM for intracellular recordings generated by weak stimuli in vitro is also longer than the model. This may result from cellular differences in the model where cells may have had smaller membrane time constants than was the case in vitro. A closer agreement between model and in vitro intracellular FWHM data may reduce the FWHM discrepancies observed for optical data.

Table 1
Comparison of model and in vitro results for single stimulus pulse. The time to peak and FWHM times (in ms) for voltage sensitive dye and membrane potential signals generated by the model are shown. For comparison with the model, in vitro figures taken directly from published data are also presented.

		Model	In vitro
VSD	Time to peak	8.41 ms ± 6.11 ms	9.5 ms ± 4.3 ms
	FWHM	12.67 ms ± 4.55 ms	30 ms ± 5 ms
Membrane potential	Time to peak	10.24 ms ± 5.73 ms	7 ms ± 1.9 ms
	FWHM	17.87 ms ± 3.27 ms	24 ms ± 1.5 ms

4. Discussion

The vast majority of efferent and afferent connections in layer 2/3 of the primary visual cortex are intralaminar (Binzegger et al., 2004). Furthermore, an apparent dichotomy shows two distinct architectures; one comprising local diffuse connectivity; the other more specific, consisting of long range patchy connections (Bosking et al., 1997; Buzás et al., 2006; Gilbert & Wiesel, 1983; Kisvárday et al., 1997; Malach et al., 1993; Schmidt et al., 1997; Sincich & Blasdel, 2001; Tanigawa et al., 2005). The specific functionality of this architecture is still unclear but elucidation is essential to understanding cortical processing of visual stimuli. In vitro focal extracellular stimulation applied to layer 2/3 slices from ferret primary visual cortex reveal population activity consistent with this architecture (Tucker & Katz, 2003b). Population activity was imaged using voltage sensitive dyes and revealed local diffuse activity and discrete patches of activity at distal locations. Superficially

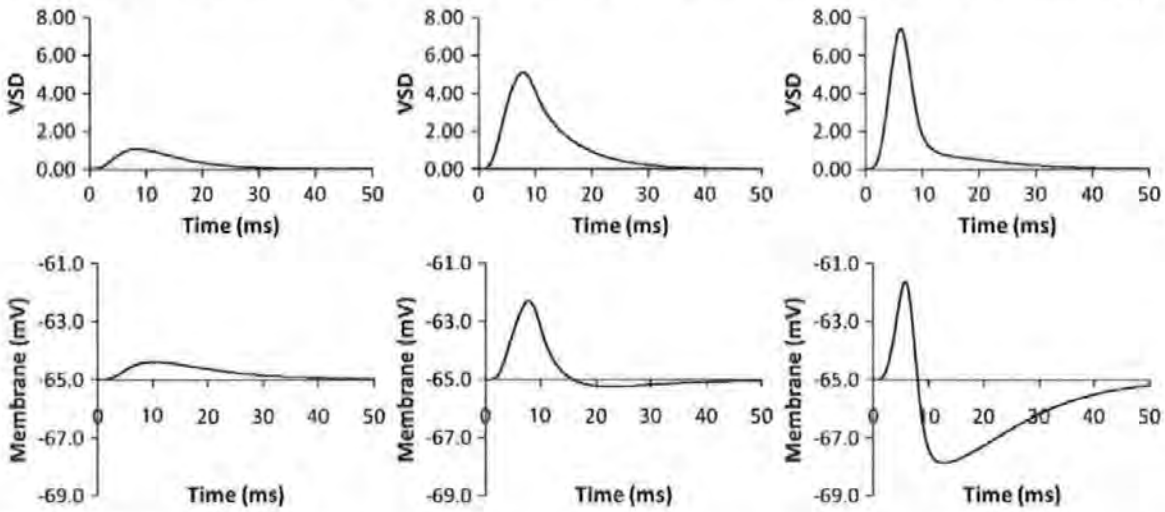

Fig. 16. Temporal activity generated by a single stimulus pulse. The upper row shows the voltage sensitive dye signal generated by a single weak, moderate and strong stimulus pulse. The increasing stimulus strength not only increased the signal amplitude but also reduced the full width at half maximum (FWHM). The lower row shows the corresponding membrane potentials after depolarisation by 5 mV to increase the resting potential and accentuate inhibition. As with the VSD signal increasing stimulus strength increased amplitude. The underlying inhibition responsible for the decreases in FWHM was weakly present for a moderate stimulus, and fully established for a strong stimulus, c.f., Fig. 11A–C.

these data are consistent with the connectivity architecture. However, interpretation of optical signals from VSD is not trivial (Ebner & Chen, 1995; Grinvald et al., 1999). Furthermore, connectivity patterns alone are insufficient to fully describe the observed population activity. Computational modelling the VSD data offers a unique opportunity to determine more precisely the physiological properties and synaptic activity that underlies the behaviour observed in large populations of cortical cells. In addition such models offer a powerful tool to predict how such in vitro data relates to in vivo behaviour of the cortical microcircuitry.

Fundamental to the development of such models was determining an appropriate input representation, or more precisely a proper model of extracellular stimulation. Two simplifying assumptions were made regarding the model of extracellular stimulation. First that the path of axonal projections follows the shortest distance between pre and postsynaptic cells. From even the most cursory inspection of the cortex it is readily apparent that the path taken by connections between cells is anything but straight. The second simplification is that an extracellular field applied to a length of axon can be treated as a number of independent contiguous segments. A more accurate compartmental model capturing the circuitous path taken by axons and the effects of large extracellular electric fields may reveal discrepancies with the model proposed here. However, for the spatial resolution of the data modelled the simplifications adopted gave good results. At this granularity the shape of the connectivity surface (Fig. 2) dominates the spatiotemporal patterns of activity observed.

A specific feature of the spatiotemporal activity is pronounced suppression of activity local to the stimulus site. A distinct region of inhibition centred on the stimulus site is observed to deepen and expand with successive extracellular pulses during repetitive stimulation. However it should be noted that such spatiotemporal activity does not appear to be entirely stereotypical with various forms of local inhibition observed such as a partial ring (figures 4 and 7 in Tucker and Katz (2003b)), and complete suppression at the stimulus site (figures 5 and 10 in Tucker and Katz (2003b)). Tucker and Katz consider the role of increased efficacy of excitation and inhibition during high frequency stimulation and synaptic plasticity. Here we show that inhibition increases and expands almost entirely as a result of temporal integration by inhibitory synapses through lateral propagation. The temporal properties of synaptic components lead to increased inhibitory activity with repetitive stimulation at 100 Hz. This expanding and increasing region of inhibitory activity is manifest as an expanding and deepening suppression of excitation. The model presented here demonstrates that the specific balance of excitation and inhibition in combination with cellular and synaptic characteristics can combine to produce the suppressive behaviour observed in vitro.

The model shows that the ring and crater of inhibition observed in vitro are attributed to extracellular stimulation of different axonal pathways. The crater of inhibition emerges as a result of strong activation of local diffuse axonal projections. Stimulation of long range circuitry elevates the signal at the stimulus site giving rise to an inhibitory signature that manifests itself more as a ring. It is proposed that the appearance of both inhibitory patterns results from variation in the number of patches formed by long range axons. Inspection of long range patchy connectivity observed in the cortex (Bosking et al., 1997; Buzás et al., 2006; Kisvárday et al., 1997; Sincich & Blasdel, 2001; Tanigawa et al., 2005) appears less uniform than suggested by the model of Buzás et al. (2006). Indeed, inspection of their Fig. 5 reveals that their model predicts more patches than the anatomical data show. In New World monkeys between 8 and 18 patches are observed (11.7 ± 3.4, mean $\pm$standard deviation, $n = 11$) (Sincich & Blasdel, 2001). In the Macaque the number of patches was between 5 and 21 (12 ± 5.6, $n = 9$) (Tanigawa et al., 2005), however these patches were not correlated with orientation tuning. Variation in the number and location of such patches will significantly influence the number of long range afferents to a given cell and the degree to which such afferents are stimulated. Consequently the combined stimulation of afferents as depicted in Fig. 7 can be expected to show features that range from the characteristic ring, as shown, to a crater, dependent on variations in the cortical microcircuitry.

The latency between stimulus pulse and corresponding peak in distal activity was observed in vitro to reduce with successive pulses. A similar characteristic was also observed in the model. The initial reduction in this latency, following the first pulse, was $\approx$74% of that observed in vitro. However, subsequent reductions in model results were significantly less than experimental data. This model result is largely attributed to temporal integration characteristics at the distal site. As such it is in opposition to the proposal of Tucker and Katz that the reduction in latency results from inhibitory activity at the distal site. Investigation of the model shows that at the distal site inhibition lags behind excitation due to the disynaptic temporal integration of the former, i.e., long range excitation of inhibitory cells and GABAergic synapses from inhibitory to excitatory cells at the distal patches. By comparison, excitation only suffers from temporal integration of long range excitation. As a consequence, the effective rise rate of inhibitory input to a distal excitatory cell is much slower than that of excitation. Further, inhibitory cell activity reaches a maximum early in the stimulus pulse train. Accordingly inhibition of excitatory cells is similar following successive pulses and does not result in a discernable reduction in latency. The introduction of conduction velocity variation provided another source of temporal integration that also reduced the latency at distal sites. Interestingly it was possible to produce latency reductions greater than that observed in vitro simply by increasing the temporal dispersal of postsynaptic activity. In general, this has clear implications when interpreting data as behaviour that initially appears inhibitory might equally be ascribed to temporal integration. It is particularly relevant when considering the compound signal of voltage sensitive dyes which confounds both excitatory and inhibitory activity. Whilst a number of sources of the latency reduction has been investigated, long range inhibitory connections have not been considered. Despite their paucity, GABAergic cells do make long range axonal projections, which in some cases are myelinated (Payne & Peters, 2001; Somogyi, Kisvárday, Martin, & Whitteridge, 1983). However, stimulation of long range excitatory connections are observed to elicit spiking activity in interneurons (Hirsch & Gilbert, 1991). Therefore it is entirely possible that both types of long range connections contribute to the observed reduction in latency.

The model was also used to predict the activity expected from extracellular stimulation of innervating axons from other cortical layers. This was considered important as it offers a more accurate representation of layer 2/3 in vivo behaviour. The results of this extra-laminar stimulation demonstrate specific differences from activity elicited by intra-laminar stimulation. A number of parameter regimes was used to weight innervating axonal connections from layer 4. These included the parameters used for interlaminar connections within layer 2/3; assuming unbiased weighting; and weighting based on data from different modelling studies (Binzegger et al., 2004; Stepanyants et al., 2008). In all cases for stimulus strength up to that used to model the in vitro data only a diffuse local region of activity was observed with no distal patches. Local inhibition was not observed under all parameter regimes. For stronger stimulus strength direct activation of layer 2/3 produced characteristically similar results to those observed under weaker stimulation. However, profound changes were observed in the activity of all other parameter regimes. These included significant attenuation of local activity for

successive stimulus pulses and more extensive lateral propagation of activity. Such predictions suggest that in vivo, the contribution of diffuse and distal activity to cortical functioning is significantly less than suggested by in vitro data. This has serious implications for predicting in vivo behaviour on the basis of activity evoked in vitro by extracellular stimulation. These results also demonstrate that current predictions of intra-laminar connectivity (Binzegger et al., 2004; Stepanyants et al., 2008) lead to profoundly different spatiotemporal patterns of activity. As such this observation highlights the need for more empirical data on cortical connectivity at the population level.

Acknowledgment

Many thanks to Thomas Tucker for additional data and its interpretation. Thanks to Zoltán Kisvárday for supplying orientation maps of cat area 18. This project was supported by funding under the Sixth Research Framework Programme of the European Union under the grant no. FP6-2004-IST-FETPI 15879 (FACETS).

Andy Symes died in July 2008, briefly after finishing the work reported here which was part of his Ph.D. project. This publication aims at posthumously honouring his outstanding work as a young scientist.

References

Beecroft, S. I., Alkhateeb, R. P., & Gaumond, R. P. (1994). Nerve fiber stimulation threshold for multiphase stimuli. In J. Masi, R. Davis, M. Fox, & R. Peura (Eds.), *Bioengineering: 20th annual northeast conference* (pp. 67–68). New York, City: IEEE Press.

Binzegger, T., Douglas, R. J., & Martin, K. A. C. (2004). A quantitative map of the circuit of cat primary visual cortex. *The Journal of Neuroscience, 24*, 8441–8453.

Bosking, W. H., Zhang, Y., Schofield, B., & Fitzpatrick, D. (1997). Orientation selectivity and the arrangement of horizontal connections in tree shrew striate cortex. *The Journal of Neuroscience, 17*, 2112–2127.

Bringuier, V., Chavane, F., Glaeser, L., & Frégnac, Y. (1999). Horizontal propagation of visual activity in the synaptic integration field of area 17 neurons. *Science, 283*, 695–699.

Buzás, P., Kovács, K., Ferecskó, A. S., Budd, J. M. L., Eysel, U. T., & Kisvárday, Z. F. (2006). Model-based analysis of excitatory lateral connections in the visual cortex. *The Journal of Comparative Neurology, 499*, 861–881.

Carandini, M., & Ferster, D. (2000). Membrane potential and firing rate in cat primary visual cortex. *The Journal of Neuroscience, 20*, 470–484.

Ebner, T. J., & Chen, G. (1995). Use of voltage-sensitive dyes and optical recordings in the central nervous system. *Progress in Neurobiology, 46*, 463–506.

Ferster, D., & Miller, K. D. (2000). Neural mechanisms of orientation selectivity in the visual cortex. *Annual Review of Neuroscience, 23*, 441–471.

Fitzpatrick, D. (2000). Cortical imaging: Capturing the moment. *Current Biology, 10*, R187-R190.

Gerstner, W., & Kistler, W. M. (2002). *Spiking neuron models: Single neurons, populations, plasticity*. New York: Cambridge University Press.

Gilbert, C. D., & Wiesel, T. N. (1983). Clustered intrinsic connections in cat visual cortex. *The Journal of Neuroscience, 3*, 1116–1133.

Gimsa, U., Schreiber, U., Habel, B., Flehr, J., van Rienen, U., & Gimsa, J. (2006). Matching geometry and stimulation parameters of electrodes for deep brain stimulation experiments? Numerical considerations. *Journal of Neuroscience Methods, 150*, 212–227.

Grinvald, A., Lieke, E. E., Frostig, R. D., & Hildesheim, R. (1994). Cortical point-spread function and long-range lateral interactions revealed by real-time optical imaging of macaque monkey primary visual cortex. *The Journal of Neuroscience, 14*, 2545–2568.

Grinvald, A., Shoham, D., Schmuel, A., Glaser, D., Vanzetta, I., Shtoyerman, E., et al. (1999). In-vivo optical imaging of cortical architecture and dynamics. In H. Johansson, & U. Windhorst (Eds.), *Modern techniques in neuroscience research* (pp. 893–969). Springer Verlag.

Hirsch, J. A., & Gilbert, C. D. (1991). Synaptic physiology of horizontal connections in the cat's visual cortex. *The Journal of Neuroscience, 11*, 1800–1809.

Jonas, P., Bischofberger, J., Fricker, D., & Miles, R. (2004). Interneuron diversity series: Fast in, fast out — temporal and spatial signal processing in hippocampal interneurons. *Trends in Neuroscience, 27*, 30–40.

Kandel, E. R., Schwartz, J. H., & Jessell, T. M. (2000). *Principles of neural science*. New York: McGraw-Hill.

Kisvárday, Z. F., Tóth, É., Rausch, M., & Eysel, U. T. (1997). Orientation-specific relationship between populations of excitatory and inhibitory lateral connections in the visual cortex of the cat. *Cerebral Cortex, 7*, 605–618.

Lumer, E. D., Edelman, G. M., & Tononi, G. (1997). Neural dynamics in a model of the thalamocortical system. I. Layers, loops and the emergence of fast synchronous rhythms. *Cerebral Cortex, 7*, 207–227.

Malach, R., Amir, Y., Harel, M., & Grinvald, A. (1993). Relationship between intrinsic connections and functional architecture revealed by optical imaging and in vivo targeted biocytin injections in primate striate cortex. *Proceedings of the National Academy of Sciences of the United States of America*, 10460–10473.

McIntyre, C. C., & Grill, W. M. (1999). Excitation of central nervous system neurons by nonuniform electric fields. *Biophysical Journal, 76*, 878–888.

Nowak, L. G., Azouz, R., Sanchez-Vives, M. V., Gray, C. M., & McCormick, D. A. (2003). Electrophysiological classes of cat primary visual cortical neurons in vivo as revealed by quantitative analyses. *Journal of Neurophysiology, 89*, 1541–1566.

Nowak, L. G., & Bullier, J. (1998a). Axons, but not cell bodies, are activated by electrical stimulation in cortical gray matter I. Evidence from chronaxie measurements. *Experimental Brain Research, 118*, 477–488.

Nowak, L. G., & Bullier, J. (1998b). Axons, but not cell bodies, are activated by electrical stimulation in cortical gray matter II. Evidence from selective inactivation of cell bodies and axon initial segments. *Experimental Brain Research, 118*, 489–500.

Nusser, Z., Naylor, D., & Mody, I. (2001). Synapse-specific contribution of the variation of transmitter concentration to the decay of inhibitory postsynaptic currents. *Biophysical Journal, 80*, 1251–1261.

Payne, B. R., & Peters, A. (2001). *The cat primary visual cortex*. San Diego: Academic Press Inc..

Petersen, C. C. H., Grinvald, A., & Sakmann, B. (2003). Spatiotemporal dynamics of sensory responses in layer 2/3 of rat barrel cortex measured in vivo by voltage-sensitive dye imaging combined with whole-cell voltage recordings and neuron reconstructions. *The Journal of Neuroscience, 23*, 1298–1309.

Roerig, B., & Kao, J. P. Y. (1999). Organization of intracortical circuits in relation to direction preference maps in ferret visual cortex. *The Journal of Neuroscience, 19*, 1–5.

Schmidt, K. E., Goebel, R., Löwel, S., & Singer, W. (1997). The perceptual grouping criterion of colinearity is reflected by anisotropies of connections in the primary visual cortex. *The European Journal of Neuroscience, 9*, 1083–1089.

Seriès, P., George, S., Lorenceau, J., & Frégnac, Y. (2002). Orientation dependent modulation of apparent speed: A model based on the dynamics of feed-forward and horizontal connectivity in V1 cortex. *Vision Research, 42*, 2781–2797.

Seriès, P., Lorenceau, J., & Frégnac, Y. (2003). The "silent" surround of V1 receptive fields: Theory and experiments. *Journal of Physiology, Paris, 97*, 453–474.

Sincich, L. C., & Blasdel, G. G. (2001). Oriented axon projections in primary visual cortex of the monkey. *The Journal of Neuroscience, 21*, 4416–4426.

Somogyi, P., Kisvárday, Z. F., Martin, K. A. C., & Whitteridge, D. (1983). Synaptic connections of morphologically identified and physiologically characterized large basket cells in the striate cortex of cat. *Neuroscience, 10*, 261–294.

Song, S., Miller, K. D., & Abbott, L. F. (2000). Competitive Hebbian learning through spike-timing-dependent synaptic plasticity. *Nature Neuroscience, 3*, 919–926.

Stepanyants, A., & Chklovskii, D. B. (2005). Neurogeometry and potential synaptic connectivity. *Trends in Neuroscience, 28*, 387–394.

Stepanyants, A., Hirsch, J. A., Martinez, L. M., Kisvárday, Z. F., Ferecskó, A. S., & Chklovskii, D. B. (2008). Local potential connectivity in cat primary visual cortex. *Cerebral Cortex, 18*, 13–28.

Szabadics, J., Tamás, G., & Soltesz, I. (2007). Different transmitter transients underlie presynaptic cell type specificity of GABAA, slow and GABAA, fast. *Proceedings of the National Academy of Sciences of the United States of America, 104*, 14831–14836.

Tanigawa, H., Wang, Q., & Fujita, I. (2005). Organization of horizontal axons in the inferior temporal cortex and primary visual cortex of the macaque monkey. *Cerebral Cortex, 15*, 1887–1899.

Thomson, A. M. (1997). Activity-dependent properties of synaptic transmission at two classes of connections made by rat neocortical pyramidal axons in vitro. *Journal of Physiology, 502*, 131–147.

Tucker, T. R., & Katz, L. C. (2003a). Recruitment of local inhibitory networks by horizontal connections in layer 2/3 of ferret visual cortex. *The Journal of Neurophysiology, 89*, 501–512.

Tucker, T. R., & Katz, L. C. (2003b). Spatiotemporal patterns of excitation and inhibition evoked by the horizontal network in layer 2/3 of ferret visual cortex. *The Journal of Neurophysiology, 89*, 488–500.